(ATINER)

Athens Journal of Technology & Engineering

(ATINER)

Volume 7, Issue 4, December 2020

Articles

Front Pages

SADDAM HUSSEIN ABO SABAH, AHMAD BENG HONG KUEH, MEGAT AZMI MEGAT JOHARI & TAKSIAH A MAJID
The Effect of Honeycomb Core Thickness on the Repeated Low-Velocity Impact Behavior of Sandwich Beams

MARIE REICHERT & CATHERINA THIELE
Evaluation of Fire Resistance Concerning Bond Failure for Injection Anchors with Variable Embedment Depths

MARCUS KURTH, MICHAELA GÖGGEL, CARSTEN SCHLEYER, JOHANNES GRATT & BURKHARD MARTIN
Filling the Industrial Data Lake in Manufacturing Companies based on KPIs

ALEXANDER KOLPAKOV & AUSTIN MARIE SIPIORA
Implications of Market Penetration of Electric and Autonomous Vehicles for Florida State Transportation Revenue

Mission

ATINER is an Athens-based World Association of Academics and Researchers based in Athens. ATINER is an independent and non-profit **Association** with a **Mission** to become a forum where Academics and Researchers from all over the world can meet in Athens, exchange ideas on their research and discuss future developments in their disciplines, **as well as engage with professionals from other fields**. Athens was chosen because of its long history of academic gatherings, which go back thousands of years to *Plato's Academy* and *Aristotle's Lyceum.* Both these historic places are within walking distance from ATINER's downtown offices. Since antiquity, Athens was an open city. In the words of Pericles, **Athens"*... is open to the world, we never expel a foreigner from learning or seeing*". (**"Pericles' Funeral Oration", in Thucydides, *The History of the Peloponnesian War).* It is ATINER's **mission** to revive the glory of Ancient Athens by inviting the World Academic Community to the city, to learn from each other in an environment of freedom and respect for other people's opinions and beliefs. After all, the free expression of one's opinion formed the basis for the development of democracy, and Athens was its cradle. As it turned out, the Golden Age of Athens was in fact, the Golden Age of the Western Civilization. *Education* and *(Re)searching* for the 'truth' are the pillars of any free (democratic) society. This is the reason why *Education* and *Research* are the two core words in ATINER's name.

The Athens Journal of Technology & Engineering
ISSN NUMBER: 2241-8237- DOI: 10.30958/ajte
Volume 7, Issue 4, December 2020
Download the entire issue (PDF)

Front Pages i-viii

The Effect of Honeycomb Core Thickness on the Repeated Low-Velocity Impact Behavior of Sandwich Beams 239
Saddam Hussein Abo Sabah, Ahmad Beng Hong Kueh, Megat Azmi Megat Johari & Taksiah A Majid

Evaluation of Fire Resistance Concerning Bond Failure for Injection Anchors with Variable Embedment Depths 257
Marie Reichert & Catherina Thiele

Filling the Industrial Data Lake in Manufacturing Companies based on KPIs 277
Marcus Kurth, Michaela Göggel, Carsten Schleyer, Johannes Gratt & Burkhard Martin

Implications of Market Penetration of Electric and Autonomous Vehicles for Florida State Transportation Revenue 299
Alexander Kolpakov & Austin Marie Sipiora

Athens Journal of Technology & Engineering
Editorial and Reviewers' Board

Editors

- **Dr. Panagiotis Petratos**, Vice-President of Information Communications Technology, ATINER & Fellow, Institution of Engineering and Technology & Professor, Department of Computer Information Systems, California State University, Stanislaus, USA.
- **Dr. Nikos Mourtos**, Head, Mechanical Engineering Unit, ATINER & Professor, San Jose State University USA.
- **Dr. Theodore Trafalis**, Director, Engineering & Architecture Division, ATINER, Professor of Industrial & Systems Engineering and Director, Optimization & Intelligent Systems Laboratory, The University of Oklahoma, USA.
- **Dr. Virginia Sisiopiku**, Head, Transportation Engineering Unit, ATINER & Associate Professor, The University of Alabama at Birmingham, USA.

Editorial Board

- Dr. Marek Osinski, Academic Member, ATINER & Gardner-Zemke Professor, University of New Mexico, USA.
- Dr. Jose A. Ventura, Academic Member, ATINER & Professor, The Pennsylvania State University, USA.
- Dr. Nicolas Abatzoglou, Professor and Head, Department of Chemical & Biotechnological Engineering, University of Sherbrooke, Canada.
- Dr. Jamal Khatib, Professor, Faculty of Science and Engineering, University of Wolverhampton, UK.
- Dr. Luis Norberto Lopez de Lacalle, Professor, University of the Basque Country, Spain.
- Dr. Zagabathuni Venkata Panchakshari Murthy, Professor & Head, Department of Chemical Engineering, Sardar Vallabhbha National Institute of Technology, India.
- Dr. Yiannis Papadopoulos, Professor, Leader of Dependable Systems Research Group, University of Hull, UK.
- Dr. Bulent Yesilata, Professor & Dean, Engineering Faculty, Harran University, Turkey.
- Dr. Javed Iqbal Qazi, Professor, University of the Punjab, Pakistan.
- Dr. Ahmed Senouci, Associate Professor, College of Technology, University of Houston, USA.
- Dr. Najla Fourati, Associate Professor, National Conservatory of Arts and Crafts (Cnam)-Paris, France.
- Dr. Ameersing Luximon, Associate Professor, Institute of Textiles and Clothing, Polytechnic University, Hong Kong.
- Dr. Georges Nassar, Associate Professor, University of Lille Nord de France, France.
- Dr. Roberto Gomez, Associate Professor, Institute of Engineering, National Autonomous University of Mexico, Mexico.
- Dr. Aly Mousaad Aly, Academic Member, ATINER & Assistant Professor, Department of Civil and Environmental Engineering, Louisiana State University, USA.
- Dr. Hugo Rodrigues, Senior Lecturer, Civil Engineering Department, School of Technology and Management, Polytechnic Institute of Leiria, Portugal.
- Dr. Saravanamuthttu Subramaniam Sivakumar, Head & Senior Lecturer, Department of Civil Engineering, Faculty of Engineering, University of Jaffna, Sri Lanka.
- Dr. Hamid Reza Tabatabaiefar, Lecturer, Faculty of Science and Technology, Federation University, Australia.

- **Vice President of Publications:** Dr Zoe Boutsioli
- **General Managing Editor of all ATINER's Publications:** Ms. Afrodete Papanikou
- **ICT Managing Editor of all ATINER's Publications:** Mr. Kostas Spyropoulos
- **Managing Editor of this Journal:** Ms. Effie Stamoulara (bio)

Reviewers' Board

Click Here

President's Message

All ATINER's publications including its e-journals are open access without any costs (submission, processing, publishing, open access paid by authors, open access paid by readers etc.) and is independent of presentations at any of the many small events (conferences, symposiums, forums, colloquiums, courses, roundtable discussions) organized by ATINER throughout the year and entail significant costs of participating. The intellectual property rights of the submitting papers remain with the author. Before you submit, please make sure your paper meets the basic academic standards, which includes proper English. Some articles will be selected from the numerous papers that have been presented at the various annual international academic conferences organized by the different divisions and units of the Athens Institute for Education and Research. The plethora of papers presented every year will enable the editorial board of each journal to select the best, and in so doing produce a top-quality academic journal. In addition to papers presented, ATINER will encourage the independent submission of papers to be evaluated for publication.

The current issue is the fourth of the seventh volume of the *Athens Journal of Technology & Engineering (AJTE),* published by the Engineering & Architecture Division of ATINER.

Gregory T. Papanikos, President, ATINER.

Athens Institute for Education and Research

A World Association of Academics and Researchers

11th Annual International Conference on Civil Engineering
21-24 June 2021, Athens, Greece

The Civil Engineering Unit of ATINER is organizing its **11th Annual International Conference on Civil Engineering, 21-24 June 2020, Athens, Greece** sponsored by the Athens Journal of Technology & Engineering. The aim of the conference is to bring together academics and researchers of all areas of Civil Engineering other related areas. You may participate as stream leader, presenter of one paper, chair of a session or observer. Please submit a proposal using the form available (https://www.atiner.gr/2021/FORM-CIV.doc).

Academic Members Responsible for the Conference

- **Dr. Dimitrios Goulias**, Head, Civil Engineering Unit, ATINER and Associate Professor & Director of Undergraduate Studies Civil & Environmental Engineering Department, University of Maryland, USA.

Important Dates

- Abstract Submission: **23 Nov 2020**
- Acceptance of Abstract: 4 Weeks after Submission
- Submission of Paper: **24 May 2021**

Social and Educational Program

The Social Program Emphasizes the Educational Aspect of the Academic Meetings of Atiner.

- Greek Night Entertainment (This is the official dinner of the conference)
- Athens Sightseeing: Old and New-An Educational Urban Walk
- Social Dinner
- Mycenae Visit
- Exploration of the Aegean Islands
- Delphi Visit
- Ancient Corinth and Cape Sounion

Conference Fees

Conference fees vary from 400€ to 2000€
Details can be found at: https://www.atiner.gr/2019fees

Athens Institute for Education and Research

A World Association of Academics and Researchers

9th Annual International Conference on Industrial, Systems and Design Engineering, 22-25 June 2020, Athens, Greece

The Industrial Engineering Unit of ATINER will hold its **9th Annual International Conference on Industrial, Systems and Design Engineering, 21-24 June 2021, Athens, Greece** sponsored by the Athens Journal of Technology & Engineering.The aim of the conference is to bring together academics, researchers and professionals in areas of Industrial, Systems, Design Engineering and related subjects. You may participate as stream leader, presenter of one paper, chair of a session or observer. Please submit a proposal using the form available (https://www.atiner.gr/2021/FORM-IND.doc).

Important Dates

- Abstract Submission: **23 Nov 2020**
- Acceptance of Abstract: 4 Weeks after Submission
- Submission of Paper: **24 May 2021**

Academic Member Responsible for the Conference

- **Dr. Theodore Trafalis**, Director, Engineering & Architecture Division, ATINER, Professor of Industrial & Systems Engineering and Director, Optimization & Intelligent Systems Laboratory, The University of Oklahoma, USA.

Social and Educational Program

The Social Program Emphasizes the Educational Aspect of the Academic Meetings of Atiner.

- Greek Night Entertainment (This is the official dinner of the conference)
- Athens Sightseeing: Old and New-An Educational Urban Walk
- Social Dinner
- Mycenae Visit
- Exploration of the Aegean Islands
- Delphi Visit
- Ancient Corinth and Cape Sounion

More information can be found here: https://www.atiner.gr/social-program

Conference Fees

Conference fees vary from 400€ to 2000€

Details can be found at: https://www.atiner.gr/2019fees

Athens Journal of Technology and Engineering - Volume 7, Issue 4, December 2020 – Pages 239-256

The Effect of Honeycomb Core Thickness on the Repeated Low-Velocity Impact Behavior of Sandwich Beams

By Saddam Hussein Abo Sabah[*], *Ahmad Beng Hong Kueh*[±], *Megat Azmi Megat Johari*[‡] *& Taksiah A Majid*[+]

In a recent study, a new bio-inspired honeycomb sandwich beam (BHSB) mimicking the head configuration of the woodpecker was developed. The beam consists of two carbon/epoxy composite face sheets, aluminum honeycomb core, and rubber core to enhance the repeated low-velocity impact resistance of sandwich structures. This paper aims to numerically enhance the repeated low-velocity impact resistance of the BHSB via optimizing the aluminum honeycomb core thickness. The beam was investigated employing three core thicknesses: 20 mm, 25 mm, and 30 mm at three impact energy levels (13.5 J, 15.55 J, 21.43 J). The results revealed that increasing the thickness of the aluminum honeycomb core to a certain level enhances the sandwich beam stiffness. The beam with the 25 mm honeycomb core thickness was the only beam that can sustain five repeated impacts achieving the highest impact resistance efficiency index, especially at high energy levels. Furthermore, the bottom face sheet of this beam developed the lowest stresses indicating that this thickness has a relatively better performance during impact events since it allowed minimal stress to reach the bottom face sheet. Overall, increasing the aluminum core thickness will increase the height of its cells subjecting it to buckling phenomenon. Therefore, this study suggests that the optimal thickness of the aluminum honeycomb core should be 65% of the overall thickness of the sandwich beam to have the best impact resistance.

Keywords: *sandwich beams, core thickness, impact behavior, finite element analysis, modeling*

Introduction

The application of fiber reinforced composite sandwich structures in various engineering areas such as civil, mechanical, automotive engineering is on the increase due to the high specific strength, high stiffness, lightweight, and corrosion resistance that these structures possess (Fatt and Park 2001). Yet, these structures are vulnerable under heavy objects, tool drops, bird strikes, and loadings impacts. Impact loads can significantly damage sandwich structures both internally and externally and reduce their tensile, compressive, shear, and bending strength. Thus,

[*]Postdoctoral Fellow, School of Civil Engineering, Universiti Sains Malaysia, Malaysia.
[±]Civil Engineering Department, Universiti Malaysia Sarawak, Malaysia.
[‡]School of Civil Engineering, Universiti Sains Malaysia, Malaysia.
[+]School of Civil Engineering, Universiti Sains Malaysia, Malaysia.

many researchers have been proposing new strategies and designs to improve the impact resistance of these structures, rendering them an interesting research topic.

Many researchers such as Aminanda et al. (2009) and Williams et al. (2008) have investigated the impact behavior of sandwich structures with various core types under low-velocity impact. Fatt and Park (2001) examined the common failure modes of a sandwich panel with a polymer core and found that the panel experienced both skin fracture and core shear. Yang et al. (2015) also studied the energy absorption of foam-filled sandwich panels with six types of skins. Panels with pure carbon skins showed poor impact resistance, while panels with pure glass skins displayed preferable properties among all the specimens. Compston et al. (2006) investigated the energy absorption capability of two sandwich structures under low and high velocity impacts loading having different cores: aluminum foam and PVC foam. It was found that both structures had similar energy absorption capabilities, but the damages were different. The sandwich with the PVC foam core experienced a localized damage in the form of matrix cracking and core indentation at low energies and skin fracture and core crushing at high energies. On the other hand, the aluminum foam sandwich structure experienced skin buckling and cell crushing at both energies.

Kolopp et al. (2013) experimentally subjected a sandwich structure to medium-velocity impacts (120 m/s) to be used as armor for aeronautical applications by investigating two skin types, aluminum plates and dry aramid stitched fabrics, and two core types, aluminum and Nomex honeycombs. It was found that the dry stitched fabrics with aluminum honeycomb core exhibited better performance due to its lightweight and strong bonding between the top skin and the core.

Recently, researchers started to adopt the new concept of having dual-core sandwich structures. Heimbs et al. (2010) developed three-dimensional structures from a flat sheet of material by a simple folding process in order to reduce impact damage. They compared the behavior of a dual-core sandwich structure with a single core sandwich structure under low-velocity impact. The test was conducted on a drop tower with a hemi-spherical steel impactor and the impact location was chosen to be in the middle of the upper skin. The dual cores were of carbon and aramid fiber reinforced polymer and separated by a carbon fiber reinforced polymer layer. They reported that the stiffness and strength properties of sandwich structures with a dual-core system are extremely higher than those of single-core ones. Abo Sabah et al. (2017) compared the behavior of a bio-inspired dual-core sandwich beam with a conventional one under low-velocity impacts. The results showed that the dual-core sandwich beam showed a superior impact performance. In addition, Xiong et al. (2012) tested two-layer composite pyramidal-core sandwich panels under both compression and impact, and they compared their performance with glass fiber woven textile truss cores. It was concluded that the two-layer carbon fiber composite pyramidal truss cores have comparable specific energy absorptions versus glass fiber woven textile truss cores. Thus, it is obvious that a dual-core system can enhance the impact resistance of sandwich structures. Furthermore, Jiang and Shu (2005) studied the local displacement of a sandwich structure when subjected to low-velocity impact. The structure consisted of two

cores and an internal sheet inserted between the two cores. The purpose of the internal layer is to spread the impact energy to the whole panels, instead of concentrating the impact energy on a local area of the impact. The results showed that the local displacement of the core was reduced significantly.

Kılıçaslan et al. (2013) investigated the impact behavior of layered trapezoidal and corrugated aluminum cores (7 cores) and aluminum skins sandwich structures. The simulation and experimental results revealed that the main deformation mechanisms were the progressive fin folding of corrugated core layer and bending of interlayer and skins.

In a most recent work, a bio-inspired honeycomb sandwich beam (BHSB) that consists of two carbon fiber reinforced plastic (CFRP) face sheets (top and bottom) and a dual-core system (rubber and aluminum honeycomb) was developed to improve the repeated low-velocity impact resistance of sandwich structures (Abo Sabah et al. 2017). Both experimental and numerical investigations were conducted, and the results exhibited that the impact resistance of the BHSB was better by five folds than that of the conventional sandwich beam. The repeated low-velocity impact behavior of the BHSB was also investigated, and its impact performance was 1.65–16.22 times higher than that of the conventional design (Abo Sabah et al. 2018). The failure mode maps for this bio-inspired beam under single and repeated low-velocity impacts were also constructed in Abo Sabah et al. (2019).

In spite of the fact that many failure modes can be experienced after low-velocity impact, face yield, face wrinkle, core failure, and indentation are the four major modes of failure (McCormack et al., 2001). While a low-velocity impact does not normally cause perforation to the structure, the damage becomes confined to the upper skin, core shearing, and minor damage in the lower skin. The damage in the impacted zone of the skin is always localized under the impactor due to the core (Lin and Fatt 2006). For thick composite skins, cracks always develop in the first layer due to the high contact stresses during an impact, while for thin composite skins, cracks appear in the lowest layer due to bending stresses. When increasing the impact energy, the cracks start to propagate until they reach the interface of the consequent layer. After that, matrix cracks develop at the interface creating interlaminar stresses allowing the occurrence of delamination. According to Dear et al. (2005), with an increase in energy, fiber breakage takes place and then indentation develops on the surface of the top skin indicating serious damage. Zhou et al. (2006) indicated that the properties of the core have a great influence on the sandwich structure damage initiation mechanisms since cores have lower densities compared to skins. Honeycomb cores, for instance, fail by buckling and crushing at the impacted region (Dear et al. 2005). Core crushing is usually associated with folds and wrinkles in the cells. The aluminum honeycomb core crushing mechanism has been extensively investigated by Mohr and Doyoyo (2003, 2004). It was suggested that buckling takes place just before the peak load and this buckling alters the cell wall stress state of the homogenous membrane causing concentrations of stress along the boundaries of the core wall. As a result, plastic collapse occurs at the edges of the honeycombs. Zhang and Ashby (1992) examined the core crushing mechanisms of Nomex honeycomb cores. Their

crushing behavior appeared to be somewhat complicated compared to the aluminum honeycombs. Even though the folds in the cells' walls were similar, the angles of these folds appeared to be sharper in Nomex due to the difference in the materials plasticity. Anderson and Madenci (2000) also identified the dynamic crash behavior of bio-inspired sandwich structures composed of carbon fiber reinforced plastic (CFRP) panels and aluminum honeycomb. The CFRP skins failed by matrix cracking and fiber breakage, while the aluminum honeycomb core experienced shear, crushing, and buckling.

The numerical simulations are necessary in the development process of sandwich structures. They are an efficient approach to explore the behavior of both small and large structures reducing both time and cost. Moreover, models developed via finite element can be efficiently optimized and can be easily adjusted to suit any complex structure. Many researchers have used different finite element softwares such as ABAQUS and LS-DYNA to simulate the low-velocity impact event in sandwich structures. Therefore, finite element models are a powerful method frequently used by authors to simulate the structural behavior and damage modes of sandwich structures. Heimbs et al. (2010) developed dynamic finite element simulations using LS-DYNA to investigate the single low-velocity impact behavior of textile-reinforced foldcores sandwich structures. The behavior of the foldcores structures was compared with the behavior of the single core structures. It was found that foldcores structures have a better impact resistance. Because of the diverse skin and core failure modes they aimed to cover, the models required a high degree of complexity. The models' results showed very good agreement with the experimental data. Ivañez and Sanchez-Saez (2013) numerically modeled the low-velocity impact behavior of honeycomb core sandwich beams with ABAQUS. Their models were also verified through experimentally conducting single low-velocity tests. Solid and shell elements were used to mesh the skins and core, respectively. The skin behavior was molded through a VUMAT subroutine based on the Hou failure criteria. It was found that the core dominates the energy absorption of the sandwich beam especially at low energies. Zhu and Chai (2013) used ABAQUS/Explicit to simulate the initiation of damage, evolution, and failure modes of composite sandwich panels subjected to single low-velocity impacts. Burlayenko and Sadowski (2012) used ABAQUS to analyze free vibrations and steady-state dynamic behavior of sandwich plates initially damaged by single low-velocity impacts. Santiuste et al. (2010) predicted the failure modes of sandwich beams under single impacts by implementing Hou and Hashin failure criteria through a user subroutine VUMAT in ABAQUS/ Explicit. The numerical results of load and displacement agreed well with the experimental results.

This study aims to optimize the thickness of the BHSB in order to decide the ideal thickness that further improves its performance against repeated low-velocity impacts. The thicknesses of the face sheets (top and bottom) and rubber core are kept constant. The sandwich beam is tested numerically with three different core thicknesses: 20 mm, 25 mm, and 30 mm, and the impact energies used in this study are 13.5 J, 15.55 J, and 21.43 J. The beams are compared in terms of impact characteristics, stress propagation, failure modes, damage area, and absorbed energy. An impact resistance efficiency index (I_e) is also introduced to evaluate the

overall performance of the numerically tested beams.

Low-Velocity Impact Finite Element Simulation

Bio-Inspired Sandwich Beam Description

For the optimization process, the four-layer bio-inspired sandwich beam layout developed by Abo Sabah et al. (2017) based on the woodpecker's head configuration was adopted. Figure 1 depicts that the beak of the woodpecker's head was represented with a CFRP layer due to its high strength, and it formed the first protective layer against impact damage. The rubber layer represented the hyoid as the beam's Core I, and its function was to distribute and absorb the stresses caused by the impact event so that the next layers of the structure were protected. The aluminum honeycomb layer employed as Core II bio-mimicked the woodpecker's spongy bone to suppress any further impact. The fourth and last layer was another CFRP layer representing the woodpecker's skull bone.

Figure 1. (a) *The Woodpecker's Head Configuration (b) Bio-Inspired Honeycomb Sandwich Beam*

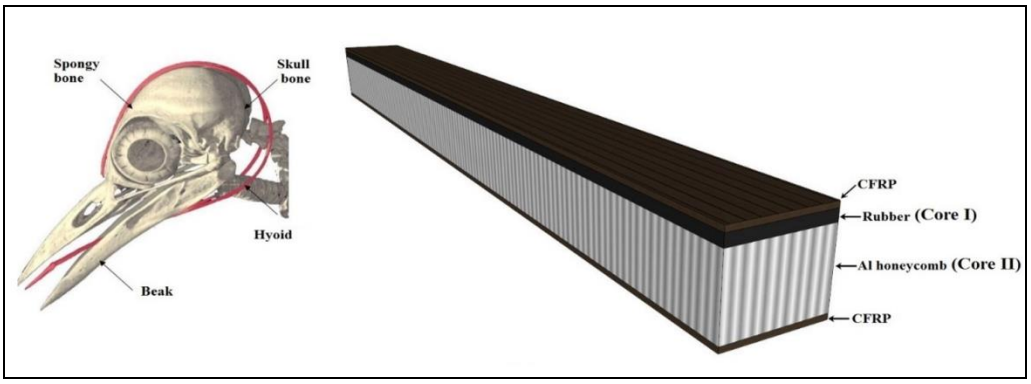

(a) *(b)*

Source: Abo Sabah et al. 2017.

Material Mechanical Properties

The face sheets (top and bottom layers) consisted of twelve layers of unidirectional T350/EP-1006 CFRP. Table 1 presents the properties of a single unidirectional T350/EP-1006 CFRP layer employed in this study (Abo Sabah et al. 2017).

Core I was a 3-mm-thick rubber with a density of 2000 kg/m^3 while Core II was a 5052-aluminum honeycomb having a cell size of 8 mm and a density of 2700 kg/m^3. The CFRP face sheet had a total thickness of 4.85 mm and a stacking sequence of $[0/\mp 90]_{4S}$. With the variation of the beam's thickness, the dimensions of the beam were 300 mm × 25 mm. The impactor was a 3 kg hemispherical steel with a 12 mm diameter. The density, Young's modulus, and Poisson's ratio of the impactor were 8050 kg/m^3, 210 GPa, and 0.3, respectively.

Modeling Description

ABAQUS 6.13-1/Explicit (2013) was employed to simulate the behavior of the sandwich beams subjected to five repeated low-velocity impact. The face sheets (top and bottom) and the aluminum honeycomb core were discretized with 4-node shell elements with reduced integration (S4R) while the rubber core was discretized with 8-node linear brick elements with reduced integration (C3D8R). The 4-node linear tetrahedron elements (C3D4) were utilized to discretize the hemispherical steel impactor.

To optimize the accuracy and computational time, the sandwich beams were finely meshed near the impact and support regions while the other regions were meshed with coarser elements. With the assumption that bonding between the beam layers was perfect, the surface-based tie constrain was used to simulate the adhesive bonding. The sandwich beam boundary conditions in this study are shown in Figure 2 where u_x; u_y; and u_z are the translations in the *X*-, *Y*-, and *Z*-directions, respectively whereas θ_x, θ_y and θ_z are the rotations about the *X*-, *Y*- and *Z*-axes, respectively. Using the predefined field, the velocity for each energy level was assigned. The beams were impacted at the center and repeated up to five times; the impact event was halted if the beam experienced ultimate failure before reaching the fifth impact.

Figure 2. *Numerical Model with Boundary Conditions*

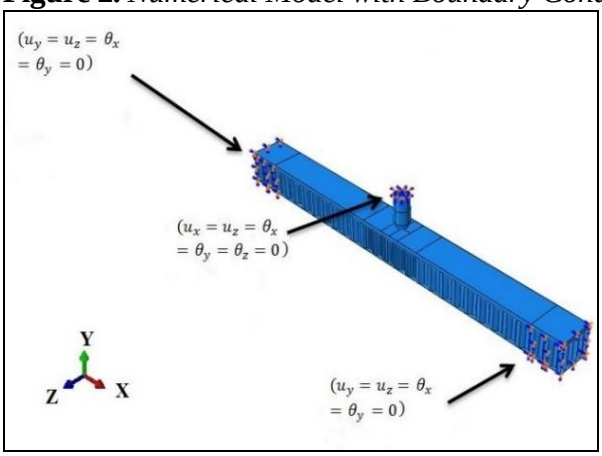

The aluminum honeycomb core (Core II) was modeled as an elasto-plastic material by defining the elastic part using the "Elastic Isotropic" option and the plastic part using the "Plastic Isotropic". Ductile and shear damage models were also incorporated to define the aluminum honeycomb core. The top and bottom face sheets were modeled as an elastic material using the properties presented in Table 1. The face sheets failure criteria introduced by Hashin (1980) were employed. The adopted failure criteria are described by the following conditions:

Tensile fiber failure ($\sigma_{11} \geq 0$):

$$\left(\frac{\sigma_{11}}{X_T}\right)^2 + \propto \left(\frac{\sigma_{12}^2+\sigma_{13}^2}{S_{12}^2}\right) = \begin{cases} \geq 1 & failure \\ < 1 & no\ failure \end{cases} \quad (1)$$

Compressive fiber failure (for $\sigma_{11} < 0$):

$$\left(\frac{\sigma_{11}}{X_C}\right)^2 = \begin{cases} \geq 1 & failure \\ < 1 & no\ failure \end{cases} \quad (2)$$

Tensile matrix failure (for $\sigma_{22} \geq 0$):

$$\left(\frac{\sigma_{22}}{Y_T}\right)^2 + \frac{\sigma_{12}^2+\sigma_{13}^2}{S_{12}^2} = \begin{cases} \geq 1 & failure \\ < 1 & no\ failure \end{cases} \quad (3)$$

Compressive matrix failure (for $\sigma_{22} < 0$):

$$\left(\frac{\sigma_{22}}{2S_{23}}\right)^2 + \left[\left(\frac{Y_C}{2S_{23}}\right)^2 - 1\right]\frac{\sigma_{22}}{Y_C} + \left(\frac{\sigma_{12}+\sigma_{13}}{S_{12}}\right)^2 = \begin{cases} \geq 1 & failure \\ < 1 & no\ failure \end{cases} \quad (4)$$

Table 1. *Properties of Unidirectional t350/ep-1006 Composite [8]*

Property	**Value**
Density, ρ (kg/m^3)	998.33
Longitudinal stiffness, E_1 (MPa)	123387.35
Transverse stiffness, E_2 (MPa)	8372.19
Poisson's ratio, v_{12}	0.319
In-plane shear modulus, G_{12} (MPa)	4278.57
Out-of-plane shear modulus, G_{13} (MPa)	4278.57
Out-of-plane shear modulus, G_{23} (MPa)	2968.86
Longitudinal tensile strength, X_t (MPa)	926.05
Longitudinal compressive strength, X_c (MPa)	345.60
Transverse tensile strength, Y_t (MPa)	8
Transverse compressive strength, Y_c (MPa)	57.60
Longitudinal shear strength, S_t (MPa)	19.45
Transverse shear strength, S_c (MPa)	19.45

Source: Abo Sabah et al. 2017.

where X_T is the longitudinal tensile strength, X_C is the longitudinal compressive strength, Y_T is the transverse tensile strength, Y_C is the transverse compressive strength, S_t is the longitudinal shear strength, S_c is the transverse shear strength, $\propto$ taken as 1.0 is a coefficient that determines the contribution of the shear stress, and σ_{ij} $(i,j = 1,2,3)$ are the effective stresses.

Finally, the rubber core was modeled as a hyperelastic material using the Mooney-Rivlin model. The Mooney-Rivlin model strain energy is defined in the following (Zhou et al. 2012):

$$U = C_{10}(\bar{I}_1 - 3) + C_{01}(\bar{I}_2 - 3) + \frac{1}{D_1}(J^{el} - 1)^2 \quad (5)$$

where C_{10}, C_{01}, and D_1 are the rubber parameters, $\bar{I}_1 = J^{-2/3}I_1$ and

$\bar{I}_2 = J^{-4/3} I_2$ are the strain invariants, and $J^{el} = \sqrt{I_3}$ is the elastic volume ratio. The element removal feature in ABAQUS/Explicit was performed for both cores and skin sheets. When the damage criteria for any element were fulfilled, the element was eliminated.

Results and Discussion

The results of the dynamic behaviors of BHSB subjected to repeated low-velocity impacts for various aluminum honeycomb core thicknesses numerically compared at impact energies of 13.5 J, 15.55 J, and 21.43 J are discussed in this section.

Impact Characteristics

Figure 3 depicts the load-time behaviors of the sandwich beams at energy level 13.5 J. It is seen that the first impact peak load for all beam thicknesses is the highest as compared to the subsequent impacts except for that with core thickness 30 mm. The peak force for the 30 mm core thick beam at the fifth impact is the highest (6521 N) as depicted in Figure 3(c). The unloading part of the curve at the fifth impact shows a sudden drop behavior indicating that the beam undergone serious damage. The contact durations for all beams increase as the number of impacts increases due to the progression of damage within each beam, which reduced the sandwich beam stiffness.

The load-time curves for the three beams at 15.55 J are depicted in Figure 4. The results show that the first impact peak load is varying from one thickness to another. The force peak dropped as the number of impacts increased and that is because no compaction of the beam occurred during the impact event so that the stiffness deteriorated. The contact durations also increased with each impact indicating that damage propagates steadily with the number of impacts.

Figure 5 illustrates the numerical load history curves for the five impacts at the highest energy level 21.43 J. It is noticed that the peak of the impact force reduced with the increase of the impact number. Only the beam with 25 mm aluminum honeycomb core thickness could sustain five repeated impacts while the other two beams failed at the fourth impact. This indicates that the 25 mm core beam could sustain its stiffness which enabled it to withstand the fifth impact. By closely inspecting the fourth impact of the three beams, the 25 mm aluminum honeycomb core peak force was higher compared to those of the other two beams. Thus, the 25 mm aluminum honeycomb core improved the performance of the sandwich beam under repeated low-velocity impacts. In addition, the impact durations for all beams were proportional to the number of impacts due to the progression of damage within each beam which reduced the stiffness of the sandwich beam.

Figure 3. *BHSB Contact Force-Time Curves for Five Repeated Impacts at Energy Level 13.5 J for Aluminum Core Thicknesses of a) 20 mm, b) 25 mm, c) 30 mm*

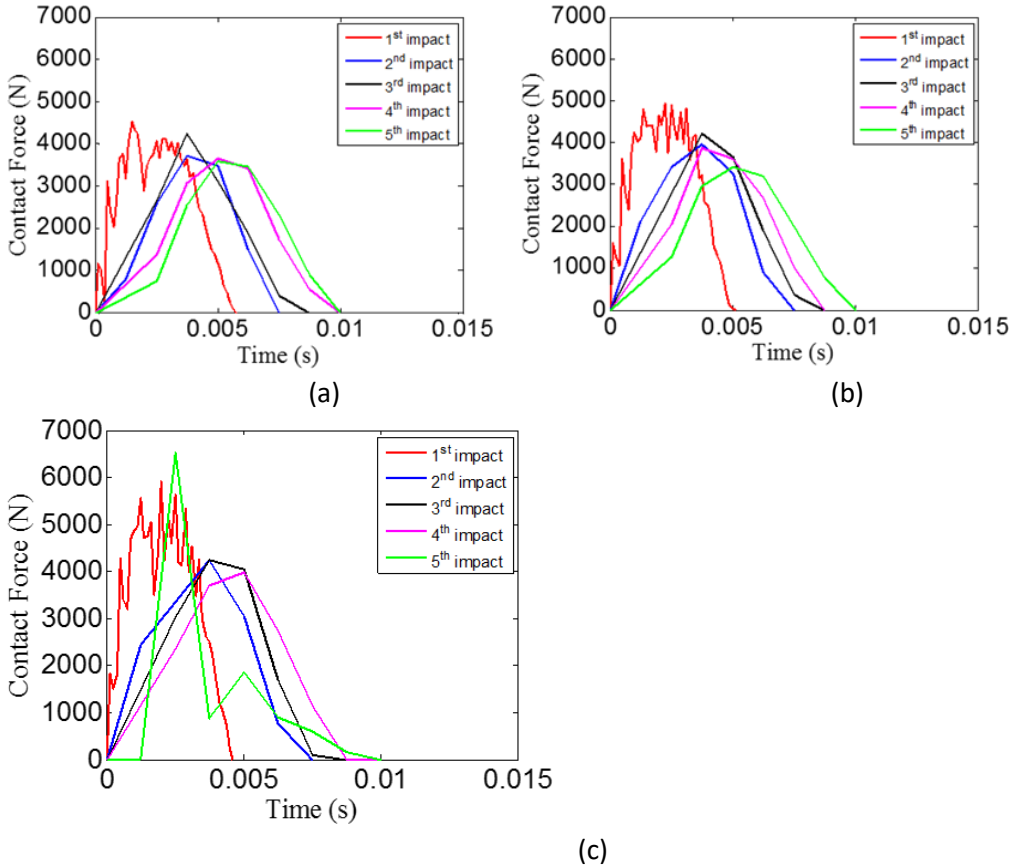

Stress Propagation

Figure 6 depicts the maximum principal stresses of the bottom face sheets for the various honeycomb core thicknesses under repeated impact energies of 13.5 J, 15.55 J, and 21.43 J. The stresses in the three beams were proportional to the impact energy. The stress in the bottom sheet of the 20 mm core beam behaved arbitrary at 21.43 J due to the severity of damage. On the contrary, the bottom skin of the beam with honeycomb core thickness of 25 mm developed the lowest stresses, especially at higher impact energy (21.43 J) because this thickness maintained the stiffness during the impact event by suppressing the contact forces and allowing only minimal forces to be transferred to the bottom face sheet. The 25 mm core beam stresses decreased as the impact number increased, and that is due to the compaction process which maintains the beam stiffness during the impact event (Sevkat et al. 2010). This indicates that the performance of this core thickness was relatively better. The 30 mm core beam developed stresses higher than those of the 25 mm core beam, especially in Figure 6(c). From Figure 6(c), it is apparent that the beam stresses increased with the impact number increase signifying that the stiffness of the beam has deteriorated allowing more contact forces to be transferred into the bottom face sheet. Generally, it can be said that both 25 mm and 30 mm core beams were comparable. Nevertheless, when the

impact energy increased, the beam with the 25 mm core exhibited a much better performance. In other words, the 25 mm core thickness enhanced the beam stiffness and did not expose the core cells to buckling. Like the 25 mm core thickness, the 20 mm core thickness did not expose the beam to buckling but it did not contribute much to the beam stiffness.

Finally, the 30 mm core thickness added stiffness to the beam but at the same time it exposed the beam to buckling reducing its damage resistance because each cell in the core acted as a slender column.

Figure 4. *BHSB Contact Force-Time Curves for Five Repeated Impacts at Energy Level 15.55 J for Aluminum Core Thicknesses of a) 20 mm, b) 25 mm, c) 30 mm*

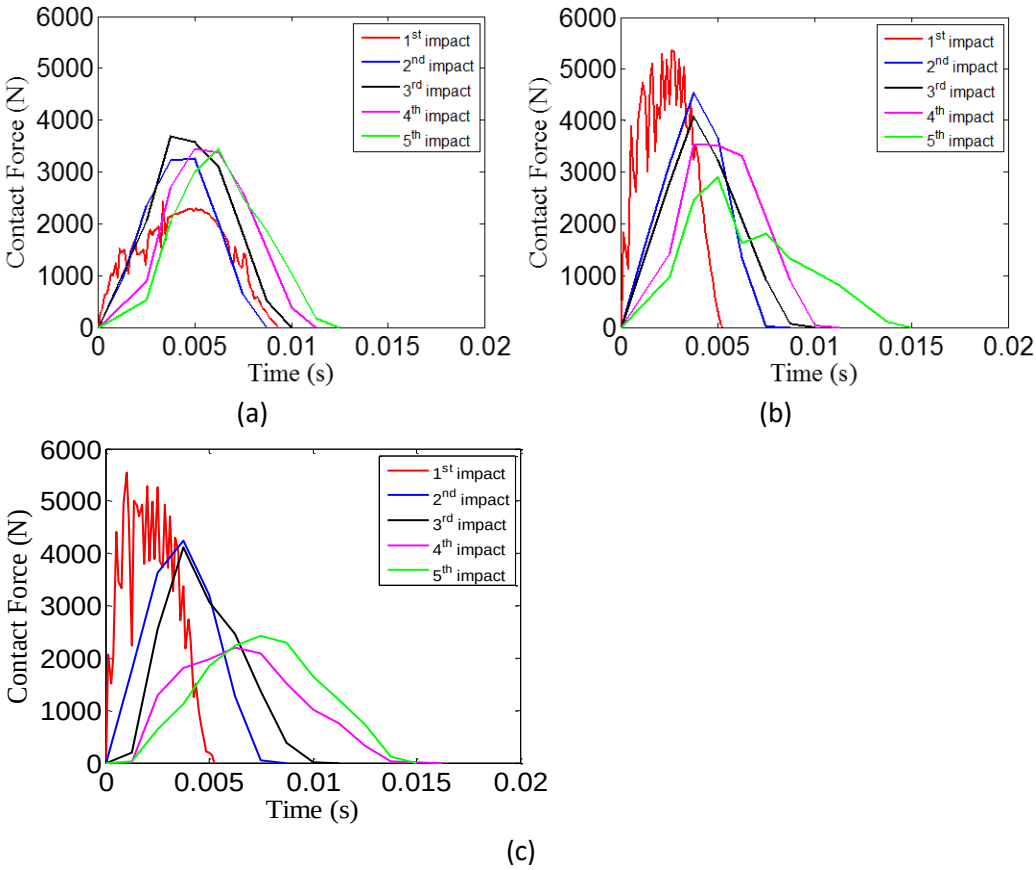

Figure 5. *BHSB Contact Force-Time Curves for Five Repeated Impacts at Energy Level 21.43 J for Aluminum Core Thicknesses of a) 20 mm, b) 25 mm, c) 30 mm*

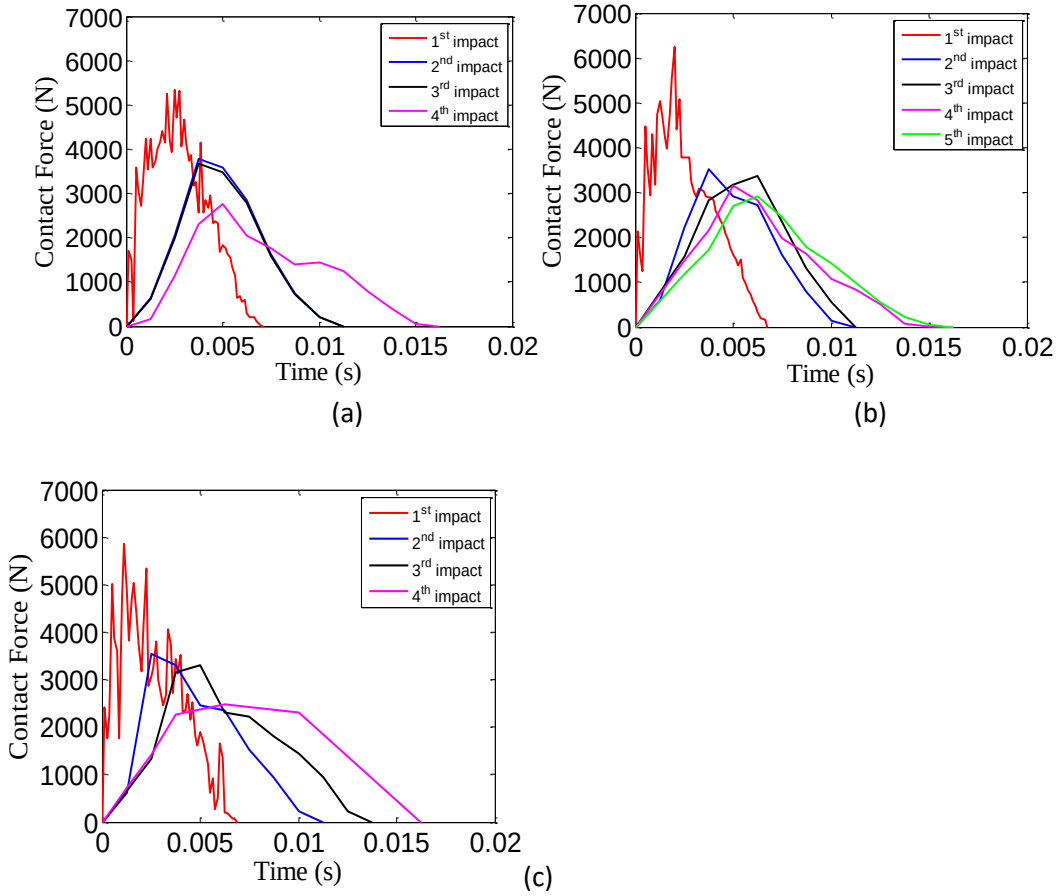

Failure Modes

For 13.5 J, Figure 7 shows that the three beams were capable of withstanding five impacts with some matrix cracking and fiber breakage (MCFB).

The three cores also experienced no sign of damage. The damage areas in the 20 mm, 25 mm, and 30 mm honeycomb core beams after the fifth hit were 356.83 mm^2, 306.09 mm^2, and 308.89 mm^2, respectively.

The damage morphologies for 15.55 J are shown in Figure 8. The 30 mm core beam developed the largest damage area in both top face sheet and core. Its core experienced some crushing at the impacted zone. The top face sheets of the 20 mm and 25 mm beams had damages in the forms of matrix cracking and fiber breakage.

Their cores also exhibited minor crushing under the point of impact. The total damage areas were 395.06 mm^2, 334.23 mm^2, and 413.84 mm^2 for the 20 mm, 25 mm, and 30 mm core beams, respectively.

Figure 9 shows the numerical failure modes the beams experienced at the end of the repeated impact event of 21.43 J. It is obvious that the 20 mm and 30 mm cores beams suffered severe damages in both upper face sheets and cores. The cores experienced buckling and shear at the impact zone. By investigating the 25 mm core beam (Figure 9 (b)), it is noticed that the beam underwent some upper

skin matrix cracking and fiber breakage (MCFB) while the core experienced only some buckling at the impact point. The calculated damage areas for the 20 mm, 25 mm, and 30 mm core beams at this energy level were 519.98 mm^2, 404.65 mm^2, and 468.5 mm^2, respectively.

Figure 6. *The Five Impacts Maximum Principal Stresses in the Bottom Face Sheets of the Beams with 20 mm, 25 mm, and 30 mm Honeycomb Cores Thicknesses at Energy Levels: a) 13.5 J, b) 15.55 J, c) 21.43 J*

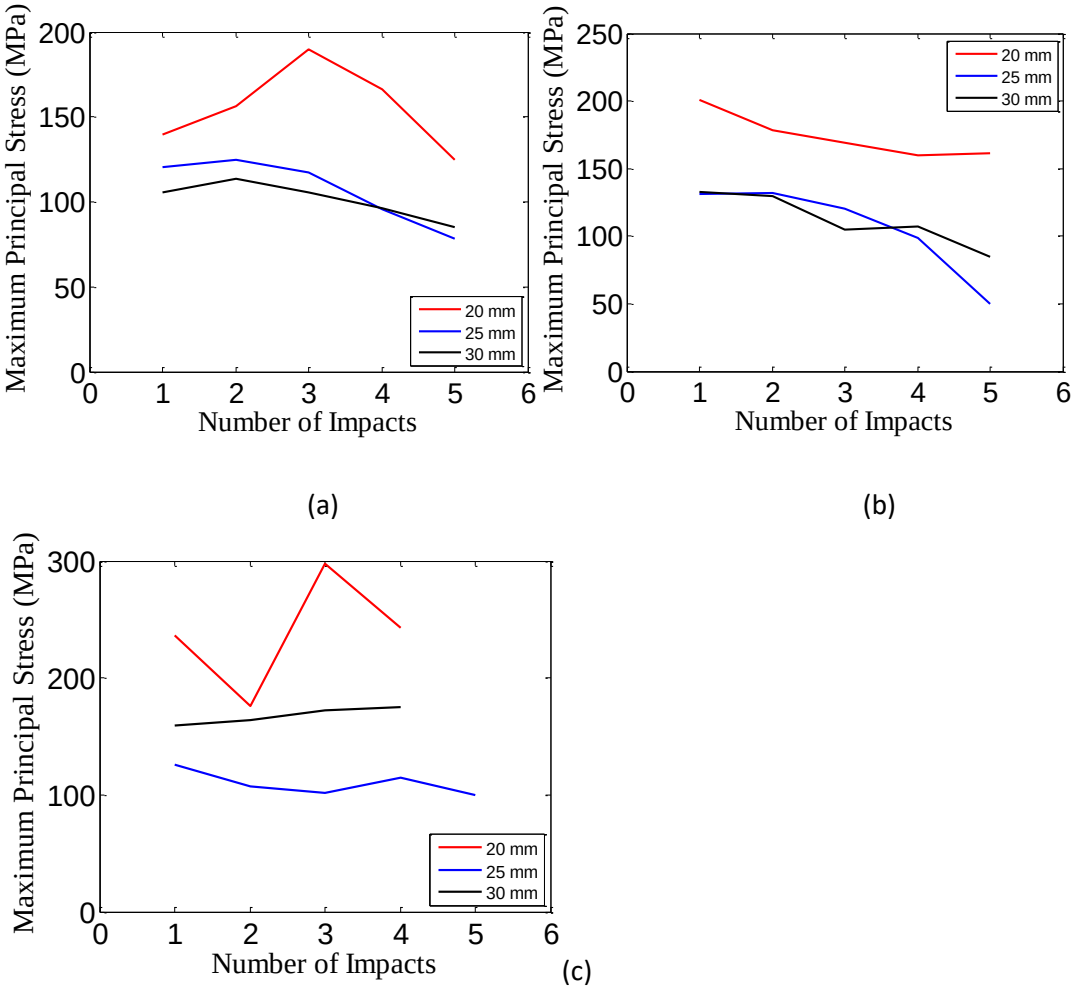

Figure 7. *Repeated Impact Damage of Honeycomb Core Thicknesses* a) *20 mm*, b) *25 mm*, c) *30 mm at 13.5 J*.

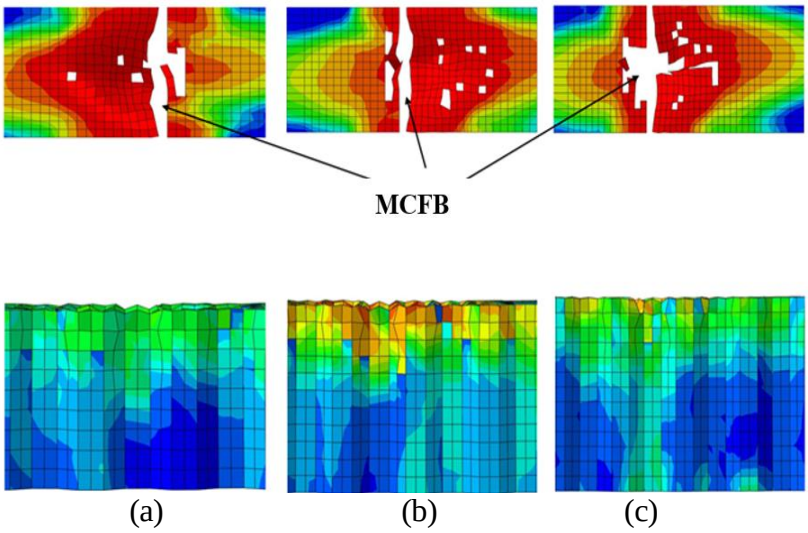

(a) (b) (c)

In each view, top row = skin top view; bottom row = core side view.

Figure 8. *Repeated Impact Damage of Honeycomb Core Thicknesses* a) *20 mm*, b) *25 mm*, c) *30 mm at 15.55 J*

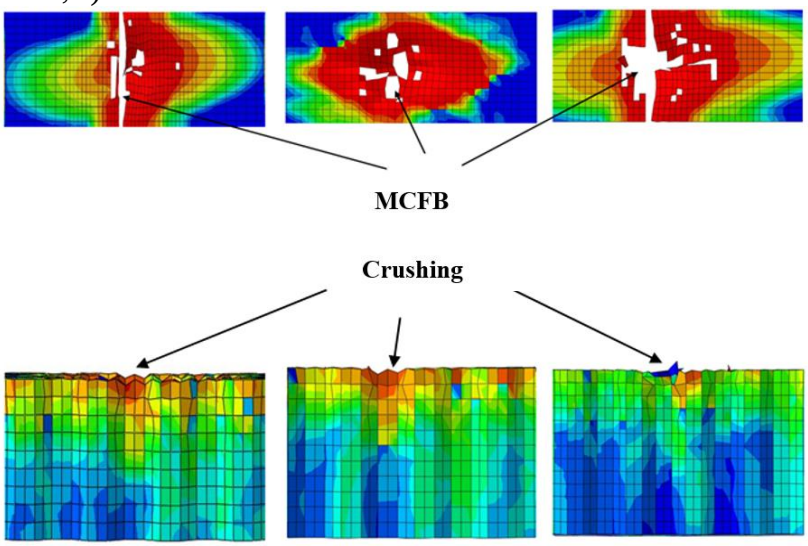

(a) (b) (c)

In each view, top row = skin top view; bottom row = core side view.

Figure 9. *Repeated Impact Damage of Honeycomb Core Thicknesses* a) *20 mm*, b) *25 mm*, c) *30 mm. at 21.43*

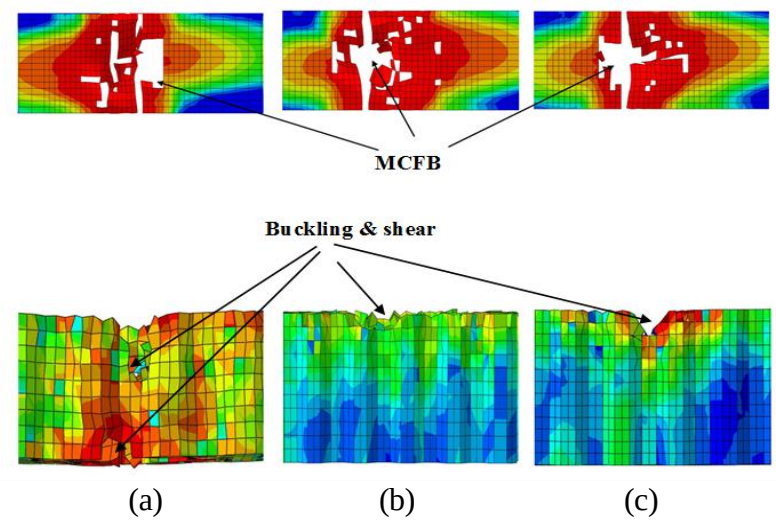

In each view, top row = skin top view; bottom row = core side view.

It can be concluded that BHSB with 25 mm core thickness had a better impact resistance. Increasing the thickness of the honeycomb core increased the height of its individual cells. As a result, the cells behaved like a column subjected to higher possibility of buckling phenomenon like the analogy of column, the higher the column goes it is easier for it to buckle because of its slenderness.

Figure 10 shows the behavior of damage area for BHSB with the 20 mm, 25 mm, and 30 mm honeycomb core thicknesses. The damage in the beams increased as the energy of impact increased. BHSB with 25 mm core thickness experienced the lowest damage for all impact energies indicating that this thickness improved the damage resistance of BHSB.

Figure 10. *Impact Damage Area vs. Impact Energy for BHSB with Different Honeycomb Core Thicknesses*

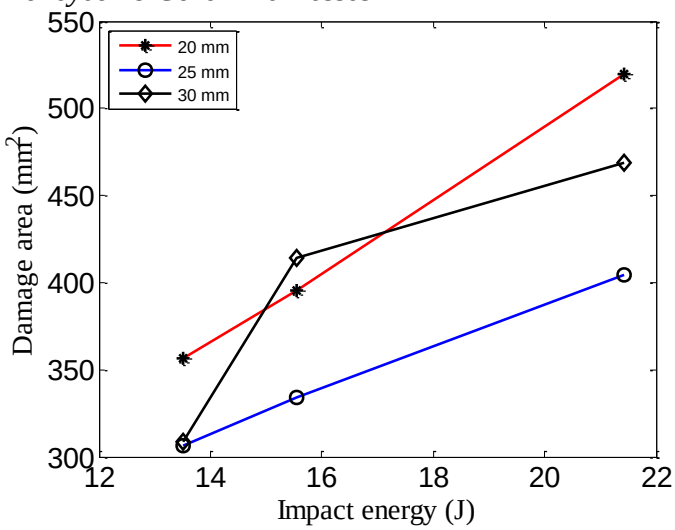

Absorbed Energy

Figure 11. *BHSB Five Impacts Energy Curves for the 20 mm Honeycomb Core Beam at a) 13.5 J, b)15.55J, c) 21.43 J*

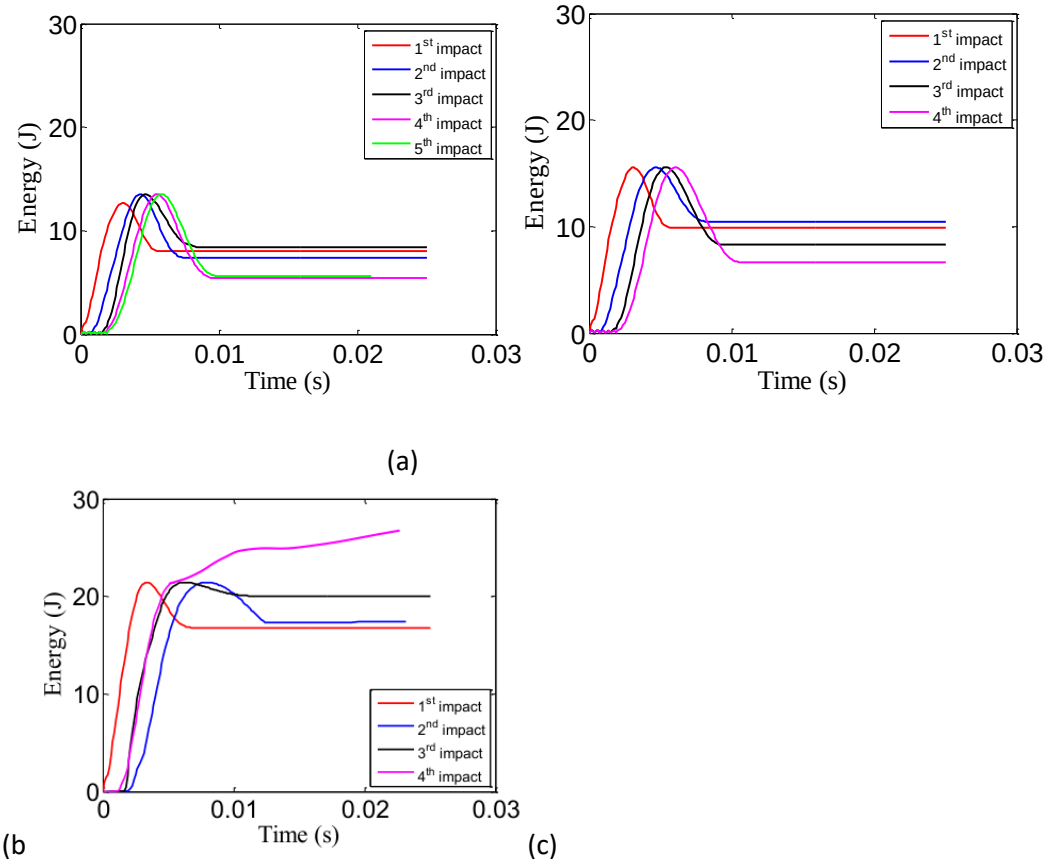

Figure 11 exhibits the energy curves for honeycomb core thickness of 20 mm for the three impact energies since there was a change in the behavior more than those of 25 mm and 30 mm core thicknesses. At energy levels 15.55 J and 21.43 J, the beams could only sustain loads up to the fourth impact, and the absorbed energy fluctuated from one hit to another. The energy curve of the fourth impact at energy level 21.43 kept increasing after reaching the peak as an indication that perforation has taken place in the beam. The fluctuation of the absorbed energy was due to the compaction process which made the beams sometimes tougher and enabled them to absorb more energy at the successive impacts.

Impact Resistance Efficiency Index

A preferred sandwich structure is the one that has the capability to absorb more energies, resist higher loads, and minimize the area of damage. Therefore, an impact resistance efficiency index (I_e) was introduced in this study to obtain a meaningful impact performance assessment. It was calculated using the following:

$$I_e = \frac{E_{abs} F_{max}}{A_d g m_b t \sigma_{max}} \quad (6)$$

where E_{abs} is the absorbed energy, F_{max} is the maximum contact force, g is the gravitational acceleration, σ_{max} is the maximum stress in the sandwich beam, A_d is the damage area, m_b is the mass of the sandwich beam, and t is the sandwich beam total thickness. Since the I_e is normalized by the thickness and mass of the sandwich beam, the comparison is mainly focused on the performance of the beams.

Table 2 introduces the impact resistance efficiency indices for BHSB at the fifth impact for the three honeycomb core thicknesses. BHSB with 25 mm honeycomb core thickness achieved the highest efficiency index, especially at higher impact energies. However, at the lowest impact energy (13.5 J), the efficiency index for BHSB with 30 mm honeycomb core thickness was the highest. The efficiency indices decreased as the impact energy increased. Therefore, the 25 mm honeycomb core thickness is considered the optimized parameter in the current case.

Table 2. *Impact Resistance Efficiency Indices of BHSB at the End of the Impact Event*

Core thickness (mm) / **Impact energy (J)**	**20**	**25**	**30**
13.5	32.57	75.99	81.11
15.55	24.38	45.40	34.42
21.43	18.66	42.55	29.31

Conclusions

The numerical investigations performed in this study proved that increasing the thickness of the aluminum honeycomb core to a certain level enhances the sandwich beam stiffness. Among the three studied thicknesses, the beam with 25 mm honeycomb core thickness was the only beam that could sustain five repeated impacts with the highest impact resistance efficiency index. In addition, the bottom face sheet of this beam developed the lowest stresses for the three impact energies. This indicates that this thickness had a relatively better performance during the impact event since it allowed minimal stress to be transferred to the bottom face sheet. It can be said that increasing the thickness of the honeycomb core increases the height of its cells. When the height of the cells increases, the cells behave like a column subjected to higher possibility of buckling phenomenon. Like the column analogy, the higher the column goes it is easier for it to buckle due to its slenderness. Thus, based on the findings, it is suggested that the aluminum honeycomb core thickness should be 65% of the sandwich beam overall thickness in order to achieve the best repeated low-velocity impact resistance.

References

ABAQUS (2013) *User's & theory manuals d release 6*. Providence, RI, USA.

Abo Sabah S, Kueh ABH, Al-Fasih MY (2017) Comparative low-velocity impact behavior of bio-inspired and conventional sandwich composite beams. *Composites Science and Technology* 149(Sep): 64–74.

Abo Sabah S, Kueh ABH, Al-Fasih MY (2018) Bio-inspired vs. conventional sandwich beams: a low-velocity repeated impact behavior exploration. *Construction and Building Materials* 169(Apr): 193–204.

Abo Sabah S, Kueh ABH, Bunnori NM (2019) Failure mode maps of bio-inspired sandwich beams under repeated low-velocity impact. *Composites Science and Technology* 182(Sep): 107785.

Aminanda Y, Castanié B, Barrau JJ, Thevenet P (2009) Experimental and numerical study of compression after impact of sandwich structures with metallic skins. *Composites Science and Technology* 69(1): 50–59.

Anderson T, Madenci E (2000) Experimental investigation of low-velocity impact characteristics of sandwich composites. *Composite Structures* 50(3): 239–247.

Burlayenko VN, Sadowski T (2012) A numerical study of the dynamic response of sandwich plates initially damaged by low-velocity impact. *Computational Materials Science* 52(1): 212–216.

Compston P, Styles M, Kalyanasundaram S (2006) Low energy impact damage modes in aluminum foam and polymer foam sandwich structures. *Journal of Sandwich Structures & Materials* 8(5): 365–379.

Dear JP, Lee H, Brown SA (2005) Impact damage processes in composite sheet and sandwich honeycomb materials. *International Journal of Impact Engineering* 32(1–4): 130–154.

Fatt MSH, Park KS (2001) Dynamic models for low-velocity impact damage of composite sandwich panels–Part A: deformation. *Composite Structures* 52(3–4): 335–351.

Hashin Z (1980) Failure criteria for unidirectional fiber composites. *Journal of Applied Mechanics* 47(Jun): 329–334.

Heimbs S, Cichosz J, Klaus M, Kilchert S, Johnson AF (2010) Sandwich structures with textile-reinforced composite foldcores under impact loads. *Composite structures* 92(6): 1485–1497.

Ivañez I, Sanchez-Saez S (2013) Numerical modelling of the low-velocity impact response of composite sandwich beams with honeycomb core. *Composite Structures* 106(Dec): 716–723.

Jiang D, Shu D (2005) Local displacement of core in two-layer sandwich composite structures subjected to low velocity impact. *Composite Structures* 71(1): 53–60.

Kılıçaslan C, Güden M, Odacı İK, Taşdemirci A (2013) The impact responses and the finite element modeling of layered trapezoidal corrugated aluminum core and aluminum sheet interlayer sandwich structures. *Materials & Design* 46(Apr): 121–133.

Kolopp A, Rivallant S, Bouvet C (2013) Experimental study of sandwich structures as armour against medium-velocity impacts. *International Journal of Impact Engineering* 61(Nov): 24–35.

McCormack TM, Miller R, Kesler O, Gibson LJ (2001) Failure of sandwich beams with metallic foam cores. *International Journal of Solids and Structures* 38(28–29): 4901–4920.

Mohr D, Doyoyo M (2003) A new method for the biaxial testing of cellular solids. *Experimental Mechanics* 43(2): 173–182.

Mohr D, Doyoyo M (2004) Deformation-induced folding systems in thin-walled monolithic hexagonal metallic honeycomb. *International Journal of Solids and Structures* 41(11–12): 3353–3377.

Lin C, Fatt MSH (2006) Perforation of composite plates and sandwich panels under quasi-static and projectile loading. *Journal of Composite Materials* 40(Oct): 1801–1840.

Santiuste C, Sánchez-Sáez S, Barbero E (2010) A comparison of progressive-failure criteria in the prediction of the dynamic bending failure of composite laminated beams. *Composite Structures* 92(10): 2406–2414.

Sevkat E, Liaw B, Delale F, Raju BB (2010) Effect of repeated impacts on the response of plain-woven hybrid composites. *Composites Part B: Engineering* 41(5): 403–413.

Williams HR, Trask RS, Bond IP (2008) Self-healing sandwich panels: restoration of compressive strength after impact. *Composites Science and Technology* 68(15–16): 3171–3177.

Xiong J, Vaziri A, Ma L, Papadopoulos J, Wu L (2012) Compression and impact testing of two-layer composite pyramidal-core sandwich panels. *Composite Structures* 94(2): 793–801.

Yang P, Shams SS, Slay A, Brokate B, Elhajjar R (2015) Evaluation of temperature effects on low velocity impact damage in composite sandwich panels with polymeric foam cores. *Composite Structures* 129(Oct): 213–223.

Zhang J, Ashby MF (1992) Buckling of honeycombs under in-plane biaxial stresses. *International Journal of Mechanical Sciences* 34(6): 491–509.

Zhou G, Hill M, Loughlan J, Hookham N (2006) Damage characteristics of composite honeycomb sandwich panels in bending under quasi-static loading. *Journal of Sandwich Structures & Materials* 8(1): 55–90.

Zhou J, Hassan MZ, Guan Z, Cantwell WJ (2012) The low velocity impact response of foam-based sandwich panels. *Composites Science and Technology* 72(14): 1781–1790.

Zhu S, Chai GB (2013) Damage and failure mode maps of composite sandwich panel subjected to quasi-static indentation and low velocity impact. *Composite Structures* 101(Jul): 204–214.

Athens Journal of Technology and Engineering - Volume 7, Issue 4, December 2020 – Pages 257-276

Evaluation of Fire Resistance Concerning Bond Failure for Injection Anchors with Variable Embedment Depths

By Marie Reichert[*] & Catherina Thiele[±]

In the last decades injection anchors became a common fastening system. With the frequent use, the requirements in load capacity and the fields of application expands. Therefore, there is also the demand for assessments in case of fire. At the same time the knowledge about the load-bearing behaviour under fire exposure is small. In this scientific work the impact of high temperature loads on anchors is determined by static calculations and thermal-transient simulations. Furthermore, the load capacity and load-bearing behaviour of bonded anchors concerning bond failure is investigated experimentally for mortar temperatures between 20°C and 400°C. Influencing factors on the bond stress-temperature behaviour of injection mortars like anchor diameter, moisture of concrete, internal and external forces and the type of test execution are examined. The work identifies bond failure and steel failure as the main failure types for injection anchors in case of fire. As a result of the presented research a calculation method for the bond failure on the basis of temperature profiles and the behaviour of the load capacity of bond materials under high temperatures is presented. The assumed temperature profile and the determination method for the BST-Curves were found as the main influencing factors on the fire resistance. In total the research work shows and evaluates the complexity of fire events and the numerous influencing factors on injection anchors. Fire resistances or rather methods for the calculation of fire resistances on the safe side can be given. Nevertheless, the confirmation with experimental tests in real fire tests cannot be completely replaced.

Keywords: *bonded anchors, fire resistance, assessment, experimental investigation, transient thermal simulation*

Introduction

An injection anchor is a fastening system for use in concrete or masonry to ensure the attachment of construction components. It consists of an anchor rod (mostly threaded rod) and the injection mortar. Figure 1 shows the setting procedure beginning with drilling and cleaning of the hole, injection of the mortar and setting of the anchor. The assessment of injection anchors is regulated by European Assessment Documents (EAD) and/or Technical Reports (TR) which are published by the European Organization for Technical Approval (EOTA). The design of anchorages is implemented in part four of Eurocode 2 (DIN EN 1992-4 2019). In case of this study only injection anchors for use in concrete are considered.

[*]Research Associate, Technical University of Kaiserslautern, Germany.
[±]Academic Councillor, Technical University of Kaiserslautern, Germany.

Figure 1. *Setting Procedure for Injection Anchors*

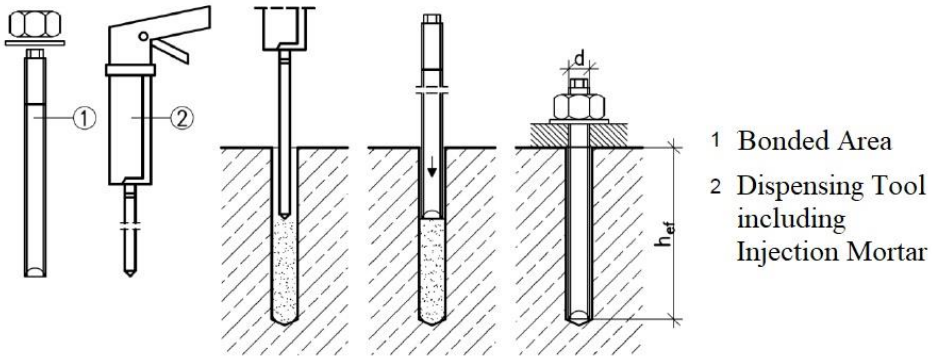

Source: EAD 330499-00-0601 2017.

The evaluation and design of injection anchors for use in constructions with requirements concerning the fire resistance are missing so far. The Technical Report which covers the evaluation of metal anchors in case of fire is TR020 (2004). The technical report defines a simplified design method and an experimental design method. The simplified design method gives design equations based on the load capacity for normal ambient temperature, which are on the safe side. For the experimental design method, the execution of fire tests where the **u**niform **t**ime **t**emperature **c**urve (UTTC) according to DIN EN 1991-1-2 (2013) is applied, is required. Because of the lack of knowledge concerning the load-bearing behavior of injection anchors this type of fastenings is currently excluded of the regulation.

In case of fire generally the same failure types as at normal ambient temperature could possibly occur. The types of failure are concrete cone failure, splitting and concrete edge failure, bond failure and steel failure. Because of the significant decrease of steel strength for temperatures higher than 500 °C, steel failure is one of the main failure modes defining the fire resistance for metal anchors. Besides that, a significant temperature dependence for injection mortars is already known. The existing assessments for post-installed rebars shows that the bond resistance of injection mortars could drop to almost zero for temperatures above 200 °C to 300 °C. The exact load bearing behavior concerning bond resistance of injection anchors is at current state of the art mainly unknown.

Literature Review

In the last decade just a few researches have dealt with the fire resistance of bonded anchors. Fuchs and Silva (2012) and Mallèe et al. (2012) published papers about the topic and the lack in regulation. They specifically pointed out that in a lot of cases steel failure is decisive and that fabricators using the experimental based design method preferably because of its higher loads in comparison to the simplified design method.

In parallel some researchers treated the evaluation and design of post-installed rebar connections in case of fire, for which in many times the same injection

mortars were used for bonded anchors. For example, Pinoteau et al. (2011) investigated the influence of heating type and heating rate on the fire test for determination of bond stress versus temperature curves for a specific product according to EAD 330087-00-0601 (2015). He could find an influence on the evaporation effects which did not lead to significantly different test results. In the last years several additional research work was published which deals with post-installed rebars or bonded anchors in case of fire, testing methods and the influencing factors, e.g., Lahouar et al. (2018) and Al-Mansouri et al. (2020).

Subsequently the idea of a simplified method for the calculation of the fire resistance concerning bond failure on the basis of the **b**ond-**s**tress-**t**emperature-curve (BST-Curve) rose. The research idea and first results were published by Patil and Thiele (2015), Lakhani and Hofmann (2017) as well as Reichert and Thiele (2017).

Methodology

First a clarification of the influences on injection anchors in case of fire should give a basis for calculations and experimental tests. Two main influences were outlined, the temperature itself and the stress distribution in concrete slabs which represents the anchorage ground. The temperature distribution along the anchorage depth was determined by transient thermal simulations with the finite element tool ANSYS. With the help of temperature distributions caused by uniform temperature-time curves (UTTCs) in concrete slabs and the thermal and mechanical properties of concrete under increased temperatures the stress distribution in concrete slabs could be calculated. A sequential calculation by using an Excel sheet was used.

Furthermore, temperature tests for the determination of BST-Curves were conducted which could replace real fire tests as far as possible. Two test setups were used. Firstly, temperature tests using a heating ring (HR-Test) according to EAD 330087-00-0601 (2015) were executed. Secondly, a new designed test setup using a heating device (cartridge) (HC-Test) in the inner of the anchor rod and with a shortened embedment depth was established. Several influencing factors like type of test execution, duration of temperature load, geometry and type of anchor rods, compression stresses in test members and moisture were examined.

Impact on Injection Anchors in Case of Fire

The main impact on anchors in case of fire is the extreme temperature load, with temperatures above 1000°C. As a consequence, restrained forces in the concrete occur and possibly also influence the sustainability of injection anchors under fire exposure. As a first step in the investigation of the load bearing capacity of injection anchors the impacts on them are described.

For the determination of temperature profiles along the embedment depth for an arbitrary anchor a transient thermal simulation was used. An anchor with

specified anchor diameter and embedment depth, as well as a concrete cylinder, were modeled. The data output was taken at the interface between anchor and concrete, see Figure 2 (right). The mortar layer was neglected in the simulations. For confirmation of the simulation results temperature measurements on anchors with the same length and diameter in a real fire test were carried out. The temperatures were measured at three points with thermocouples. The thermocouples were positioned with a distance of 10 mm from the surface, at half of the embedment depth and at a distance of 10 mm from the end of the embedment depth. For the example shown in Figure 2 and Figure 3 with an embedment depth of 80 mm, it leads to a measurement at 10 mm, 40 mm and 70 mm distance from the heated surface. In both simulation and real fire test the UTTC was applied. The comparison between the measured and simulated temperatures shown in Figure 2 and Figure 3 confirm each other. That means the simulation of temperatures along the embedment depth with transient thermal simulations is possible with a good comparison to the test results. Further investigations with simulated and measured temperatures showed the following influencing factors on the temperature distribution of anchors:

- **Anchor diameter**: Bigger anchor diameters lead to higher temperatures at the same point of embedment depth (Thiele et al. 2017).
- **Anchorage depth**: Anchors with bigger embedment depth can emit more heat to the concrete. A bigger embedment depth therefore leads to smaller temperatures at the same point of embedment depth (Thiele et al. 2017).
- **Moisture**: With rising temperatures the combined water in concrete evaporates. This phenomenon leads to a cooling effect. Location, time and amount of released water are unknown and it is not possible to replicate this effect with simulations (Reichert 2020).
- **Fixture**: Presence and size of a fixture has a high influence on the measured temperatures in fire tests. This shielding effect can just be simulated in parts, because it is also influenced by moisture and air streams (Reichert 2020).

Figure 2. *Comparison of the Measured and Simulated Temperatures over Time (left), Model of the Anchor (right)*

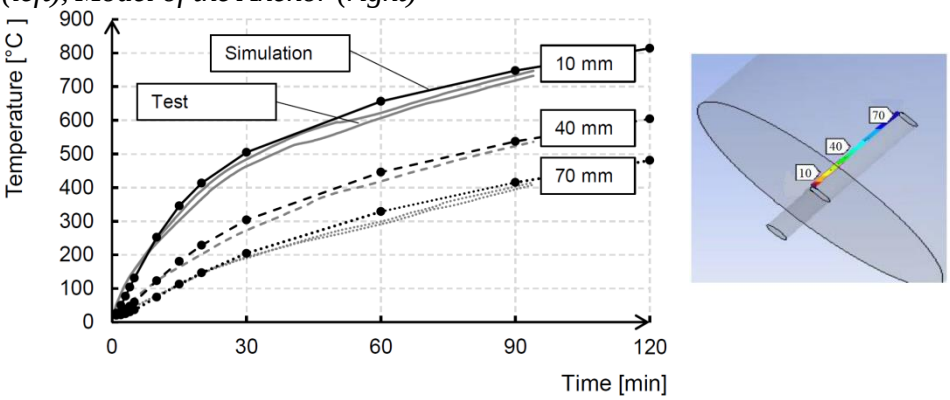

Figure 3. *Comparison of Measured and Simulated Temperatures over Embedment Depth*

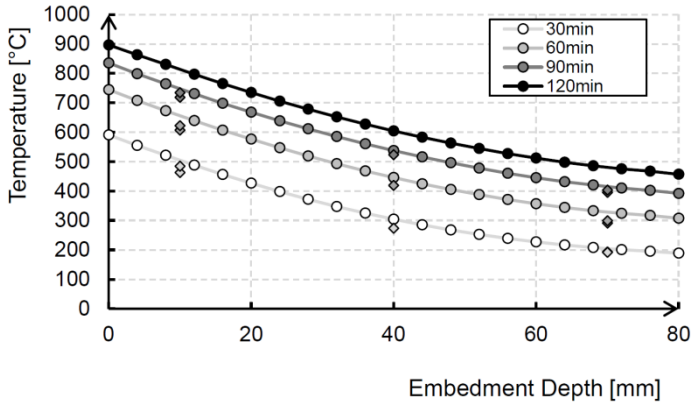

Besides temperature profiles for anchors the transient thermal simulation allows the determination of temperature distributions in the concrete. Due to the relatively small thermal conductivity of concrete (1.3-2.0 W/mK at 20 °C) and the very high temperatures during a case of fire (>1000 °C) there is a high difference in temperature between the fire side and cold side results. This leads to a bending of concrete slabs when they are exposed to fire from one side only. Figure 4 (left) shows the free thermal strain ε_{th} of concrete concerning the actual temperature in a concrete slab (dotted line) and the total strain ε_{res} of the slab regarding Bernoulli hypothesis (see Equation (1) line 1). In the following, the difference between these strains is called the stress-generating strains $\varepsilon_{\sigma,}$ see Equation (1) line 2 and 3, see Hosser and Richter (2013). They depend on time in the UTTC, thickness of the slab and percentage of reinforcement. A typical qualitative distribution is shown in

where: ε_{res} Total strain
ε_0 Diameter of anchorage
k Curvature
z Height of the section
ε_σ Stress-generated strain
ε_{th} Free thermal strain

Figure 4 (right). It shows positive strains on the edge areas and negative strains in the middle of the slab.

$$\begin{aligned} \varepsilon_{res} &= \varepsilon_0 + k \cdot z \\ \varepsilon_{res} &= \varepsilon_\sigma + \varepsilon_{th} \\ \varepsilon_\sigma &= \varepsilon_{res} - \varepsilon_{th} = \varepsilon_0 + k \cdot z - \varepsilon_{th} \end{aligned} \tag{1}$$

where: ε_{res} Total strain
ε_0 Diameter of anchorage
k Curvature
z Height of the section

ε_σ Stress-generated strain
ε_{th} Free thermal strain

Figure 4. *Total and Free Thermal Strains in Concrete Slab (left), Stress Generating Strains in Concrete Slab (right)*

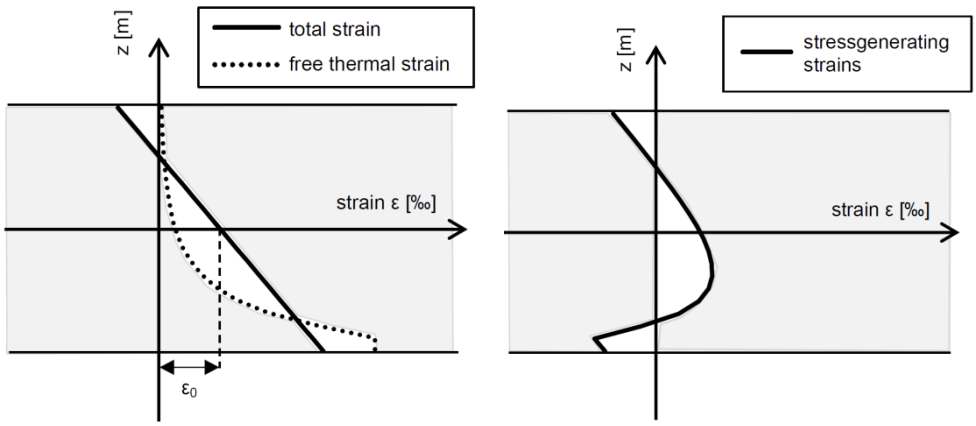

Figure 5. *Reduction Factor of Concrete Strength over Strain (left), Obtained Stresses in Concrete Slab (right)*

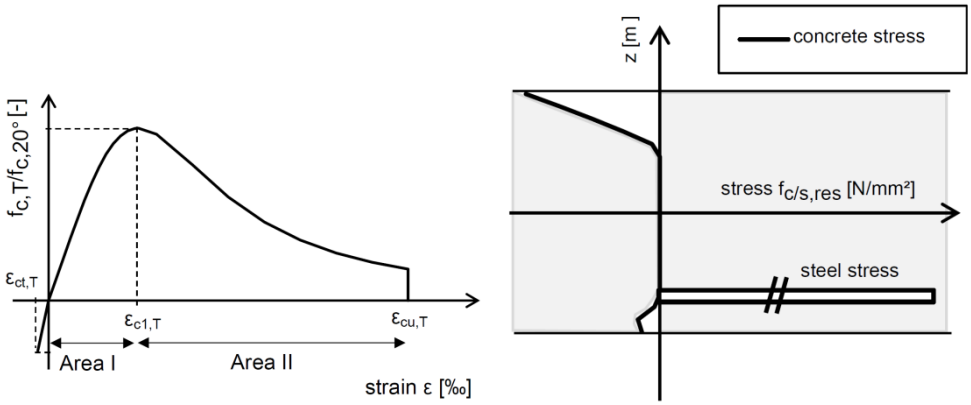

In consideration of the load-bearing behavior of concrete at a particular temperature (Figure 5, left) the calculation of the concrete stresses in the cross section of the concrete slab is possible. The procedure is also described by Reick (2001). Figure 5 (right) shows a typical distribution, which indicates high concrete compression stresses on the "cold side" of the slab, small compression stresses (due to the very high temperatures) on the fire exposed side of the concrete slab and a cracked area in the middle of the cross section. The influence of the compression stresses and the inner cracks on the fire resistance of injection anchors is unknown and requires further research.

The presented calculation of the restrained forces caused by the temperature distribution in concrete slabs under fire exposure neglects the influence of anchors on the temperature distribution. Due to the high thermal conductivity of steel (54 W/mK at 20 °C) the temperature of the anchor itself and the surrounding concrete is higher than the temperature of the remaining concrete cross section. It could be followed that in the surrounding area of an anchor due to the higher

temperatures bigger thermal strains occur and lead to a reduction of tension stresses, as well as an increase of compression stresses.

Experimental Investigation of Bond Failure

As described in Introduction, the fire resistance of post-installed rebar connections can be evaluated according to EAD 330087-00-0601 (2015). The test setup used to determine the BST-Curve for an injection mortar is shown in Figure 6. The test setup consists of a rebar installed in a steel coated concrete member according to the fabricator's manual. The shell surface of the concrete member can be heated by a heating device. In the test executed in the framework of this research an electrical heating ring with a maximum temperature of 600 °C was used. The heating ring leads to a temperature distribution similar to the reality, which indicates that the temperature increase is initialized through the concrete and a constant temperature distribution along the embedment depth follows. In the HR-Tests according to EAD 330087-00-0601 (2015) a transient test execution is scheduled, that indicates that the anchor is loaded by a constant load while the concrete member is heated, see Figure 8 (left). The test ends by failure of the anchor. The mortar temperature at the time of failure (measured with two thermocouples at position TE1 and TE2) can be related to the bond stress with which the anchor was loaded. With a minimum number of 20 tests the BST-Curve can be defined.

Figure 6. *HR-Test Setup according to EAD 330087-00-0601 2015*

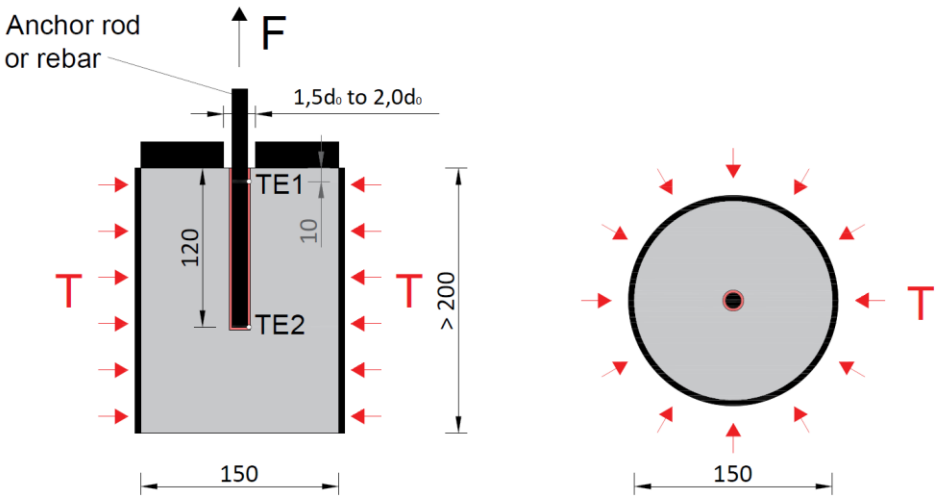

Besides that a new test setup was developed to study the load bearing behavior of injection anchors under increased temperatures, see Figure 7. The test setup enables a direct heating of the anchor rod due to a heating cartridge inside the concrete. This follows the curcumstances in reality where the temperature increase in the mortar is also initialzed through the anchor rod. Furthermore the new test

setup allows a measurement of the anchor displacement s_{ub} on the unloaded side of the anchor, which shows the slippage of the anchor.

Figure 7. *HP-Test Setup*

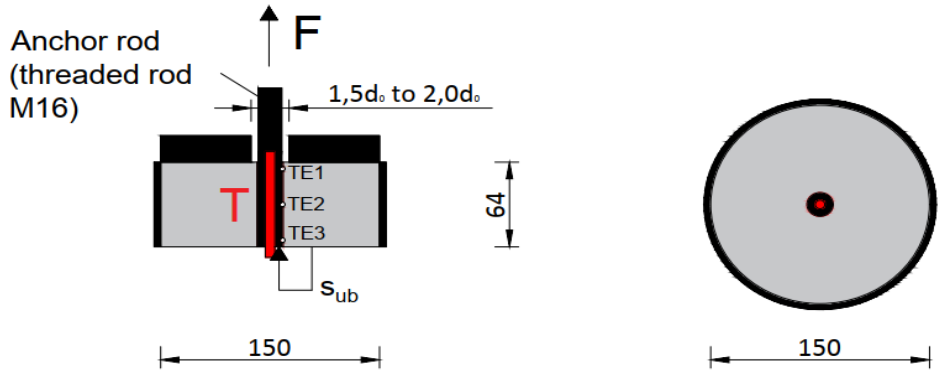

Due to the direct heating different types of test procedures are possible. Beside transient tests, like in the HR-test setup, also pullout tests at constant temperature (see Figure 8 right) or creep tests at constent load and temperature can be executed.

Figure 8. *Test Procedure for Pull-Out Tests (left) and Transient Tests (right)*

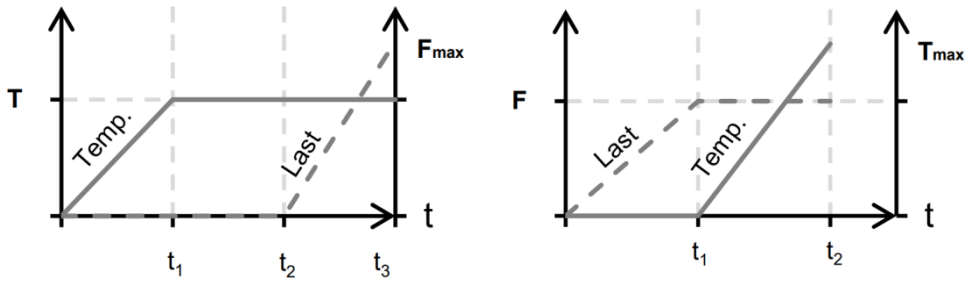

Influence of Test Setup

In Figure 9 test results from the transient tests and pullout tests executed in both types of test setup with two mortar types are shown. It can be seen that the type of test setup can have a significant influence on the BST-Curves. In the HP-Test setup higher failure temperatures occurred for same loading than in HR-Tests.

Figure 8. *Comparison of BST-Curves Determined with Different Types of Test Setup on Two Mortar Systems, left: Polymer Resin, right: Epoxy Resin*

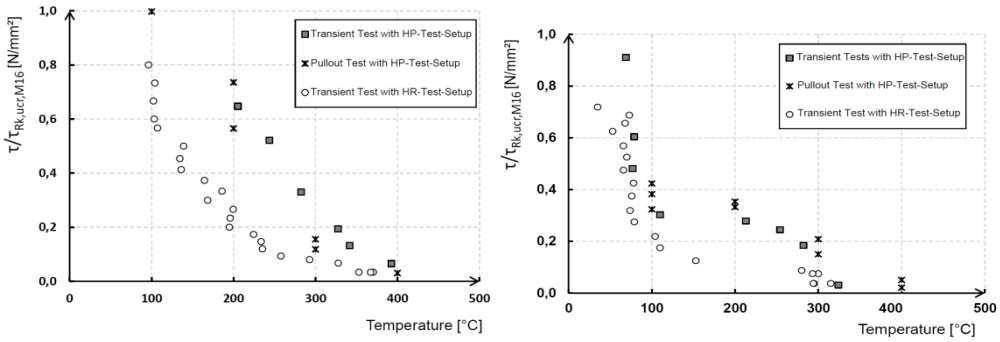

In the authors' opinion one main reason for the differences is the restrained forces caused by the temperature distribution in the concrete member. Due to the direct heating on the anchor the mortar temperature can be increased fast while the temperature in the surrounding concrete increases slowly. This leads to a temperature profil with high temperatures in the inner part of the concrete member (up to 400°C) and low temperatures at the shell surface (ambient temperature, about 20°C) and prevents deformations. According to the considerations made above compression stresses inside the concrete member occur. This could have a positive effect on the load capacity of the injection anchor and could be the reason for the differences in the obtained BST-Curves in the HP-Test and HR-Test. Besides this explanation the heating rate, the heating direction including insulating properties of the mortar and moisture streams as well as gemoetry and size of the anchor could be a reason for the differences in the obtained BST-Curve.

Influence of Duration of the Temperature Load

The HP-Test setup allows a direct and instant temperature load on the anchor, as well as the option of holding the temperature at a specified level. On the two types of resin introduced before the influence of a duration of the temperature load was investigated. Therefore, pullout tests in the HP-Test setup were conducted at 200°C. In the executed tests the times after reaching the specified temperature of 200°C t_1 and beginning of the pullout test t_2 (see Figure 8, left) differ between 0 min and 120 min. As the reference value the average value of the test results for t_2-t_1 equal to 0 min was used. The relationship between the bond stresses and the temperature duration is shown in Figure 10.

Figure 9. *Relation of Bond Stress and the Bond Stress in Reference Test over Temperature Duration, left: Polymer Resin, right: Epoxy Resin*

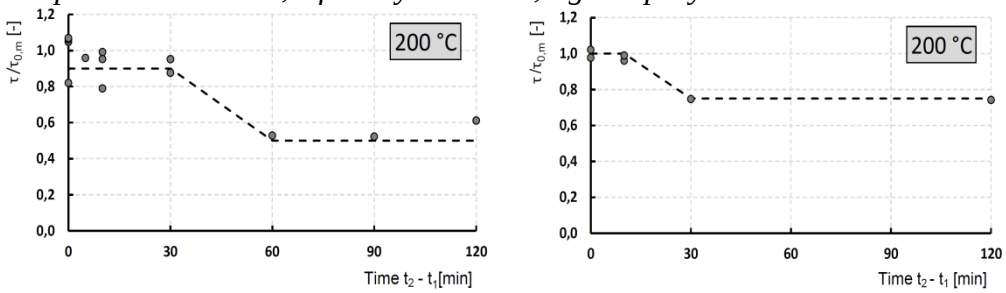

It can be seen that the obtained bond stress in the presented pullout tests decreases with the increase of temperature duration t_2-t_1. For the polymer resin the obtained bond stresses are constant up to a duration of 30 min and drops subsequently at 50% of the bond stress in the reference tests. In the tests with epoxy resin a drop to 75% can already be seen after a 30 min duration of temperature before the start of test execution.

As a reason for the phenomenon shown in Figure 10, two main explanations can be given. Firstly, during the heating on the anchor, the temperature distribution in the concrete member changes. With an increase of temperature duration, the temperatures in the concrete member are getting uniform. This reduces the restrained forces caused by the temperature profile. Secondly, time dependent chemical effects in the mortar could change the load bearing behavior with the increase of time.

Influence of Geometry of Anchor Rod

The HR-Test discribed in EAD 330087-00-0601 (2015) was developed to determine the fire resistance of post-installed rebar connections. Therefore, reinforcement bars were used in the test setup. If the BST-Curves determined with this test method are to be used and transferred onto the injection anchors the influencing factor of geometry and diameter of the anchor rod has to be excluded.

To investigate the influence of anchor type, which means the difference in using a threaded rod and reinforcement bars, HR-Tests with different anchor types were executed. Two different types of rebars with differences in the related rib area f_R were used. All values are normalized by $(f_R/0.08)^{0.4}$. Also a threaded rod and a prestressing steel by the company GEWI were used. All anchor rods had an anchor diameter of 12 mm. The obtained BST-Curves are shown in Figure 11.

Figure 10. *Comparison of the BST-Curves Obtained on Different Types of Anchor Rods in the HR-Tests*

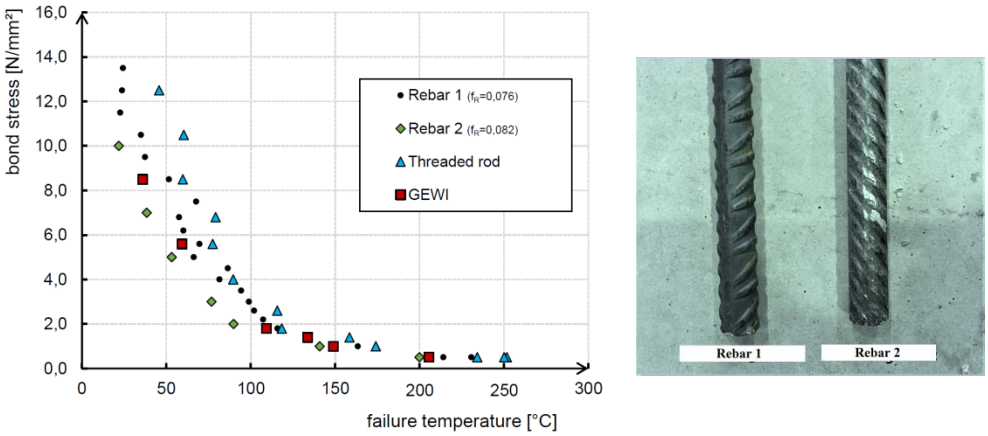

It can be seen that the type of anchor rod does not influence the main bond stress – temperature behaviour. For temperatures near to normal ambient temperatures the transient tests with threaded rods lasted longer with the same bond stress while with rebar type 2 lower failure temperatures can be detected. With the increase of temperature the BST-Curves converge. For temperatures above 100 °C no difference in the BST-Curves can be seen.

In the frame work of Thiele et al. (2017) and Reichert (2020) further investigations on the influence of anchor type and anchor diameter were done. The result is that the influences which can be determined at ambient temperature decrease with the rise in temperature. In the authors' opinion this influence can therefore be neglected for the definition of the fire resistance.

Influence of Compression Stresses on Concrete Members

Due to the findings concerning the restrained forces caused by temperature profiles the hypothesis assumes that compressive loading could have a positive influence on the sustainability of injection anchors. To investigate this assumption, pull-out tests in the HP-Test setup were conducted under compression stress on the concrete member. Therefore, cubic concrete members instead of cylinders were used. A biaxial compression stress of 5%, 40% and 70% was applied on the shell surfaces whiles the pull-out test was executed. Figure 12 shows the test results at a temperature of 200°C. Again, in the left figure a polymer resin and in the right figure an epoxy resin were used.

Figure 11. *Maximum Bond Stress in Pull-Out Tests with Biaxial Compression Stress, left: Polymer Resin, right: Epoxy Resin*

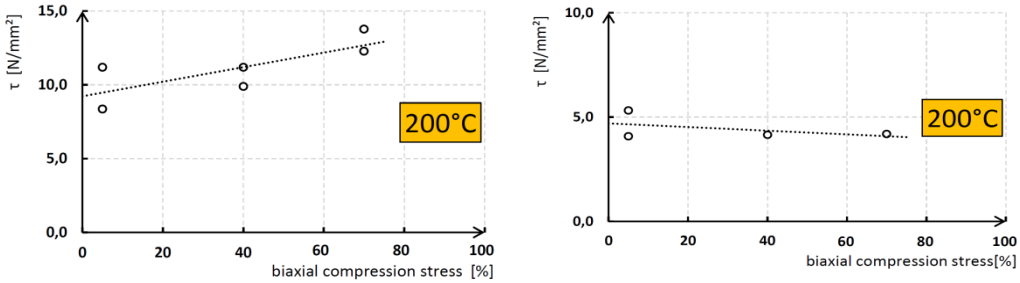

The results are showing a different behaviour for the two mortar types tested. While the tests conducted with the polymer resin show an increase of about 20% in the compressive strength, while from 5% to 70% of the tests conducted with the epoxy resin show no influence. In the frame work of the research by Reichert (2020) this type of test was executed also at 20°C, 100°C, 300°C and 400°C. The behaviour detected at 200°C can be confirmed from the further tests. This shows that that the influence of compression stresses depends on the mortar type used in the tests.

Influence of Moisture

The investigation of the impacts on anchors in case of fire showed that the moisture in concrete influences the temperature profiles in a relevant way. When the differences in the test results between the test execution in the HR-Test setup and HP-Test setup were found, the question rises up that moisture could be an influencing factor also in this case. The reason for this hypothesis is that in the HR-Tests water evaporizations can be observated during the tests, which indicates the existance of moisture streams. Evaporated water is moving from hot to cold concrete areas until it reaches the concrete surface and is condensing there. The assumed moisture stream flows first in radial direction to the core of the cylinder and subsequently longitudinal through the mortar layer, see Figure 13 the left part. For investigation of the influence of moisture streams through the mortar layer a test series with injection anchors installed in steel members instead of the use of concrete were conducted, see Figure 13. To recreate a bond surface, an internal thread was generated. The anchors were set in the internal thread, so that the contact surfaces with interal thread-mortar and mortar-external thread occur. The tests were carried out as the transient tests at the same heating rate.

Figure 12. *Left: Assumption of Moisture Stream in the HR-Test, Right: Rebar Installed in Steel Test Member*

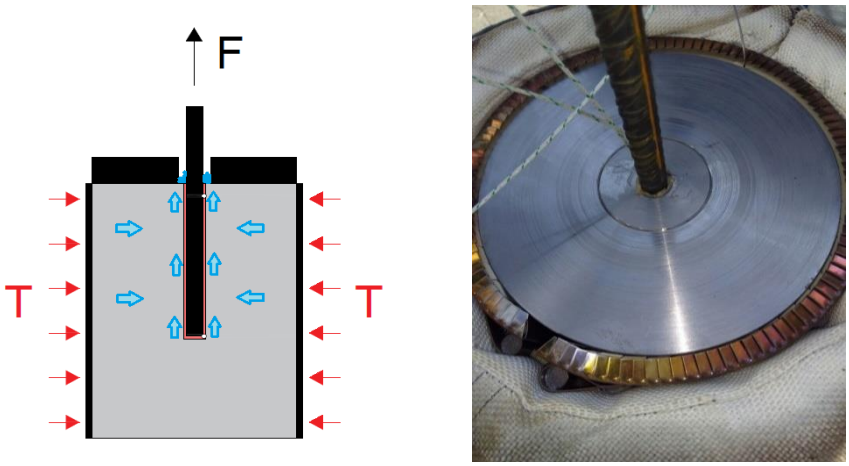

Figure 14 shows the test results compared to the test results conducted in the HP-Test-Setup and HR-Test-Setup with the polymer resin. It can be seen that the transient tests executed on the steel members to exclude the influence of concrete moisture show the inhanced test results compared to the tests executed on concrete members in the HR-Test. Nevertheless the comparison to the HP-Test shows lower failure temperatures for the same load level. Despite the small number of tests, the test resutls indicate that the moisture of the concrete has a negative influence on the test results in the HR-Tests.

Figure 13. *Test Results in Steel Test Members Compared to Transient Tests with the HP-Test-Setup and HR-Test-Setup*

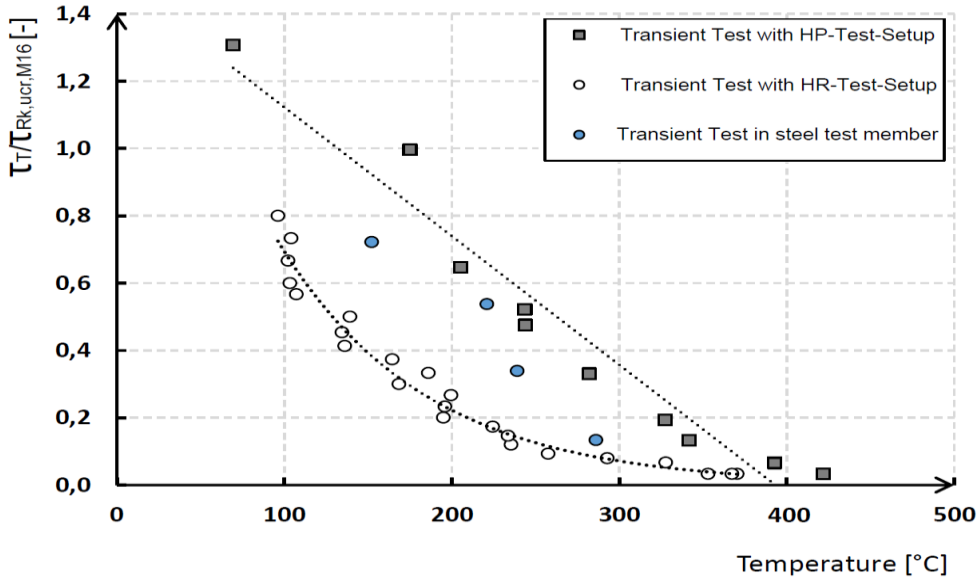

In addition to these tests by Reichert (2020) also the transient tests in the HR-test setup with different moisture contents were executed and compared. Therefore, different forms of storage were used. Tests in dried concrete at 80°C and 110°C as well as concrete members with storage in water bath or at normal ambient

temperature were done. The different types of storage lead the moisture contents to vary between 0.3% and 3.0%. The results showed no significant influence of moisture content on the BST-Curve.

Summary of Influences on the BST-Curve

This paper resulted in the framework of the research described in by Reichert (2020). The work includes several more tests to describe the influences on the BST-Curve for injection anchors. Table 1 summarizes all influencing factors and findings.

Table 1. *Influences on the BSC-Curve*

Influence	**Test setup**	**Execution**	**Result**
Test Setup	HP/HR	Transient	Type of test setup can have significant influence on the BST-Curve Up to 100% higher bond stress with the same failure time *Statement: Reason can be due to the restrained forces caused by temperature distribution or the effects caused by moisture stream.*
Duration of temperature load	HP	Pull-out	The increase of load duration leads to the decrease of bond stress by up to 50%. *Statement: increase of duration leads to decrease of restrained forces in the concrete member or time dependent chemical effects in the mortar.*
Geometry of anchor rod	HR	Transient	Type of anchor rod (rebar/threaded rod or diameter) can have an influence on the BSC-Curves but the overall behavior stays the same. *Statement: Influence of anchor type can be classified as small. It occurs mostly for temperatures < 100°C and is product-specific.*
Compression stress on concrete member	HP	Pull-out	The increase of the compressive stress on concrete member leads to an increase of bond stress by up to 20%. *Statement: The effect is product specific and differs with temperature.*
Moisture	HR	Transient	Tests with the concrete moisture between 0.3 to 3.0% show no significant influence. Tests on the steel member (0% moisture) lead to higher BSC-Curves up to the level of the HP-Test *Statement: Concrete members always have a residual moisture (also dried), and the moisture streams could have an influence on the BST-Curve*

Calculation of Bond Failure in Case of Fire

The information about temperature profiles of an anchor and the BST-Curves of the used mortar can be used to calculate the fire resistance for an injection anchor. Therefore, the time in the UTTC for which the fire resistance should be

calculated, has to be chosen. In the example explained later the fire resistance for an anchor with an M16 threaded rod and 80 mm embedment depth after a30 min of fire is calculated. The first step of the calculation is to read out the temperatures 2 for each embedment depth 1, see Figure 15 (left figure). Subsequently, the temperature information 2 can be related to a bond stress 3 (or reduction factor of bond stress) with the help of the BST-Curve, see Figure 15. The two pieces of information can be used to link every step of the embedment depth 1 to a bond stress 3. This is done in Figure 16. It shows that for the first 35 mm of embedment depth the temperature is higher than the limit temperature T_{max}, which means no loads can be transferred. In the rear part of the embedment depth stresses up to 2 N/mm² can be transferred according to the BST-Curve. The integral of the bond stress over the embedment depth results in the fire resistance N_p 4 for the chosen time in the UTTC, see Equation (2).

Figure 14. *Temperature Profiles for M18-80 (left), BST-Curve for the Used Mortar (right)*

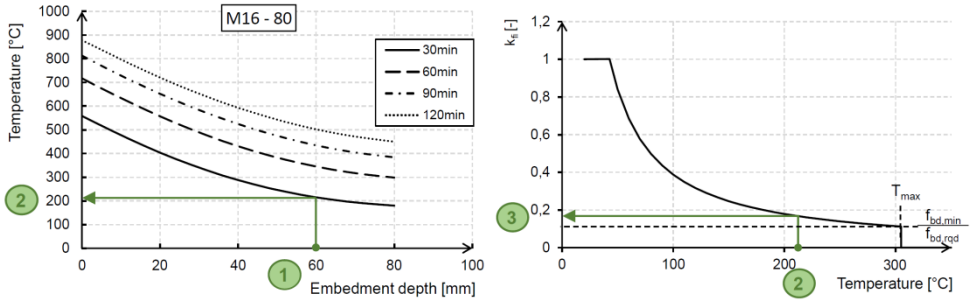

Figure 15. *Bond Stress Distribution along Embedment Depth*

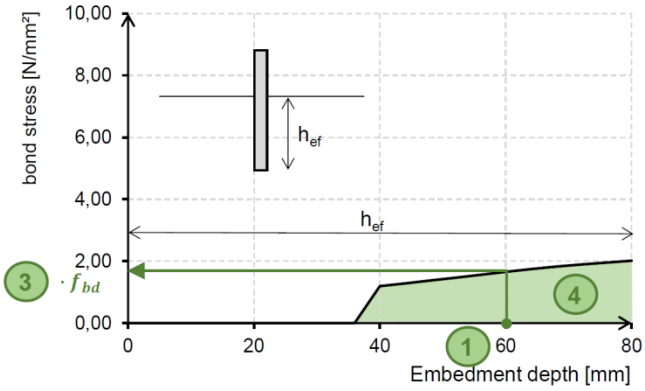

$$N_p = \pi \cdot d \cdot \int_0^{h_{ef}} f_{b,T}(h_{ef})\, \partial h_{ef} \qquad (2)$$

where: N_p Fire resistance concerning pull-out failure
d Diameter of anchorage
h_{ef} Embedment depth
$f_{b,T}$ Mortar specific bond stress in dependence of temperature

To confirm the calculation method the predicted fire resistances are compared with the results from the real fire tests. Figure 17 shows comparisons of two different mortar types: on the left side a polymer system, and on the right side an epoxy system. The prediction where the BST-Curve determined on the transient tests in the HR-test setup was used is presented with the black dashed line. The prediction where the BST-Curve determined on transient tests in the HP-test setup was used is presented with the green dashed line. It can be seen that the prediction is in any case on the safe side. Meanwhile the quality of accordance differs greatly. Especially for durations of fire longer than 60 minutes the predicted resistance drops to values of almost or even zero while the anchors are able to carry small loads for much longer. The results also show that the prediction based on the BST-Curves determined in the HP-Tests sometimes overestimates the fire resistance.

Figure 16. *Comparison of the Prediction of the Fire Resistance and Test Results*

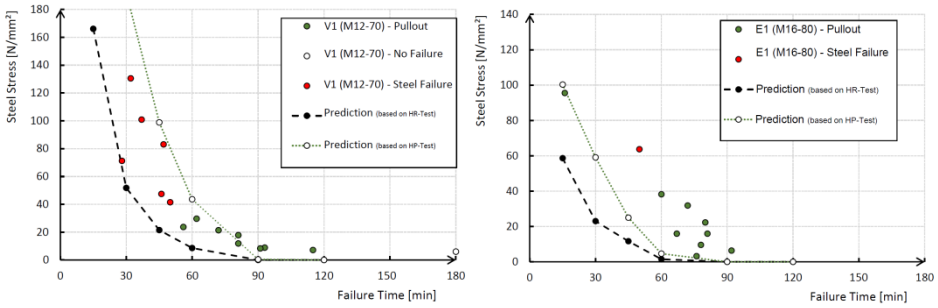

Within the scope of this research influencing factors on this prediction method were investigated. Four main aspects were considered as follows.

- **Temperature Profiles:** This example is presented before the temperature profiles determined without considering shielding influences of a fixture. Having regard to this and vaporization of water lower temperatures can be anticipated. This could be one reason for the results on the safe side. An overall implementation of these effects in the temperature profiles is in the authors' opinion neither feasible nor advisable.
- **The BST-Curve for the temperatures higher than T_{max}:** Caused by the test procedure for determination of the BSC-Curves the information about the bond resistance of mortars above the temperature T_{max} is missing. Nevertheless, fire durations up to 180 min can be monitored by fire tests with small loads ($f_b < 0.5$ N/mm²). A "grain-to-grain-support" could be a reason for that. The determination of a minimum bond strength $f_{b,min}$ related to the grain diameter could be a solution. This needs further research.
- **Determination of the BST-Curve**: The previously shown studies on determination of the BSC-Curves indicated many influences on the resulting curve. Especially the type of test execution shows a great impact. The restrained forces caused by temperature distribution in the test slabs of the real fire tests could be a reason for predictions on the safe side. For an explicit statement to the influence further research to this topic is necessary.

- **Anchor displacements:** The prediction method shown above does not consider the displacement and deformation of the anchor during loading. In the research work this paper refers to Reichert (2020) an exemplary calculation is presented, which considers stress induced strains and thermal strains of the anchor and uses load-displacement curves determined by the pullout tests in the HP-Tests. In conclusion of the calculated example no significant reduction of the predicted fire resistance is necessary.

Influence of Cracks on Bond Failure

The investigations on stress distribution in concrete slabs during fire showed that for common dimensions of slabs inner cracks occur. The influence of cracks for injection anchors are described by two hypotheses:

- Cooling effect: One explanation is that the cracks yield space for evaporated water and lead to a cooling effect and therefore higher fire resistances.
- Bigger displacements: On the other hand, the cracks should consequently lead to lower fire resistances like at room temperature, because of bigger displacements and the interruption of the adhesive bond.

For the assessment of the influence of cracks real fire tests on the cracked and uncracked concrete were conducted. The condition (cracked or uncracked) of the concrete is estimated before the start of the test. For the tests on the cracked concrete, bending cracks were caused and the anchors are installed in the cracks. Also, during fire exposure the slabs are loaded with a dead weight which causes a steel stress of 270 N/mm². For the test on the uncracked concrete no preloading is done and also during the test the slab is not loaded. Nevertheless, the occurrence of inner cracks is not prevented. The tests were conducted for two mortar types. The results are shown in Figure 18. It can be seen that for mortar type V1 (left) no influence of cracks developed, and the anchors installed in the cracks lasted even longer (average +6 min). For mortar type E1 a negative influence of cracks could be interpreted. The anchors failed on average 7 min earlier.

Figure 17. *Steel Stress versus Failure Time for Anchors in the Cracked and Uncracked Concrete*

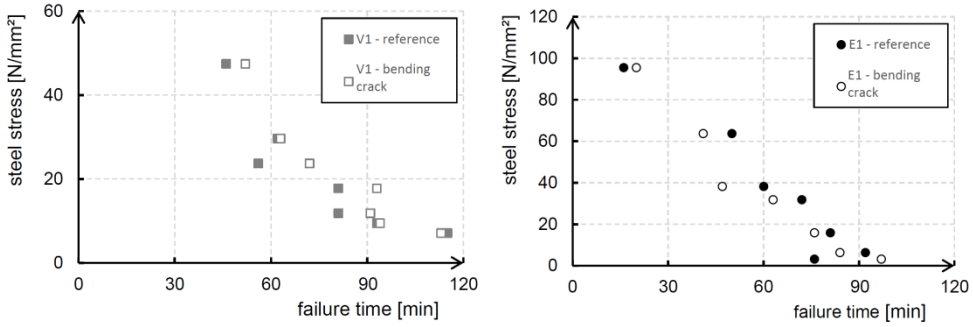

Overall the tests are showing failure times with a typical scatter for fire tests (± 10 min) so that no significant influence of precracked concrete for the described type of test execution can be concluded. It can be recorded that a classification in cracked and non-cracked concrete, as it is done for normal ambient temperatures, is not useful for tests under fire load. Instead, the definition of the dimensions and supporting conditions for real fire tests should be clearly defined. Bigger span widths should be preferred in contrast to smaller ones. Furthermore, hinged and horizontal sliding supports should be used.

Discussion

In case of fire a complex combination of temperature distribution and stresses are influencing the sustainability of injection anchors. The research work identifies bond failure and steel failure as the main failure types for injection anchors in case of fire.

The determination of temperature profiles with use of transient thermal finite element simulations is possible. This study finds anchor diameter and anchorage depth as well as moisture and presence of a fixture as the main influencing factors. The anchor geometry can be implemented easily into the simulation, while the presence of moisture and/or fixture leads to lower temperatures and can therefore be neglected as an assumption on the safe side.

Also, the usage of the BSC-Curves determined for post-installed rebar connections seems to be an assumption on the safe side. The study showed that the BSC-Curve can be influenced by many influencing factors. Especially the determination of the type of test execution and the influence of the restrained forces caused by the temperature profile in the concrete members require further research.

The presented prediction method gives a simple opportunity to calculate the fire resistances on the safe side. However the safety level can differ largely by different mortar types. Therefore, further research is recommendable for a better understanding of the load bearing capacity and its influencing factors. The presented HP-Test could be a good opportunity to get a better understanding of the load-bearing behaviour because of its ability to measure displacement and regulate temperature specifically.

The considerations due to the restrained forces caused by the temperature profile in concrete slabs show that a concrete member in case of fire has a cracked cross section in most cases. A definition of cracked and non-cracked concrete at it is handled at normal ambient temperature is not possible or useful for real fire tests. Tests with anchors installed in bending cracks could not prove a clear influence.

Conclusions

The research gives an overview to the load-bearing behaviour of injection anchors in case of fire and the main influencing factors. It deals mainly with the

bond failure mode. An opportunity for the calculation of bond failure is given. Further research is recommended to clarify the influence of fixture, moisture and test execution for determination of stress-temperature curves.

References

Al-Manouri O, Mège R, Pinoteau N, Guillet T, Piccinin R, McBride K et al. (2020) Numerical investigation of parameters influencing fire evaluation tests of chemically bonded anchors in uncracked concrete. *Engineering Structures* 209(Apr): 110297.

DIN EN 1991-1-2 (2013). *Eurocode 1: Einwirkungen auf Tragwerke, Teil 1-2: Allgemeine Einwirkungen – Brandeinwirkungen auf Tragwerke*. (Eurocode 1: actions on structures - Part 1-2: general actions - Actions on structures exposed to fire). Berichtigung 1. Berlin.

DIN EN 1992-4 (2019) *Eurocode 2: Bemessung und Konstruktion von Stahlbeton- und Spannbetontragwerken – Teil 4: Bemessung der Verankerung von Befestigungen in Beton*. (Eurocode 2 - Design of concrete structures - Part 4: design of fastenings for use in concrete).

EAD 330087-00-0601 (2015) *Systems for post-installed rebar connections with mortar*. EOTA.

EAD 330499-00-0601 (2017). *Bonded fasteners for use in concrete*. EOTA.

Fuchs W, Silva JF (2012) EOTA Approach to qualification and design of post-installed adhesive anchors for fire exposure. In *Understanding Adhesive Anchors: Behaviour, Materials, Installation, Design*. Chicago, Illinois, USA: ACI Spring Convention.

Hosser D, Richter E (2013) *Vereinfachtes Rechenverfahren zum Nachweis des konstruktiven Brandschutzes bei Stahlbeton-Kragstützen*. (Simplified design method for the structural fire resistance of brackets made of reinforced concrete). Berlin: Deutscher Ausschuss für Stahlbeton.

Lahouar M, Pinoteau N, Caron J-F, Foret G, Rivillon P (2018) Fire design of post-installed bonded rebars: full-scale validation test on a $2.94 \times 2 \times 0.15 m^3$ concrete slab subjected to ISO 834-1 fire. *Engineering Structures* 174(2018): 81–94.

Lakhani H, Hofmann J (2017) A numerical method to evaluate the pull-out strength of bonded anchors under fire. In *3rd International Symposium on Connections between Steel and Concrete*, 1079–1090. Stuttgart.

Mallée R, Fuchs W, Eligehausen R (2012) *Bemessung von Verankerungen in Beton nach CEN/TS 1992-4*. (Design of fasteners in concrete according to CEN/TS 1992-4). Beton-Kalender 2012. Berlin: Ernst, Wilhelm & Sohn.

Patil M, Thiele C (2015) Thermal study of bonded anchors to determine temperature distribution. In *Workshop Heißbemessung Braunschweig*.

Pinoteau N, Pimienta P, Guillet T, Rivillon P, Rémond S (2011) Effect of heating rate on bond failure of rebars into concrete using polymer adhesives to simulate exposure to fire. *International Journal of Adhesion and Adhesives* 31(8): 851–861.

Reichert M, Thiele C (2017) Qualification of bonded anchors in case of fire. In *3rd International Symposium on Connections between Steel and Concrete*, 1091–1099. Stuttgart: IWB.

Reichert M (2020) *Zur Bestimmung des Feuerwiderstands von Injektionsankern mit variabler Verankerungstiefe in Beton*. (determination of fire resistances for injection anchors with variable embedment depth). Dissertation. Kaiserslautern: TU Kaiserslautern (in press).

Reick M (2001) *Brandverhalten von Befestigungen mit großem Randabstand in Beton bei zentrischer Zugbeanspruchung*. (Fire Behaviour of Fastenings with high Edge Distances for centric Tension Loads). Dissertation. Stuttgart: Universität Stuttgart.

Thiele C, Reichert M, Patil M (2017) *Verbunddübel im Brandfall: Abschlussbericht eines Forschungsvorhabens des DIBt.* (Bonded anchors in case of fire: final report of a research project for DIBt). Kaiserslautern: TU Kaiserslautern.

TR020 (2004) *Feuerwiderstandsfähigkeit von Metalldübeln*. (Evaluation of anchorages in concrete concerning resistance to fire). EOTA.

Athens Journal of Technology and Engineering - Volume 7, Issue 4, December 2020 – Pages 277-298

Filling the Industrial Data Lake in Manufacturing Companies based on KPIs

By Marcus Kurth[*], Michaela Göggel[±], Carsten Schleyer[‡], Johannes Gratt[+] & Burkhard Martin[§]

An efficient implementation of digitalisation projects in manufacturing is highly challenging. Usually a transformation to digitalisation based on a technology-oriented perspective leads to vast investments and implementation costs. In order to exploit the potential of digitalisation entirely, defined digitalisation targets derived from an overall corporate strategy are required. This paper describes a new systemic methodology based on a generalised automation pyramid allowing the optimal placement of required sensors in a production line based on highest impact key performance indicators (KPIs) identified from the corporate strategy broken down to production level. The new approach is demonstrated on the hand of the vial production line of Sola Messwerkzeuge GmbH exploiting synergy effects systemically achieving cost efficiency.

Keywords: *digitalisation, industry 4.0, KPIs, data analysis, systems engineering*

Introduction

Production planning and control as well as quality management in a production facility always require up-to-date production data. While information is always available in the same, high-resolution cycle in continuous or sequential systems, object-related processes in logistics or manufacturing industry are characterized by random events. For example, employees arrive at a plant at different times in the morning, or the material arrives at the production facility at exactly the time it is processed - just in time or as an enhancement: just in sequence. This reduces stocks in production and thus avoids unnecessary investments or costs, especially because the proportion of non-value-added activities is minimized.

With the introduction of these principles, it is no longer possible to exactly calculate the moment an event will take place - like the arrival of material. Such systems are not deterministic and follow stochastic distributions. Non-deterministic systems can only be automated with stochastic models. The quality of these models depends here on the accuracy of the identification of underlying distributions in a production line. In practice, that identification is highly challenging as the broad

[*]Professor, University of Applied Science Constance, Germany.
[±]Research Assistant, University of Applied Science Constance, Germany.
[‡]Professor, University of Applied Science Constance, Germany.
[+]Sola GmbH, Austria.
[§]Sola GmbH, Austria.

necessary database is usually not available. And if figures are available, these distributions are highly time variant, e.g., with product variance.

In many companies, the status quo is usually a manual collection of operational data - either in paper or in digitalised form. The required data is entered manually into a form and confirmed or signed. This usually works well until problems in production occur. In the latter case the forms are often handed in collectively, i.e., at the end of a shift. And this means that there is no longer a sufficiently precise data basis for an optimal production planning or control. However, to achieve the paradigm shift to Industry 4.0, where the product determines the path through production, an order must necessarily be clearly identifiable and precisely traceable at any time.

Companies facing that challenges with automation, digitalisation and big data technology are driven by various external and internal factors such as e-commerce, increased customisation combined with reduced batch sizes or cost reduction and competitiveness.

These drivers have different influences on the company's motivation for digital transformation. Especially hygiene factors have an essential impact. In this context, hygiene factors, referred to product perspective, represent an economic imperative for implementation, otherwise the product cannot be sold anymore. As a consequence, customers are not willing to pay for automation. In order to remain competitive, manufacturers are forced to implement automation without being able to generate financial added value by the end customer, e.g., by increasing sales prices. Other hygiene factors are, for example legal regulations or increased customer demands.

That paper addresses that challenges by introducing a systemic methodology compromising technology and costs against a company's strategy using only highest impact production indicators. The described methodology was developed with Sola Messwerkzeuge GmbH in Austria. The paper shows the application of the methodology exemplary on the hand of a production line for vials as part of Sola's spirit level production.

In a former project, Sola targeted that challenge like many other companies driven by technology. A data lake should be implemented sourced by ident sensors providing track and trace for the product focussing a part-production line. The suppliers offer regarding the required industrial-standard sensors with their related hard- and software equipment plus further required touch screens led to high estimations of investment costs – compared to the benefit. As for tracking parts and tracing processes, a cost-effective, reliable and industry-compatible technology is required. In the beginning, several technologies for part tracking and tracing have been investigated with regard to their usability, applicability and profitability in the considered context. As a result, RFID technology has been identified as being well suited but involving very high investment costs. Further investigations show that the benefits of this technology are limited to little advantages specific for the focussed part of the production line.

That has stopped the project – again like in many other companies. However, there was a demand for a more methodical and application-oriented approach for standardized use in the complete companies' production lines.

Based on the actual intention of that first project – turning the event driven production line deterministic by generating production line data in real time – the systemic methodology was developed. The paper shows the exemplary application of the methodology on the example of one KPI and starts with a determination of the most impacting parameter targeting the strategic goals driven here by hygienic factors of the market. By exploiting the information technology driven layer principles of the automation pyramid that goal is broken top-down to the digital twin of the vial production line to determine the required locations of sensors and appropriate sensor types. A following bottom-up approach through the information layers allows a further cost consideration. That process repeated in an iterative manner to find the optimal trade-off between corporate strategy and location of sensors in the production line by identifying its required production data resolution by the described iterative process leading to a cost-effective choice.

By applying that methodology consequently to other related production data indicators, the already determined devices can then be exploited optimally leading to an adequate generation of key performance indicators of production, keeping databases or data lakes lean and that under minimal implementation and maintenance cost.

In the exemplary case of Sola, the shown key performance indicator extracted from the corporate strategy could be implemented even without placing further sensors in the production line. The methodology showed, that the indicator could be implemented by simple correlation of already acquired data from the database. Further, that data can be easily augmented by few ident sensors in the production line to extract other key performance indicators.

Basics of Digitalisation and Automation - Impact by Technology and Costs

Industry 4.0 in production is driven by several technological developments accompanied by mass application and the related cost reductions of the required automation technology.

Before digitalisation and automation efforts are implemented in a production line it is recommended to analyse their potentials in the specific production. Figure 1 illustrates the implementation of automation in production in a stepwise approach, by

(1) **O**rganising workflows and workstations
(2) **M**echanising work processes and finishing with
(3) **A**utomated production

Usually, these steps are summarized by the term “OMA-principle”.

Figure 18. *General Procedure of Production Automation*

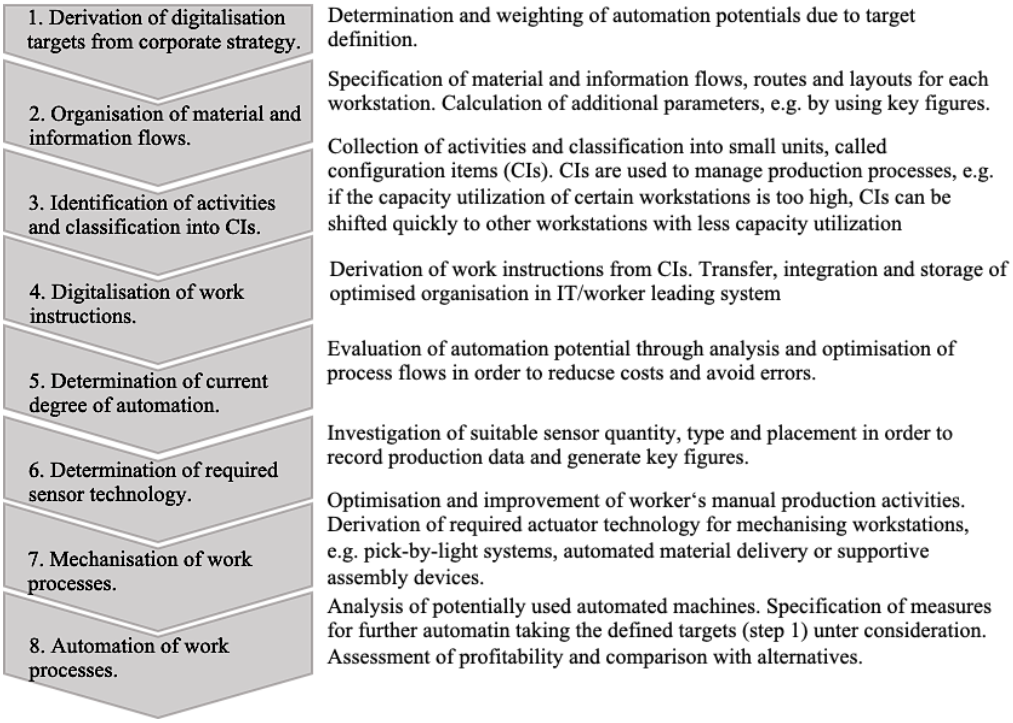

Source: Adapted from Kurth, 2020.

As shown in step 6, selection of suitable sensors and the generation of operational and business data is an essential part of production automation procedure. Information from ident systems are the basis for that step. These systems are a decisive development in sensor technology for improving the automatic acquisition of operating data in Industry 4.0 applications. They allow a clear identification of objects such as workpieces, tools or transport containers. For the hardware-technical implementation, a unique identifier or marking for identification must therefore be attached to the object. That identifier can be en masse printed, engraved or similar on objects, e.g. in the form of bar-, UDI- or QR-codes. Or in an intelligent variant in the form of a programmable data carrier with radio technology. Then further information can be transferred and read out contactless and dynamically on the object. This means that further information is also available when there is no contact to the database, e.g. in logistics.

By linking to a database, additional information, such as the corresponding customer order, is also available.

Since this database is filled permanently with data from sensors in production, the amount of information in this database is constantly increasing. Therefore, that database it is also called a data lake. The goal of a data lake in production must be to have a complete digital image of the physical system from which all the required data can be derived. In that case this data lake forms a complete digital twin over the entire lifecycle, from factory planning to product ideas and the disposal of products.

In a data lake, a wide variety of data such as technical information, production and quality data or information from the supply chain is collected by the various IT systems involved and checked for consistency and correctness. This step is necessary to comply with requirements such as single source of truth. Only in that case, it can be ensured that the stored inventory is generally valid and therefore reliable at a certain point in time.

Data in the data lake can be further used in shop floor analytics to make system dynamic predictions. Such a forecast could be the identification of demand. It could also take into account special events that will generate exceptional demand. For example, a major sporting event that will create exceptional demand for television sets. This requires system dynamic models which can be adapted based on historical data - self-learning and improving and in further developments even combined with artificial intelligence (AI).

With such predictive methods in demand management, delivery reliability can be improved while reducing reserve stocks at the same time. In addition, these methods can also be used as a smart service to manage customer inventories.

However, the data lake is not only crucial for data storing, analysis or future smart services – it also links the IT world with automation technology. The role of production and its automation in digital transformation is undisputed. Körner et al. (2019) argue that automation "requires multiple IT-systems to cope with resulting challenges due to complex manufacturing systems". The merging of IT (virtual world) with classical industrial processes (physical world) by embedded hardware and software systems leads to Cyber-Physical Systems (CPS) that demonstrate the core elements of smart factories. This evolutionary, technological transformation represents the vision of Industry 4.0 (Schreiber 2013).

At that point - where physical systems meet information technology - it must be noted that the prioritization of the requirements of classical IT clearly differs importantly from that of automation technology. In classical IT, the highest priority is given to confidentiality. This means that data may only be read, transmitted or modified by authorized users. In second place are the requirements for integrity: data must not be changed unnoticed and must be consistent. In third place is the availability, the prevention of system failures or access to data within a certain period of time. In automation technology, the exact opposite ranking applies, which requires i.e., other safety concepts.

For a CPS, it is therefore decisive whether it is derived from classic IT or automation technology. Notwithstanding the non-hierarchical approach of CPS, the established model of automation pyramid "to structure the different applications in a functional and hierarchical manner […] is still present and very common" (Körner et al. 2019).

The automation pyramid is based on various information layers commonly found in IT systems combined with the hardware-based approach of automation technology. The number of hierarchy layers of the pyramid varies, as in research some layers are removed or merged together (Körner et al. 2019). In the given context, the automation pyramid is considered with three layers for simplification (see Figure 2).

Figure 19. *The Automation Pyramid in its Common Representation as a Triangle*

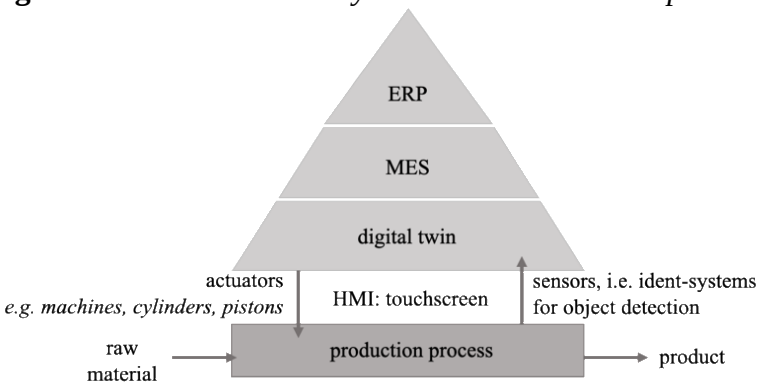

With the increasing use of sensor technology in production, the number of data stored will also rise rapidly. A concept or ontology must be elaborated at an early stage to determine not only the type (in what form) and place (where) data will be stored but also a time variant rating or importance of the data. In the case of central databases, for example, a distinction can be made according to the time at which the data is stored and the associated number of server accesses. It must also be taken into account that the data can have different meanings and must be evaluated appropriately. But over time, data can also become meaningless or even harmful. If data is randomly written to a database without a structure, a data grave is quickly created in which no user can find or assign data. The hope in practice is then often that at some point an AI or other big data analysis tools will be invented and developed that structure and analyse the chaos. However, this is currently not foreseeable and does not correspond at all to the systems dynamics-based principles of lean production: avoiding waste (Ohno 1988).

An important role in production planning plays a well-defined, manageable set of KPIs. They are the basis to bring the principles of lean thinking to databases allowing an easier organization and assignment of data by keeping communications and the number of database entries slim. Also, that reduces the maintenance effort of the database - see also the takt principle of lean manufacturing.

The Role of KPI and Key Figures in Digitalisation

The previously mentioned lean approach for filling the data lake with production data must be transferred to the generation of KPIs. Finding the KPI with the highest impact on a target of the corporate strategy is crucial for the company's success. This importance of KPIs and machine availability data (MAD) is confirmed by several authors.

Schuster (2018) highlights the importance of continuous measurement, monitoring and reporting of key figures like machine availability (MA) or Overall Equipment Effectiveness (OEE) for efficient production management (planning and control). Moreover, he suggests using supportive IoT-solutions that prepare and provide real-time machine and production information for variance/root-cause analysis and deriving measures. Kang et al. (2016) describe KPIs such as

efficiency, availability or throughput as "critical for manufacturing operation management and continuous improvement".

As this paragraph shows, in literature and practice, the terms "key figure" and "KPI" are often used synonymously. Thus, a clear definition of both terms is required.

According to the International Organization for Standardization (ISO 22400-1 2014), a key performance indicator (KPI) is defined as a "quantifable level of achieving a critical objective". Kang et al. (2016) take up this definition and add that KPIs are "a set of quantifiable and strategic measurements […] that reflect

the critical success factors of an enterprise". Moreover, they demonstrate that "KPIs are not independent and may have intrinsic mutual relationships" (Kang et al. 2015).

When differentiating KPIs and key figures, the terms "strategic measurement" and "a company's success" are crucial, as these reflect the main characteristics of a KPI.

In the context of this paper, KPIs are related to a strategic context by indicating the degree of strategic target achievement. With reference to the definition of indicators, a KPI consists of two components:

- Measurable: key figures based on specific, quantifiable values
- Non-measureable: indices, like corporate reputation, employee motivation or satisfaction (Sterman 2000)

That means, KPIs should essentially be based on key figures and rely as little as possible on indices. The key figures are measured whereas the indices are extracted from the data lake.

For example, the above mentioned MA represents a typical key figure which can be measured. Whereas the superordiante OEE as KPI is built out of the product of the figures for availability, effectiveness and quality ration. Hence, the MA influences as part of availability the OEE.

However, it must be mentioned that different definitions of MA exist in literature – having the same key statements (Kang et al. 2015). MA represents production data by expressing the percentage of actual operating time (AOT) relative to planned operating time (POT) (Kang et al. 2015, 2016).

Due to that reliance on the MA e.g., Boschi et al. (2017) define the MA as a key business factor (KBF) and a KPI, too, because it considers "the production parameters used to evaluate the production trend and the process behaviour […]".

Those relationships and interdependencies of KPIs with system quantities and between other KPIs are discussed in further detail in Stricker et al. (2016). Their paper establishes relationships between several "KPIs in the field of maintenance and machine monitoring" with MA and OEE under consideration.

Methodology

The newly developed methodology describes a systemic approach for generating a KPI systemically broken down from corporate strategy level and implemented on production level with adequate hardware and software components.

The methodology is characterized by an iteration loop-based approach with the aim to structure KPI's in order to identify the KPI with the greatest effect on achieving corporate strategy's objectives.

Its aim is to determine the clear definition of optimal sensor placements for filling the data lake, i.e., generating the required data at production level such as machine data, by considering implementation costs and other driving factors for data analysis like resolution, update rate, margin of error.

As previously described, KPIs have relationships and interdependencies. Thus, another aim of the framework is to implement the generation of related KPI deviated from the existing sensor data at production level without generating additional effort or costs.

The methodology is developed with respect to the automation principle and its prioritisation of availability, integrity and confidentially. As a consequence, requirements like single source of truth principle can be fulfilled even in combination with an IT driven data lake. In combination with the IT and automation technology approach of thinking in hierarchical information layers the costs of investment can be controlled.

For that reason, the core characteristic of the previously described automation pyramid with its multi-dimensionality is exploited. In contrast, the generic literature rarely considers that multidimensionality as shown in Figure 3 (cf. Körner et al. 2019, Bildstein and Seidelmann 2017).

Figure 20. *General Use of Automation Pyramid as Multidimensional Hierarchical Layer Model, Linking Process Driven Automation Technology and IT*

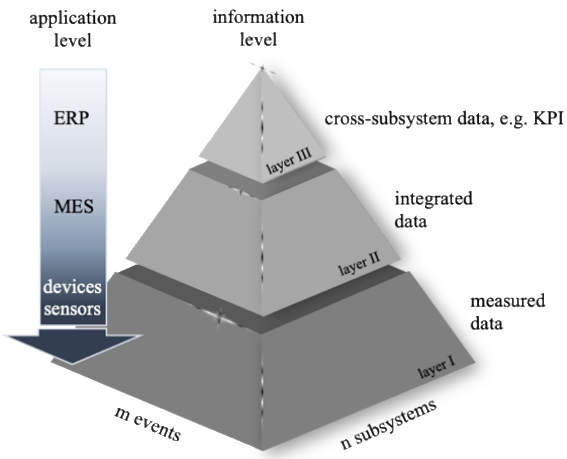

The focus of this multidimensional pyramid illustration is the key subject of the developed methodology – the systemic and iterative generation of KPIs by applying and executing a stepwise reference modell of the pyramid in a top-down and bottom-up approach.

In the context of this paper, layer I represents the lowest level, where the actual manufacturing process with its physical sub-processes "controlled by devices and sensors" (Körner et al. 2019) is imaged. Simultaneously, layer I is the foundation for the upper generation of KPIs. The multidimensionality of layer I reflects the real-world manufacturing processes. Subsystems represent, according to their respective systemic definition and interpretation, e.g. individual machines of the production line or warehouse, machine groups or complete production lines. Events then are states that trigger the transmission of data and communicate the results of a process step, for example signal of completion or arrival of material. Events are thus initiated by a trigger signal, e.g., timestamps at the beginning or end of processing.

Besides manufacturing operations control, layer II integrates the transmitted data from layer I and external data from other systems (MES, ERP from layer III). This data is gathered over the entire system, or here production landscape or network, for generating the KPIs. In this layer, the sensor values recorded in layer I are compared with the target values. The data measured in layer I is converted to integrated data, which is required for the calculation of the KPIs (layer III). Layer III, the top level, represents the target level and defines the short- and long-term objectives. It is linked to the ERP system and entails the definition, calculation basis and visualisation of the KPI, derived from the long-term corporate strategy and digitalisation project objectives. Körner et al. (2019) highlight that in practice, business planning in this layer is executed by applying ERP tools for managing tasks, inventory and resources.

Systemic Procedure for KPI Generation

The newly developed systemic methodology is characterized by its idea to generate KPI systemically by abstracting the general pyramid hierarchy to the specific required information for KPI calculation with a top-down and bottom-up approach meeting the corporate strategy. This methodology retains the strict, hierarchical procedure from IT (see Figure 4).

Basis for the implementation of the methodology is a clearly defined, abstract project target. The targets of the digitalisation projects are derived again from the objectives of digitalisation. This requires a holistic digitalisation strategy that is aligned with the corporate strategy and vision of the company. In order to verify the target achievement of the digitalisation projects, it is necessary to determine and generate specific KPIs. The stepwise application of the pyramid model enables the methodological generation of such KPIs by defining and specifying the requirements for KPI generation. A systemic approach to the generation of KPIs is essential in order to identify and assess the overall relationships and correlations between them. As a result, before applying the methodology, potential correlations between KPIs must be considered. Thus, similar KPIs can be generated additionally

with little effort by using synergies in the collection of data for calculating key figures and KPIs.

Figure 21. *Automation Pyramid with its Multi-Dimensionality and Derived from Overall Corporate Strategy*

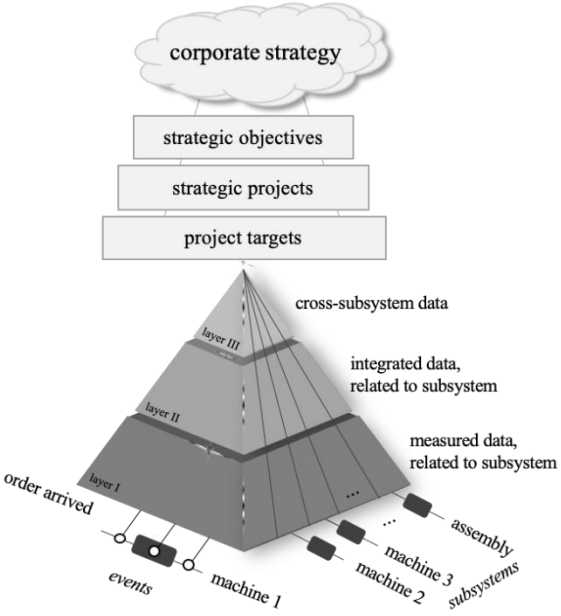

Although the methodology is characterized by a systemic manner, the procedure for applying the concept is described stepwise. Another important characteristic of the methodology is its user-driven data collection and generation. User-driven means that data generation is not randomly performed by the subsystems themselves but is selectively and solution-oriented initiated by the end user. This is an important prerequisite for keeping the data lake lean and controllable. This is supported by an automatically generated KPI specification data sheet during application of that methodology.

Step 1: Derivation of the KPIs from the Strategic Objectives

After determining the corporate strategy and deriving strategic projects with specific project targets, the first step is to identify the KPIs to be determined, which are derived from the general strategic objectives of the company. An important requirement for KPI definition is that the specific KPI is measured with at least one key figure. Thus, the key figure to be determined has to be defined and abstracted from the KPI. Secondly, the purpose and goal of KPI generation and key figure calculation is described in this step. With regard to this, the linking context and reference between key figure and determined goals as well as additional key figures is created. Therefore, related key figure and KPI are gathered.

Step 2: Determination of the Basic Structure of the Pyramid

In this step, each layer of the pyramid is elaborated. Starting with layer III, the KPI is defined and the calculation basis for KPI and key figure is determined. For layer II, the data for calculation are described. The data are differentiated between required data for calculation on layer III and measured data from layer I and external systems, like from MES-/ERP systems such as transaction-related data or master data. This step completes with the determination of data types for data collection on process level (layer I).

Step 3: Identification and Specification of Iteration Criteria

In order to take into account the effort required to implement the KPI generation system and the requirements for the KPIs in terms of time resolution and update rate, it is necessary to define iteration criteria for the respective KPIs. With these criteria, the KPI generation is evaluated in several iteration cycles and a after each iteration a decision on termination or further optimization is made. Therefore, the criteria must be differentiated into soft and hard criteria. Soft iteration criteria are merely guiding and non-quantifiable, whereas hard iteration criteria are quantified, i.e., they are measured with a unit and allow a clear decision about an abortion, continuation or completion of the iteration process. Hard iteration criteria are either of variable character, i.e., all values can occur and are acceptable, or of decisive character, i.e. there is a fixed target value to be reached. During this process step, a unit and a start or target value will be assigned to the hard iteration criteria.

Step 4: Top-Down Approach – Definition of KPI Requirements for Each Layer

In that step, the requirements for real-time performance and resolution are developed for each layer. Real-time behaviour is usually distinguished between soft, hard or no real-time. The hard real-time is in the safety context, i.e. a failure to meet this time requirement leads to damage, e.g. high costs or useless values. In contradiction, a violation of the soft real-time does not lead to additional costs. Thus, hard real-time is mainly necessary at the lower layers of the automation pyramid (for operational control). It is needed for information evaluation, so that the information can be time stamped. A soft real-time is sufficient for planning activities.

Update rate and resolution are decisive inputs for the sensor level. The resolution refers to the object being viewed and represents, for example, the unit that is measured, e.g. individual part, tray or pallet.

The update rate refers to the time period of the observation: e.g.: on an hourly, shift-related or daily rate.

These factors represent aspects of data processing and data storage by providing information about

(1) How many measuring points are desired (resolution)?

(2) How often should be measured (update rate)?

These criteria are essentially determined by the characteristics of the technologies (e.g., sensors) used. For this reason, the logically shortest detection interval on the one hand and the critical minimum detection interval on the other hand must be determined for the resolution.

Finally, the margin of error and the trigger response have to be defined. Margin of error also affects the selection of the sensors.

Trigger response represents the origin signal for a layer's processing or detecting activity, i.e. a layer is triggered by an upper (top-down) or a lower layer (bottom-up). Additionally, the trigger response can be initiated actively or passively.

Step 5: Bottom-Up Approach – Description of Layer Functionality in Detail

In this step the data to be recorded is specified. For this purpose, the data including a description of the criteria is compiled in a list and compared with the data from the systems (e.g., MES or ERP). The data is also re-examined for the use of synergy effects in order to be able to generate new KPIs as required with minimal effort. In addition, the data still to be generated is identified.

For layer I, it is specified how often, where and what kind of data is generated, i.e., with regard to the type of data defined in step 2.

In layer II, it is defined what kind of data are required for KPI calculation, e.g. data from subsystem (layer I), cross-subsystem data (from layer III), external data from other systems (ERP, MES). Furthermore, methods for possible verifications of the data, e.g., plausibility checks or cross-checks are determined. To conclude the specification of layer II, the integration of the internal IT, e.g., other departments or into existing systems is investigated.

This step is finalized by giving details about the functionality of layer III. This includes the definition of filters for modifying the KPI, e.g., by merging several subsystems and for collecting additional information e.g., for application such as interfaces or data formatting, storage and integration. In the end of this step, the list of related KPIs, created in step 1, are investigated in terms of their completeness and correctness and updated if necessary.

Step 6: Establishment of Quantity Structure from Defined KPI

The iterative application of the methodology is finalized within that step. The results of this step indicate if an iteration cycle is completed, and the results fulfil the iteration criteria.

In this step, the requirements for the investigated KPI are summarized and the costs and efforts for the implementation are examined in detail. This step represents a feedback loop to review bottom-up the performed steps regarding the initially defined goals and strategic objectives and the defined budget.

For this purpose, a list is established that

(1) Summarises the data required for the calculation including a description of the criteria in detail (unit, resolution, update rate, real-time behaviour, origin, etc.)
(2) Checks which data are already available in the MES and whether the defined criteria are fulfilled
(3) Designates the remaining data to be generated, including a description of the method of collection, and
(4) Estimates the costs and efforts for implementing the KPI system i.e., for purchasing and installing the required sensors, integrating data into existing IT, managing and analysing the data lake and for ongoing operation such as service and maintenance of hardware, software infrastructure and system merging.

In other words, in this step, the generated data is linked to a cost function in order to evaluate it in monetary terms and to determine when this data becomes redundant. This linkage to costs is an essential step to maintain the lean structure of the data lake by deleting or updating non-valuable data.

Step 7: Evaluation and Assessment of Results

With a final evaluation of results, it is decided whether the stepwise application of the methodology is completed, aborted or if a further iteration is needed, where e.g., the objects under consideration are revised with respect to the number of subsystems or kind of events, real-time requirements or the margin of error are changed, or the quality of the resolution and update rate is adjusted.

In the last two steps, it is also necessary to consider and comply with the previously described requirements for automation projects, e.g., lean data lake, data consistency and single source of truth.

As the production key figures are in many cases derived from similar data bases, synchronisation with other digitalisation subprojects is possible and recommended. In turn, this means that the implementation of the first subproject is the most cost-intensive regarding the required sensor technology.

In conclusion, the methodology aims to determine:

(1) What data are required to extract the desired information from the data lake?
(2) Whether order tracking or detailed tracking of individual components of an order is being pursued?
(3) In which time periods/intervals signals are to be recorded and data generated by the sensors (per second, minute or hour, per cycle, shift-specific, once a day, etc.)?
(4) How many sensors are needed to generate the required data?
(5) What characteristics the sensors must have (cost, quality, industrial suitability)?
(6) How the acquired signals are transmitted (via Bluetooth, via bus interface, according to which standards and with which protocols)?

Therefore, the results of the iterative application of the methodology show which data are needed from the production, in which order, how they are composed and in which temporal resolution they have to be generated.

The ranking then shows which digitalisation subproject should be carried out first as well as the number of sensors required to achieve the target. With consistent use of incremental data processing the e.g., the number of sensors can be reduced significantly once again in a further iteration cycle.

Exemplary Implementation of the Methodology

The methodology has been developed in collaboration with the company Sola Messwerkzeuge GmbH, headquartered in Götzis (Austria). Sola is an internationally operating SME specialized in the production of high-precision measuring tools. With its 200 employees and subsidiaries in Germany, Hungary, Switzerland and the US, the company develops, produces and distributes a comprehensive product portfolio with approximately 1,500 products in more than 70 countries all over the world.

With regard to software that is required for data collection, analysis and evaluation, the company already uses comprehensive MES- and ERP-systems. The integration of the systems is planned for the next two years. Thus, there is already a solid database for production data implemented, e.g. machine availability data (MAD) or feedback data transmitted to the system for production data acquisition (PDA).

Description of Sola's Production Processes

In order to explain the methodological generation of the key figure MA in the subsequent chapters by using a real-world scenario from the company Sola, firstly the sample production process under consideration is described.

The total production line is built up by two main sections. The vial production (VP) as the first section, takes place independently of the spirit level production (SLP). SLP is the second section and is physically separated from the VP.

The two sections are connected by a Kanban system. The Kanban system is filled manually by an employee using a Kanban card when a requirement is reported.

The plastic injection-moulded parts for the VP are initially produced in a separate plant of Sola in the same town. In addition to caps, lids and the end caps for the spirit levels, the transparent acrylic glass vials are also produced there. Special demands are made on the high accuracy and the high quality of the acrylic glass (very clear surface) as well as the precise dimensions.

Figure 22. *Sample Production Line for Vial Processing at Sola*

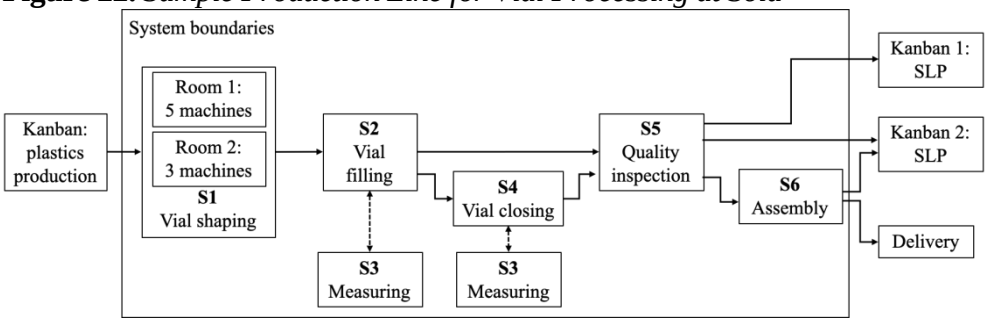

In the VP, different machines are required for the processing steps, visualized in Figure 5.

The first processing step is the vial shaping for processing the inner radius and markings (step S1). Next, the vials are filled with a liquid (step S2). Then the first test procedure (step S3) takes place at two different workstations in order to ensure that the high requirements mentioned above are met. Using a special manufacturing process, the vials are closed (step S4). This is followed by another high-precision quality inspection (step S5). Finally, the assembly of the modules takes place (step S6).

The finalized modules are stored and placed in the Kanban system for the subsequent SLP or for delivery.

As an innovative and competitive SME, Sola recognized the need to promote digitalisation to maintain productivity and efficiency, and to react flexibly in order to meet the customer's diverse demands and develop high-precision and optimised products (Sola Messwerkzeuge GmbH 2020). Sola's drivers for digitalisation are summarized in Table 1.

Table 2. *The Company's Driver for and Objectives of the Digitalisation Project*

Drivers and Objectives	**Challenges**
Hygiene factor	Competitiveness
Strategic objectives	Improved process stability and transparency; Increased process availability; reduced quality losses.
Strategic project	Process optimisation through reduced quality losses at a high degree of capacity utilization; Data analysis and reporting through generation of defined key figures/KPIs.
Project targets	Traceability of the production process through standardization, documentation and evaluation of KPIs; Tracking of individual parts (regarding inventories) in production.

Table 1 reflects the initial situation for the development of the described methodology for systemically generating and implementing a corporate key performance indicator (KPI) system.

The previously mentioned concept with a focus on application-orientation in comparison to a technology-oriented approach is described in Table 2.

Table 3. *Differentiation between Technology- and Application-Oriented Approaches in Digitalization Projects*

	Technology-Orientation	**Application-Orientation**
Step 1	Selection of adequate technology.	Specification of application.
Step 2	Identification of appropriate application for selected technology at production level.	Identification and evaluation of suitable technology for identified application.
Findings	High costs for investment and implementation; RFID-technology not beneficial.	Reduction of implementation costs; consideration of overall corporate strategy, clear definition and differentiation of key figures and KPIs

Sample Application of the Methodology

Based on the systematic approach described in Chapter 3, this chapter shows the systemic application of the developed methodology on the hand of the vial production at Sola. Congruently with that comes a proof of concept with regard to its applicability and problem-solving contribution.

The specific application of the pyramid model in a top-down and bottom-up approach according to the previously described steps, aims to increase process stability and avoid high quality losses in the long term by introducing digitalisation.

The associated track and trace implementation will improve the extracted values and their reliability. Particular attention must be paid to the relationships and interdependencies between the key figures. At the same time, the aim is to save costs during implementation (through the consideration of key figures' interrelationships).

Step 1: Derivation of the KPI from the Strategic Objectives

In accordance with the stepwise procedure described in chapter 3, the corporate strategy at Sola aims at increasing competitiveness in the long term as well as continuous quality improvement. Both objectives are reflected by the companies specific KPI OEE – to be more precise, in its term "plant productivity" (see Figure 6).

In the case of Sola, a prior performed bottleneck analysis already clearly identified that in VP section, process stability is determined by the machines. Therefore, the machine availability (MA) has the dominating impact compared to the total production availability on the KPI and is therefore chosen as measured key figure and is calculated as followed:

MA = actual operating time (AOT) / planned operating time (POT)

Hence, the purpose of this subproject is to increase data quality and interpretability of PDA and maximize MA. Related KPI is OEE, related key figures are performance, quality and downtime.

On the one hand, POT represents the difference between calendar time and planned time for non-production, e.g. time for maintenance and service. On the other hand it is calculated as the sum of operating time and availability losses such as setup times or downtimes.

The key figure MA further is applied for validating and verifying the feedback data and for synchronising it with the production cycle. This leads to an increased interpretability and transparency for production management. Thus, this key figure has a high practical relevance. In addition, with little effort, further key figures can be generated from the MA and KPIs such as the OEE itself can be specified in figures.

Step 2: Determination of the Basic Structure of the Pyramid

The application-specific structure of the pyramid is illustrated in Figure 6. The key figure machine availability (MA) is distinguished in linked and individual MA. Layer III calculates the linked MA in vial production according to the individual MA. When considering the availability of the overall production line (linked MA), the calculation of the key figure MA results from the individual MA.

Figure 23. *Structure of the Pyramid in the Context of Sola's Vial Production for Calculating Linked Machine Availability (MA)*

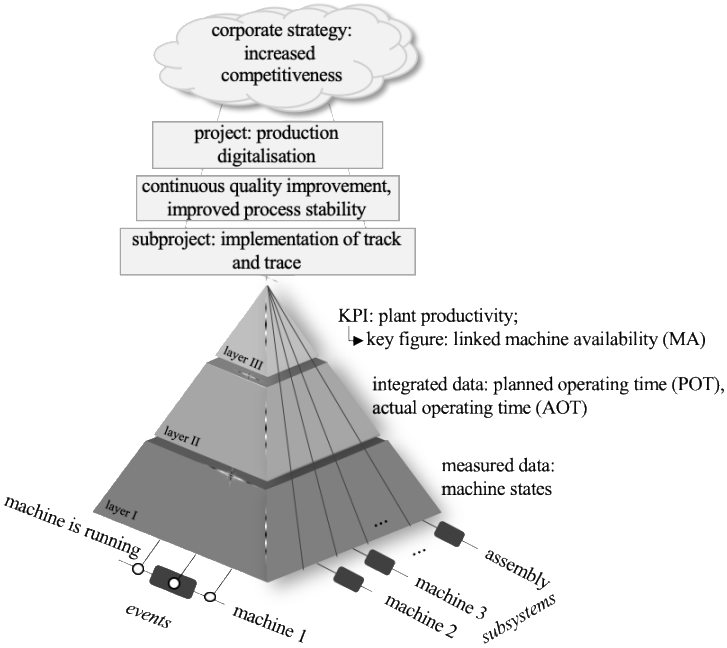

The individual and linked MA is a function of the specific structure. The structure reflects the order and layout of the machines, i.e. in serial sequence (multiplication of individual MA values) or in parallel order (summing up of individual MA values). The structure also refers to the processing steps. For each processing step the structure of the machines have to be defined. Therefore, each individual machine here represents a subsystem and the merging across the

structure (parallel or sequential) takes place in layer III. In order to generate useful results, a clearly defined meaning of the term "structure" is required. The calculation of individual MA takes place in layer II, whereas the planned operating time (POT) is delivered from external systems (PPS) and the actual operating time (AOT) is delivered from each machine autonomously. That means, layer I delivers each individual machine status to layer II for calculation. Machine states are differentiated in "machine is running", "machine is stopped", "machine is in malfunction". Malfunction means, there is no OPC signal available. The real AOT is derived from machine status "machine is running" and defined by the time, the machine is actually producing parts actively. Ramping up or waiting for new material to arrive are not included in AOT. Layer II transfers the calculated individual MAs in a standardized form to Layer III, as a basis for the calculation of the linked MA on layer III.

Figure 7 summarizes all steps of the methodology applied to the Sola sample. Step 1 and step 2, described previously in detail, are illustrated on the right side of the figure, followed by step 3.

Figure 24. *Overview of Performed Steps for Exemplary KPI Generation for Machine Availability at Sola*

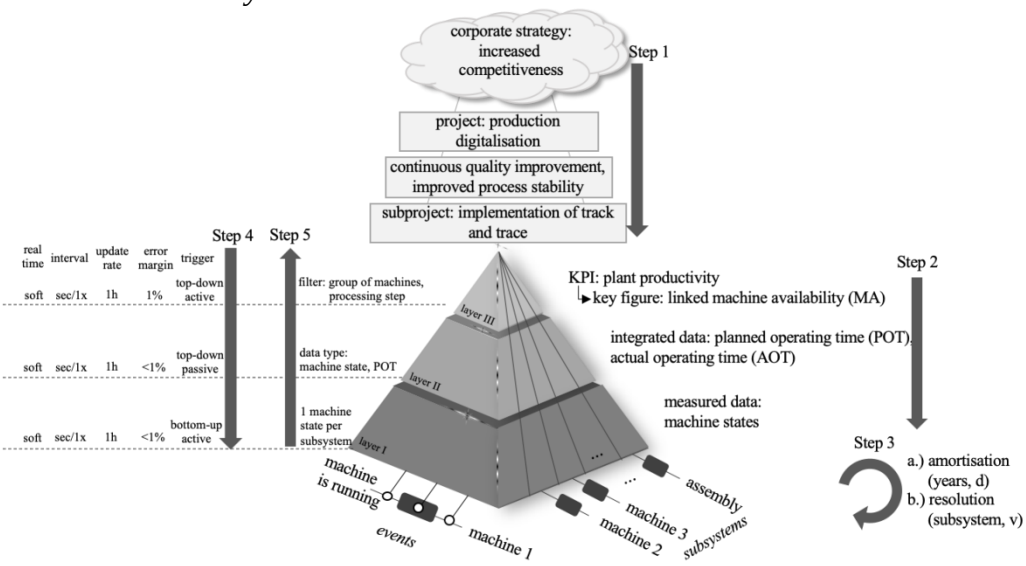

Step 3: Identification and Specification of Iteration Criteria

Several iteration criteria for top-down and bottom-up approach for Sola's example have been identified.

The type of criteria is either soft or hard, as explained in chapter 3. A unit is assigned to each hard iteration criteria (see term in brackets) as well as a differentiation is made between variable (v) and decisive character (d). A target value has to be added to the decision criteria.

For the sample set of Sola, the two most important iteration criteria, amortisation of the implementation and resolution have been selected.

Amortisation of implementation refers to costs in relation to benefit. The costs for implementation include the installation costs for sensor technology (hardware) as well as the expenses for database integration and maintenance as well as assigned, proportionate costs for already existing software architecture and systems (e.g., PDA in MES system).

The benefit refers to the improved transparency in production, which makes it easier to optimize production processes. The benefit is more difficult to quantify than the costs. Therefore, an estimation of benefit is essentially necessary here. For calculation the amortization it is important to have the same unit for both, costs and benefits.

The amortization is a function depending on resolution and quality. This signifies that the resolution has a fundamental influence on the amortization. For example, with increased resolution, i.e., resulting in more installed sensors, the costs increase proportional. This implies that it must be determined what benefits can be derived from an improved resolution. As a consequence, resolution is identified as a variable criterion (v), being adjustable in relation to each subsystem. In contrast, amortisation is a decision criterion (d), measured in years and used for countercheck. The amortisation's target value for indicating a successful iteration cycle has to be less than three years.

Step 4: Top-Down Approach – Definition of KPI Requirements for Each Layer

Starting in Layer III, the requirements for the KPI are defined. The real-time performance of the key figure "linked MA" in layer III is analysed as soft real-time. This means that real-time is required for the calculation of the key figure, but the time of value delivery is not that sensitive. The decisive factor is that the value is delivered. For example, for linked MA it does not have a huge negative effect whether the value is available at 6:00 pm or 6:30 pm, but a value delivery at 00:00 am is not acceptable. Interval is differentiated in logically shortest detection interval and critical minimum detection interval. For layer III and linked MA, the shortest detection interval is per second, as it is determined by the lower layers. The critical minimum detection interval depends on various influencing factors for the benefit. For example, if the shift influences the benefit of the implementation and thus the amortisation of implementation, it is necessary to evaluate the key figure once per shift. In the case of Sola, it is necessary to generate the key figure at least once per production batch. This also influences the update rate. Therefore, update rate is set to hourly, which means with every change in production batch. Margin of error refers to error tolerance. If error tolerance, as an iteration criterion, is set to 99%, the acceptable margin of error is 1%. For layer III, trigger response "top-down, active" means, that this layer actively requests new values for calculation from subordinate layer II.

This procedure is repeated for layer II and layer I. In layer II, the individual MA in standardised form is calculated. Its real-time performance is determined by the real-time performance of superordinate layer (layer III). Trigger response of layer II is "top-down, passive" because layer II does not send the information to layer III without a request.

Here can be highlighted that the newly applied methodology shows for layer I that no further sensor devices are required here for fulfilling the iteration requirements as the machine state signal is generated by the machine autonomously and actively forwarded to layer II for calculation. Hence, trigger response is "bottom-up, active".

Step 5: Bottom-Up Approach - Description of Layer Functionality in Detail

Starting with layer I, for calculation of the individual MA, the machine state (e.g., "machine is running") has to be delivered to layer II once per subsystem. In layer II, data from several sources is gathered, i.e., machine state from layer I and information about planned operating time (POT) from production planning and steering (PPS) system. This layer also required a definition of possible plausibility checks for data verification. For the example of individual MA, the machine state "machine is running" can be counterchecked on the one hand, by validating the machine state in accordance with the output counter signal. If machine is in state "machine is running" and parts are produced, the output counter signal has to increase. On the other hand, by summing up the three different machine states at the end of a day, the total time must meet exactly 24 hours.

For layer III, potential filters summarise information for further derivation, e.g., by gathering same types of machines or machines of the same processing step, an overall linked MA can be calculated to extend the expressiveness of the key figure.

With this step, the exemplary explanation of the developed methodology is completed.

If the definition of the criteria and the top-down and bottom-up approach is successful, implementation can be started immediately. If iteration criteria are not yet met, new iteration is necessary by adjusting one iteration criterion and applying the iterative method (top-down and bottom-up) once again in order to complete the KPI definition.

Conclusions

In many manufacturing companies, the users of data proclaim, that they do not have sufficient and transparent data for interpretation, analysis and evaluation. As a consequence, the users often start to place sensors by gut feelings at production level that generate more and more data and fill the data lake unstructured. Several sensors then deliver same or redundant information or, if they have a different resolution, they deliver different data at different time stamps. This leads to an exponential growth of databases as well as increasing costs and effort, and reduced controllability and transparency of the data lake. And single source of truth principle can't be warrantied.

In the last years, Sola implemented, besides the existing MES and ERP systems, in a structured manner a system for machine status feedback using the

OPC-UA standard. On this base a highly cost-effective solution for KPI generation by application of the new systemic methodology was found in collaboration.

The data lake mentioned in the title of this paper connects two worlds – the world of the process and its availability, and the world of IT with confidentiality as the highest priority. As previously described, for keeping the data lake small, lean and controllable, it is mandatory to have a systemic and stepwise procedure, based on production automation principles and applicable to each company-specific use case by bringing the hierarchical levels to IT and leading to an optimised choice of sensors investment in order to keep the payback time.

Derived from the overall corporate strategy, the novel methodology and its requirements of data consistency and single source of truth principle, simplifies the integration of the KPI into existing systems like MES or ERP.

Thus, filling the industrial data lake takes place in a methodological approach. This procedure delivers a specification for KPI generation. Therefore, the developed methodology provides a useful tool to generate KPI in compliance with the requirements for data analysis and storage.

The application of the methodology achieves among other things the following findings:

(1) How many sensors are needed where at the lowest level?
(2) Which processing programs are needed for the integrating layer (is MES or ERP needed and if so, which one?)
(3) What does this implementation cost, such as sensor installation or software integration?
(4) What specification does that KPI need to fulfil?

At Sola, the initiation phase for calculating the linked MA as a basis for generating the KPI OEE is performed. Currently, the installation of sensors at production level is completed and the integration of the generated data into the existing systems is in progress.

It was found out, that the application of the methodology leads to a target-oriented, solution-driven and cost-effective implementation.

Due to that, a Sola internal guideline describing the developed methodology was established (Gratt and Martin 2019). In the next step, the methodology is applied to other sections of the production line as well as to the other departments. Finally, the KPI specification data sheet can be used as blueprint for further derivation or modifications of related KPIs.

References

Bildstein A, Seidelmann J (2017) Migration zur Industrie- 4.0-Fertigung. (Migration to industrial 4.0 manufacturing). In *Handbuch Industrie 4.0 Bd. 1 Produktion*. Berlin: Springer Vieweg Germany, 227–242.

Boschi F, Zanetti C, Tavola G, Leitao P, Barbosa J, Pereira A (2017) From key business factors to KPIs within a reconfigurable and flexible cyber-physical system. In *2017*

International Conference on Engineering, Technology and Innovation (ICE/ITMC), Madeira Island, Portugal, 2017.

Gratt J, Martin B (2019) *Tracking and Tracing - Vorstellung Leitfaden zur Generierung von KPIs.* (Tracking and tracing - Presentation of company guidelines for the generation of KPIs). Götzis: Sola.

ISO – International Organization for Standardization: ISO 22400-1:2014 (2020) *Automation systems and integration — Key performance indicators (kpis) for manufacturing operations management — Part 1: overview, concepts and terminology: iso online browsing platform*, 2014. Retrieved from: https://www.iso.org/obp/ui/#iso:std:iso:22400:-1:ed-1:v1:en. [Accessed 5 June 2020.]

Kang N, Zhao C, Li J, Horst JA (2015) Analysis of key operation performance data in manufacturing systems. In *IEEE International Conference on Big Data (Big Data),* 2767–2770.

Kang N, Zhao C, Li J, Horst JA (2016) A hierarchical structure of key performance indicators for operation management and continuous improvement in production systems. *International Journal of Production Research* 54(21): 6333–6350.

Körner M-F, Bauer D, Keller R, Rösch M, Schlereth A, Simon P et al. (2019) Extending the automation pyramid for industrial demand response. In *52nd CIRP Conference on Manufacturing Systems*.

Kurth M (2020) *Smart Factory - Motivation und Einordnung.* (Motivation and classifiacation). N.p.p.: AKAD University.

Ohno T (1988) *Toyota production system - Beyond large-scale prodcution.* Cambridge Massachusetts: Productivity Press.

Schreiber S (2013) *Entwicklung einer Vergleichs- und Bewertungsmöglichkeit von dezentralen Steuerungsarchitekturen für Produktionssysteme.* (Development of a comparison and evaluation possibility of decentralized control architectures for production systems). Doctoral Thesis. Köln/Hamburg.

Schuster B (2018) Mehr Zeit für Innovationen durch Digitalisierung. (More time for innovation through digitization). In *Innteract Conference, Chemnitz*.

Sola Messwerkzeuge GmbH (2020) *Über Sola: Unternehmen.* (About Sola: the company). Retrieved from: https://www.sola.at/de-de/ueber-sola/unternehmen. [Accessed 5 June 2020.]

Sterman J (2000) *Business dynamics: systems thinking and modeling for a complex*. N.p.p.: McGraw-Hill Education Ltd.

Stricker N, Micali M, Dornfeld D, Lanza G (2016) Considering interdependencies of KPIs – Possible resource efficiency and effectiveness improvements. In *14th Global Conference on Sustainable Manufacturing, GCSM, Stellenbosch, South Africa*.

Athens Journal of Technology and Engineering - Volume 7, Issue 4, December 2020 – Pages 299-318

Implications of Market Penetration of Electric and Autonomous Vehicles for Florida State Transportation Revenue

By Alexander Kolpakov[*] & Austin Marie Sipiora[±]

Electric vehicle (EV) and autonomous vehicle (AV) technologies represent what seems to be beneficial, but potentially disruptive, shift in the way people and goods are transported. Wider use of EVs offers an opportunity to reduce harmful emissions, while widespread adoption of AVs has the potential to significantly improve vehicle safety, reduce congestion and impact vehicle ownership and travel habits. Since EVs do not consume petroleum fuels, they do not pay gas taxes that are used to fund transportation infrastructure. With EVs currently representing a small share of vehicle fleet, gas tax losses are minor, but as the market penetration increases, legislative bodies will encounter continuous pressure to address growing shortfall in transportation infrastructure funding. A study by the Florida Department of Transportation (FDOT) projected that the combined cumulative effect of increased EV and AV market penetration on total transportation revenue losses in Florida will reach $18.3 billion by 2048, including $5.3 billion loss from federal taxes, $9.7 billion loss from state taxes and $3.3 billion loss from local transportation taxes. Addressing these shortfalls may require to adjust motor fuel excise taxes to better reflect growing fuel economy, impose EV fees and taxes, implement mileage-based transportation fees or other funding models.

Keywords: *electric vehicle, autonomous vehicle, electric vehicle miles travelled, fuel efficiency, revenue loss*

Introduction

Widespread adoption of electric vehicles (EV) and autonomous vehicles (AV) are expected to have the most profound impact on transportation planning and investment since the invention of the automobile. Vehicle manufacturers and transportation providers around the world are investing substantial resources developing and refining these technologies. Significant changes can be expected in how we travel, what mode and vehicle type we use, how our goods are transported and how our living, working, and travel patterns are determined.

There is high uncertainty regarding how electric and autonomous vehicle technologies will develop, when their acceptance in the marketplace will occur, what additional investments may be needed to facilitate their adoption, what potential savings may be realized, and what impacts they may have on traditional

[*]Senior Research Associate, Center for Urban Transportation Research, University of South Florida, USA.
[±]Research Associate, Center for Urban Transportation Research, University of South Florida, USA.

transportation infrastructure funding sources. As such, there exists significant degree of risk with respect to what actions state governments should take to prepare for the ensuing implications on infrastructure needs and revenue funding flows. Such risks include the potential for underinvesting in required transportation infrastructure, resulting from underestimating the development of EV and AV technologies, or directing limited financial resources in areas that do not address future transportation needs.

To effectively plan for the influx of electric and autonomous vehicles and to create a transportation system for the future, transportation officials at the national and state levels must gauge the market penetration rate of these technologies and monitor how they will contribute to fleet fuel efficiency, vehicle miles travelled (VMT) and changes in travel habits, as well as forecast the impact of these new technologies on traditional infrastructure funding mechanisms.

The current paper summarizes the result of comprehensive market penetration analysis of EV and AV technologies in Florida and reports on projected impacts of these technologies on VMT and state transportation revenue collection. The long-range (30-year) forecast presented in this analysis was developed to assist Florida Department of Transportation (FDOT) in addressing future transportation infrastructure needs and revenue requirements as EV and AV market penetration rates increase.

Market Penetration Analysis and Literature Review

Electric Vehicles

In 2018, global electric vehicle, including EVs and plug-in hybrid electric vehicles (PHEV), sales exceeded 2 million units, with the United States being the third largest EV market in the world, following Europe and China (Loveday 2019). From 2011 through 2018, the global EV market averaged an annual growth rate of about 50%. Dramatic improvements in EV performance, safety, and reliability contributed to the increased adoption of these vehicles. In 2018, about 361,000 EVs were sold in the United States, representing 2% of national light-duty vehicle sales, with nearly half of EV sales taking place in California. In June 2019, U.S. EV sales reached approximately 2.5% of all light-duty vehicle sales (Loveday 2019). While the electric vehicle market share remains low, its compound annual growth rate ranged between 20% and 30% over the past seven years. This growth may slow, at least temporarily, as federal purchase incentives (up to $7,500 per vehicle) are phased out for manufacturers who exceed 200,000 EV sales. In 2018, Tesla and General Motors reached this threshold.

The U.S. EV stock continues to grow with vehicle sales but remains relatively low. Despite national sales growth, the current EV/PHEV stock is estimated at slightly over 1 million vehicles, or approximately 0.37% of the total light-duty vehicle stock (AAM 2019).

The major factors influencing EV market penetration relate to government policies, vehicle costs, consumer attitude and awareness, availability of EV

models, and fueling infrastructure. Major government policies that affect national EV sales include the California zero-emission vehicle (ZEV) program, the California Global Warming Solutions Act of 2006 that requires sharp reductions in greenhouse gas (GHG) emissions and a federal tax credit that provides up to $7,500 for purchasing EV/PHEVs, as well as CO_2 credits provided under the Environmental Protection Agency (EPA) Corporate Average Fuel Efficiency (CAFE) standards. Some states have also implemented various incentive and policy programs aimed at accelerating EV adoption, including grants, tax incentives, loans and leases, rebates, and exemptions. Incentives play a vital role in developing the EV market, particularly those that provide direct financial benefits to vehicle owners.

From a technological standpoint, the primary driver of EV/PHEV costs and sales is the battery cost. Between 2010 and 2018, the cost of automotive batteries (measured per kilowatt hour) decreased by 80%, from over $1,000/kilowatt hour (kWh) to approximately $200/kWh, and is projected to continue declining, potentially falling below $100/kWh by 2030 (Lutsey and Nicholas 2019). Industry experts believe that electric vehicles will be able to reach true price parity with traditional gasoline/diesel-powered vehicles when battery costs fall below $100/kWh, which is conservatively projected to occur between 2025 and 2030. Battery management systems and technology improvements are extending battery durability. Lithium-ion technology is projected to remain the primary technology for automotive batteries in the near future and will see further improvements in energy density and efficiency, making batteries smaller and lighter.

EV Market Projections

EV market penetration projections vary significantly from source to source. The Energy Information Administration (EIA) forecasts that sales of EV/PHEVs will exceed 1.1 million vehicles per year, accounting for 7% of all light-duty vehicle sales in 2025. EV/PHEV sales are also projected to reach 14% of annual vehicle sales in 2050 (EIA 2018). The National Renewable Energy Laboratory (NREL) forecasts that EVs will account for 20% of all light-duty vehicle sales in the United States in 2030. More aggressive forecasts place the share of EV sales at 35% of new light-duty vehicle sales in 2040, and up to 60% of all light-duty vehicle sales in 2050.

Overall, the reviewed EV sales forecasts imply short-to-medium-term (10–15 years) annual growth rates ranging from 20.6% to 25.1%, and long-term (20+ years) growth rates ranging from 7.5% to 16.0%. The projections regarding the stock of EVs found in the literature range from 7 million vehicles in 2025 to 15 million in 2030, and 41 million vehicles in 2040. Even the most aggressive forecasts, however, indicate that the electric vehicle fleet is not expected to exceed 15% of the overall U.S. vehicle stock in 2040.

Autonomous Vehicles

Although AV technology is still in the testing phase, there is a growing body of research focused on its impact on travel demand as measured by vehicle miles traveled. The Society of Automotive Engineers (SAE) International established functional definitions of AV capabilities, ranging from Level 0 to Level 5, where higher level describes wider range of functions that the vehicle can perform without human involvement. SAE levels of automation are described in Table 1.

Table 1. *Levels of Driving Automation*

<table>
<tr><th>SAE Level</th><th>Name</th><th colspan="2">Definition</th></tr>
<tr><td>0</td><td>No Automation</td><td colspan="2">The full-time performance by the human driver of all aspects of the dynamic driving task, even when "enhanced by warning or intervention systems"</td></tr>
<tr><td>1</td><td>Drive Assistance</td><td>The driving mode-specific execution by a driver assistance system of "either steering or acceleration/deceleration"</td><td rowspan="2">using information about the driving environment and with the expectation that the human driver performs all remaining aspects of the dynamic driving task</td></tr>
<tr><td>2</td><td>Partial Automation</td><td>The driving mode-specific execution by one or more driver assistance systems of both steering and acceleration/deceleration</td></tr>
<tr><td>3</td><td>Conditional Automation</td><td rowspan="3">The driving mode-specific performance by an automated driving system of all aspects of the dynamic driving task</td><td>with the expectation that the human driver will respond appropriately to a request to intervene</td></tr>
<tr><td>4</td><td>High Automation</td><td>even if a human driver does not respond appropriately to a request to intervene</td></tr>
<tr><td>5</td><td>Full Automation</td><td>under all roadway and environmental conditions that can be managed by a human driver</td></tr>
</table>

Source: Society of Automotive Engineers (SAE 2018).

AV Market Projections

The reviewed literature indicates that autonomous vehicles will likely enter the private vehicle market in a top-down pattern, first arriving in the larger and luxury car segments and only after that becoming available in the medium, small, and compact or pick-up vehicle categories. Level-4 functionality will initially become available in testing environments in 2020–2025 and will diffuse through vehicles of different categories by the early to mid-2030s. In the early 2030s, the smaller and lower-priced vehicle categories will include Level-4 capabilities. In the early 2030s, the Level-5 technology will debut in the larger and luxury segments. By the 2030–2040 timeframe, these features will be introduced into the

medium to compact vehicle market segments. Given the current technological developments and regulations, it can be expected that by 2035, Level 4-5 AV technology will encompass 35% of the private vehicle market share and anywhere from 11% to 14% of the private vehicle fleet.

One way AVs can affect vehicle travel demand is through supplying shared mobility services to the currently underserved, including youth, the elderly, and those with driving-prohibitive medical conditions. The shared mobility concept, which enables users to gain short-term access to transportation on an as-needed basis, is gaining popularity, especially with the younger generation of drivers. Recent developments in vehicle automation create additional opportunities for a wider adoption of the shared vehicle model. If fully autonomous vehicles become a reality, they can be used more efficiently to provide mobility to multiple users.

The literature review indicated that the estimated impact of new travel demand from the underserved population can result in a 2% to 14% increase in VMT (Harper et al. 2016).

Florida Market Penetration Analysis – EVs

The market acceptance of EVs depends on many factors, including demographics and socioeconomics, geography and climate, gasoline and electricity pricing, charging infrastructure availability, government incentives, as well as consumer perception, personality, and social influences.

During the past 20 years, Florida's population grew almost twice as fast as the overall population of the United States and that trend is expected to continue. Additionally, Florida's population density is significantly higher than the national average and future growth in Florida is expected to concentrate mainly within urban areas. Population growth and density are expected to have a positive effect on the adoption of plug-in electric vehicles (PEVs) in the state.

In addition to demographic, socioeconomic, and population factors, geography and climate considerations could affect EV growth, though to a lesser degree. Climate and regional temperature variation can affect the performance, efficiency, and range of EVs, which depends on battery capacity and vehicle efficiency. With its subtropical climate, Florida experiences the highest average annual temperature compared to other states. Due to its climate and temperature patterns, Florida yields some of the most optimal energy efficiency and EV range in the country, making it a favorable market for electric vehicle adoption.

Battery electric vehicles make up a greater share of electric vehicle sales in Florida than in most other states. As of June 2018, Florida battery electric vehicle sales accounted for 61.3% of total plug-in electric vehicle (PEV) sales, which is higher than the national average share of 51.3%. During the period of 2013–2018, Florida's PEV sales grew at an average annual rate of 20% per year, faster than other non-zero-emission vehicle states, which grew at an average annual rate of 16.5%. In 2018, approximately 42,962 plug-in electric vehicles were registered in the state, including 17,807 plug-in hybrid-electric and 25,155 battery electric vehicles (AAM 2019).

EV infrastructure availability is often cited as an important factor in accelerating PEV adoption. Florida's network of electric vehicle charging infrastructure continues to grow rapidly. As of August 2019, there were more than 3,300 charging outlets, including 1,139 Level 2 charging locations (with 2,640 ports) and 163 fast charging stations (with 630 ports) (AFDC 2019). While Florida has roughly 3.6% of the national stock of electric vehicles, its Level 2 and fast chargers account for approximately 5.0% of the national EV charging infrastructure. The state is expected to add an additional 530 public EV charging stations through 2022 as a result of the Duke Energy Park and Plug Program.

At present, Florida lacks any rebate, grant, or tax incentive program to accelerate PEV adoption. However, in recent years state electric utilities began offering rebate and incentive programs incentivizing PEV ownership and lowering the installation cost of charging infrastructure.

Overall, there are a number of positive factors that contribute to Florida's increasing growth in PEV sales, including favorable climate, a greater preference for automobiles over light trucks than most other states, relatively low electricity costs, and a relatively high population density to support the developing vehicle charging infrastructure. Factors that may inhibit PEV growth, or delay growth until PEV costs decline, include lower than national average household incomes, a large sector of lower wage service jobs, and relatively few state and local incentives, including non-participation in the Zero-Emission Vehicle Program.

Florida Market Penetration Analysis – AVs

Various studies project that by 2030, AVs will make up around 18.5% of the U.S. vehicle fleet. The share will gradually increase to 25.4% in 2035 and 30.0% by 2040. The reviewed literature suggests that by 2045, approximately 43.0% of the U.S. fleet may consist of AVs, and that by 2050 AVs can make up almost half of the nation's vehicle fleet (Bansal and Kockelman 2017, Bierstedt et al. 2014, Trommer et al. 2018).

Several state-specific factors may impact Florida's AV adoption rates to diverge from these national trends, including population age, income level, education level, and urban density. Several studies find that AV acceptance is positively associated with a younger population (Haboucha et al. 2017, Nielsen and Haustein 2018, Schoettle and Sivak 2014), higher income levels (Howard and Dai 2014, Kyriakidis et al. 2015, Zmud 2016), higher levels of education (Haboucha et al. 2017, Nielsen and Haustein 2018), and urban environments (Nielsen and Haustein 2018, Bansal and Kockelman 2017, Nordhoff et al. 2018). According to the U.S. Census Bureau, the median household income measured in Florida in 2012–2016 was $48,900 in 2016 dollars (US Census 2018), relatively lower than the national median of $55,322. On the other hand, the distribution by income levels in Florida is similar to the rest of the country. Assuming some similar accessibility to AVs across different income groups, it will be difficult to discern a clear relationship between income levels and AV VMT.

Florida's population currently includes a larger percentage of persons 65 and over compared to the rest of the United States. According to the U.S. Census, as of

July 2017, 20.1% of Florida's population is 65 and over, compared to 15.6% nationally. The Bureau of Economic and Business Research (BEBR) projects that by 2040, this group will represent about a quarter of the state's population. Based on the existing demographic characteristics and BEBR projections, and assuming the association between AV acceptance and age remains constant, it is expected that these population forecasts will result in a somewhat more moderate AV market acceptance in Florida compared to national trends.

New mobility options exist in population-dense, urban areas, which provide the opportunity for economies of scale. Nine of the large and population-dense metropolitan areas in the United States contain 70% of Uber and Lyft trips (Schaller 2018). Florida is more densely populated than the rest of the country, with a population density of 350 persons per square mile compared to a national average of 87 persons per square mile. Florida is also the eighth most population-dense state. Combined with the population growth that is faster than the national average, this makes urban Florida among the fastest growing areas in the nation, increasing the likelihood of options such as shared mobility services provided by transportation network companies (TNCs).

TNCs may lead individual adoption by providing mobility services in the form of shared autonomous vehicles (SAVs) or pooled autonomous vehicles (PAVs), which are SAVs that may pick up other passengers en route. Interest of TNCs in implementing practical AV solutions combined with reduced individual willingness to own vehicles, suggests that TNCs may be primary early adopters of AV technologies.

Methodology

The analysis presented in the current paper is based on forecasting total state VMT and VMT driven on electric propulsion (eVMT) during the period from 2018 through 2048. This involves estimating market penetration of EVs in Florida fleet during the 30-year projection period based on the national trends and Florida-specific factors that affect the adoption of electric and autonomous vehicle technologies.

Florida VMT estimate is produced by adjusting 2017 FHWA 30-year national VMT forecast for light-duty (LD) vehicles, single-unit trucks (SUT), transit buses and combination trucks (CT) to Florida-specific socio-economic factors that are assumed to affect VMT generation, including population growth, growth in real GDP, growth in disposable income per capita and gasoline prices. The forecasting approach assumes that Florida VMT growth will follow the general pattern of the U.S. VMT, growing faster during the first 20-year period and slowing down during the last 10 years of the 30-year projection period.

Electric VMT projections are obtained by combining forecasted number of electric vehicles in three vehicle subcategory (passenger vehicles, single-unit trucks and buses, combination trucks) with projected VMT per electric vehicle. The per-vehicle eVMT estimates are based on the assumptions regarding the shares of battery-electric vehicles (BEV) and plug-in electric vehicles (PHEV) in

Florida EV fleet, as well as the estimated electric range of these vehicles during the 30-year forecast period. Autonomous vehicles are not expected to account for a significant portion of VMT until at least 2035.

All forecasts are generated using modeling techniques consistent with the ones currently employed by the state of Florida (with minor adjustments to address the goals of the assessment) and are based on publicly available data and research results from reputable sources, such as FHWA, U.S. DOT, U.S. Department of Energy (DOE), National Renewable Energy Laboratory (NREL), EPA, FDOT, etc.

Florida Office of Economic and Demographic Research Revenue Estimating Conference (REC) produces forecasting for economic, demographic, and revenue impacts to inform the development of planning and budgeting for state resources. The current analysis incorporates REC assumptions for the period of state fiscal year 2018–2019 through 2027–2028 for the purposes of consistency with state forecasts and demographic assumptions, with the exception of REC projections for current and future miles per gallon (MPG) levels. Projections beyond 2028 utilize the same approach employed by REC, with minor adjustments.

Estimating fleet fuel efficiency is based on modelled state fleet mix and reflects the smaller share of combination trucks in Florida than is found nationally - approximately one-third less compared to national share. While the percentage change in combination truck VMT share is small (1.8%), the effect on revenue impact is considered to be a material factor since combination trucks on average consume four times more fuel per VMT compared to LD vehicles.

Results

Under baseline VMT growth forecast, total Florida VMT is projected to reach 335.9 billion annually by the year 2048. Under high VMT growth scenario, VMT is forecasted to be as high as 379.9 billion. The low growth scenario results in VMT projection of 295.1 billion per year in 2048.

The projection of the number of EVs in Florida, in comparison with the national EV market, employs a weighted index approach, similar to the one that has been used for baseline VMT projections in the state. Key macroeconomic parameters that are used as predictors of EV market development in Florida include growth in disposable income per capita, gasoline prices, availability of government EV rebates/incentives, residential electricity rates, and prices of photovoltaic panels in Florida in comparison to national averages.

eVMT Forecasting

Total electric VMT in Florida is estimated by combining the projections of the number of EVs in Florida with the forecasted average annual eVMT per electric vehicle. Separate eVMT projections were developed for each subcategory of vehicles in the fleet (LD, SUT and buses, CT). Total eVMT in Florida is

projected to reach 47.5 billion by 2048, accounting for about 14.0% of the overall VMT in the state.

Table 2 presents the summary of the forecasted eVMT in Florida during the period from 2020 through 2048.

Table 2. *Projected eVMT Forecast for Florida (2020–2048)*

eVMT Forecast (Millions)				
Year	**Total**	**Light-duty**	**SUT/B**	**Combination Trucks**
2020	**559.6**	559	0.5	0.0
2025	**2,893**	2,873	19.2	0.5
2030	**6,629**	6,564	48.9	16.7
2035	**11,669**	11,451	160.0	57.6
2040	**20,039**	19,358	482.2	198.7
2045	**34,573**	32,372	1,515.2	686.0
2048	**47,502**	43,010	3,049.7	1,442.7

AV Impact on VMT and Fuel Economy

This analysis projects a rather modest penetration rate of AV technologies. AVs are not expected to account for a significant portion of VMT until at least 2035. By 2035, VMT from AVs is projected to account for 3.8% of total Florida VMT, increasing to 7.29% of total Florida VMT by 2040 and 14.56% of total Florida VMT by 2048. The analysis assumes that all AV VMT in Florida will be eVMT from light-duty vehicles.

Autonomous vehicles are expected to drive more VMT per vehicle compared to other vehicles due to reduced cost of travel offered by AV technologies and likely use of AVs for ride sharing applications. Autonomous driving is projected to increase the average eVMT per electric vehicle by 35% starting from 2035.

Starting from 2029, AVs are projected to generate noticeable impact to VMT generation in Florida. In 2035, implementation of AV technologies is projected to add 0.6 percentage points to annual growth rate of VMT in Florida. By 2040, AV technologies will be responsible for adding 0.8 percentage points to annual VMT growth of 1.1%, accounting for 42.1% of the overall VMT growth in that year.

Total VMT from AVs in Florida is projected to reach 11 billion VMT by 2035, 22.6 billion VMT by 2040, 45.7 billion VMT by 2045 and almost 49.0 billion VMT by 2048. Figure 1 presents forecasted Florida VMT under different growth scenarios, accounting for the impact of AV technologies.

Figure 1. *Projected Florida VMT with AV Impact*

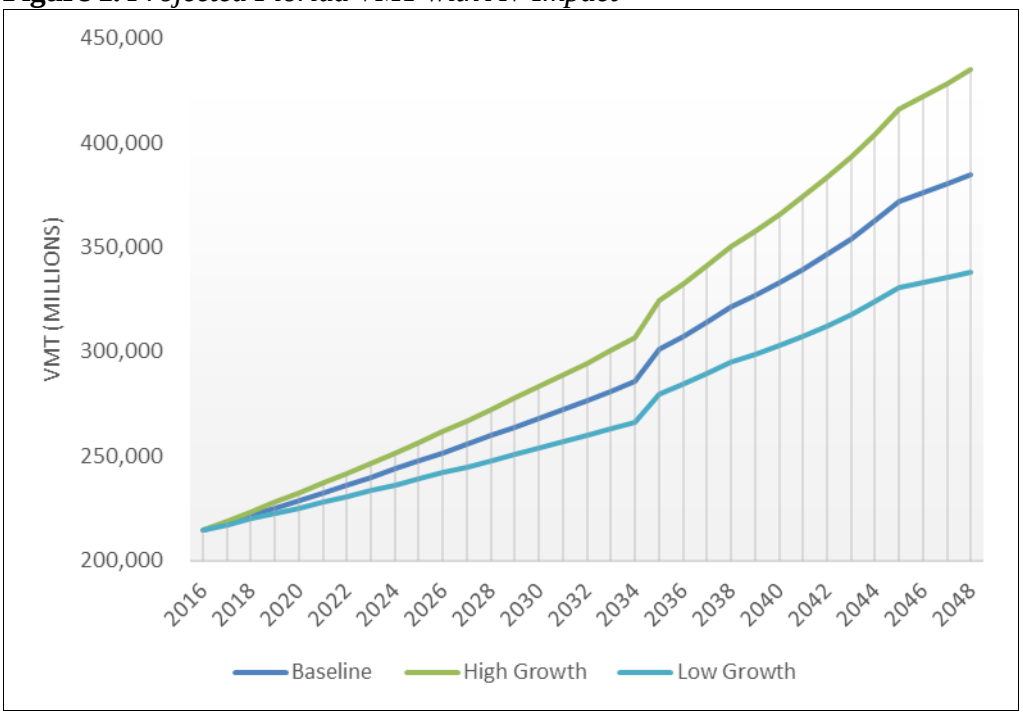

Projected Growth in EVs

The current analysis projects that the number of EVs will increase in Florida from 43,000 units in 2018 to 278,275 units in 2025 and over 3.6 million by 2048, with the majority of those vehicles to be concentrated in the higher density metropolitan areas. Light-duty vehicles are expected to account for the vast majority of EVs in Florida through the entire projection period, and will account for 93.0% of the total Florida EV fleet in 2048. The current approach also forecasts that by 2048, 18.0% of single-unit trucks and 10.0% of semi-trucks in Florida will be battery-electric.

Overview of Florida Transportation Revenue Sources

In 2017, $7.8 billion in transportation taxes and fees were collected in Florida. This consisted of $2.6 billion in federal fuel, heavy truck, and aviation taxes, $1.4 billion in local option fuel taxes and state fuel taxes that are dedicated for local use, and $3.9 billion in state fuel taxes, vehicle-related fees, and impact fees. Approximately one-half of these revenues are collected for state purposes, one-third - for federal, and one-sixth by and for local governments. Federal highway funds are appropriated to state highway departments and transit funds to state and local entities (FDOT 2017).

Taxes based on motor fuel consumption accounted for 72% of total collections. As of January 1, 2019, the combined rate for federal, state and local motor fuel taxes in Florida totaled 56.7 cents per gallon on diesel and ranged from 50.3 cents to 56.3 cents per gallon on gasoline based on the level of local option

gasoline tax levies in individual counties. Statewide, gasoline taxes averaged 54.0 cents per gallon. These rates include the January 1, 2019, 0.6 cents per gallon state motor fuel taxes increase as a result of annual consumer price index (CPI) adjustment provisions.

In 2017, federal, state and local transportation taxes and fees generated approximately 3.6 cents per mile of vehicle travel in Florida: 1.2 cents per mile from federal taxes, 1.6 cents per mile from state taxes and 0.6 cents per mile from local taxes. Of this total, the motor fuel tax collections accounted for approximately 2.6 cents per mile: one cent each from federal and state taxes and 0.6 cents from local taxes (FDOT 2017).

State Revenue Impact from EV and AV

In general, the growth in eVMT is expected to reduce demand for gasoline and diesel fuel and, in turn, negatively affect revenue generation. Lost motor fuel tax revenues resulting from the increasing use of battery electric vehicles and plug-in hybrid electric vehicles are expected to have a significant impact on transportation revenues over time, assuming the present transportation tax structures in Florida remain unchanged. This impact will remain relatively small in comparison to total transportation revenue collections until the time when EV fleet reaches significant numbers and approaches parity with internal combustion engine (ICE) vehicles.

A number of factors tend to lessen the initial impact of EV/PHEV and eVMT on transportation revenue losses, including average miles driven, utility factor and average fuel economy of vehicles replaced by EVs.

Average Miles Driven

A report from the California Air Resources Board indicated that, while owners of PHEVs drove on average a similar number of miles when compared to traditional ICE vehicle users, battery electric vehicles were driven approximately 80% of ICE annual vehicle miles (CARB 2017). This difference is likely due to current range and recharging limitations with EVs that should lessen over time as battery capacities increase and more recharging options become available.

Utility Factor

An analysis of PHEVs purchased in the U.S. in 2016 indicates an average utility factor (the percentage of eVMT to total miles driven) of 0.52, meaning that 48% of miles driven were powered by an internal combustion engine and consuming motor fuel (EPA 2016). With a utility factor of 0.52, the effect of PHEVs on lost consumption of motor fuel per vehicle is approximately one half of the total motor fuel that would have been consumed by the ICE comparable vehicle. Utility factors are expected to increase as battery costs fall and higher capacity batteries are installed in PHEVs. Additionally, as battery-electric vehicles (EV) represent larger percentage of plug-in electric vehicle (EV and PHEV) sales, the average utility factor of the electric vehicle fleet will increase.

Age and Fuel Economy of Vehicles Replaced by EVs

New cars and trucks are typically more fuel efficient than the average of the entire state fleet of registered vehicles, which contains a large percentage of older, less efficient vehicles. For example, new cars and trucks sold in 2017 were, on average, 19% more fuel efficient than vehicles sold ten years prior. It has been noted that, EV purchases are often offsetting more efficient vehicles compared to the average efficiency of the state's vehicle fleet, given that available EVs tend to be comparable in size to smaller, more efficient ICE vehicles. An analysis of 2017 vehicle sales suggested that EV vehicles replaced ICE vehicles that averaged 1.4 MPG, or 5.5% greater efficiency than the average MPG for all car and light truck sales in that year. This results in fewer gallons of motor fuel not consumed relative to vehicle miles traveled than is found for the statewide vehicle fleet on average, and the corresponding reduction in motor fuel taxes not levied are less than the state average per average car.

EV Impact on Motor Fuel Consumption

Improvements in conventional vehicle technology and emission regulations result in continuing improvements in vehicle fuel economy. As vehicle fleet becomes more efficient, it consumes less fuel resulting in less fuel tax revenue for the state. The effect of fleet fuel efficiency improvements is moderated by the growth in the number of vehicles and increases in VMT. Depending on the magnitude of the effects of VMT, size of the fleet and average vehicle efficiency, the resulting fuel consumption can either decrease or increase. The increase of the number of battery-electric vehicles in the fleet can result in the increase in the average fuel economy of the entire fleet and cause reductions in the consumption of motor fuel.

Figure 2 demonstrates the impact of EVs on projected fuel consumption in Florida over the 30-year period. The projection shows, that without EVs in the fleet, motor fuel consumption in Florida is projected to continue growing throughout the entire 30-year projection period (due to the effects of VMT and fleet size), but at a decreasing rate (due to the effects of fuel efficiency improvements). EVs cause a faster decline in the fuel consumption growth rate. Starting from 2033–2034, the use of EVs is projected to result in a consistent reduction in the amount of motor fuel consumed annually in the state.

Figure 2. *eVMT Impact on Fuel Consumption Forecast (2018–2048)*

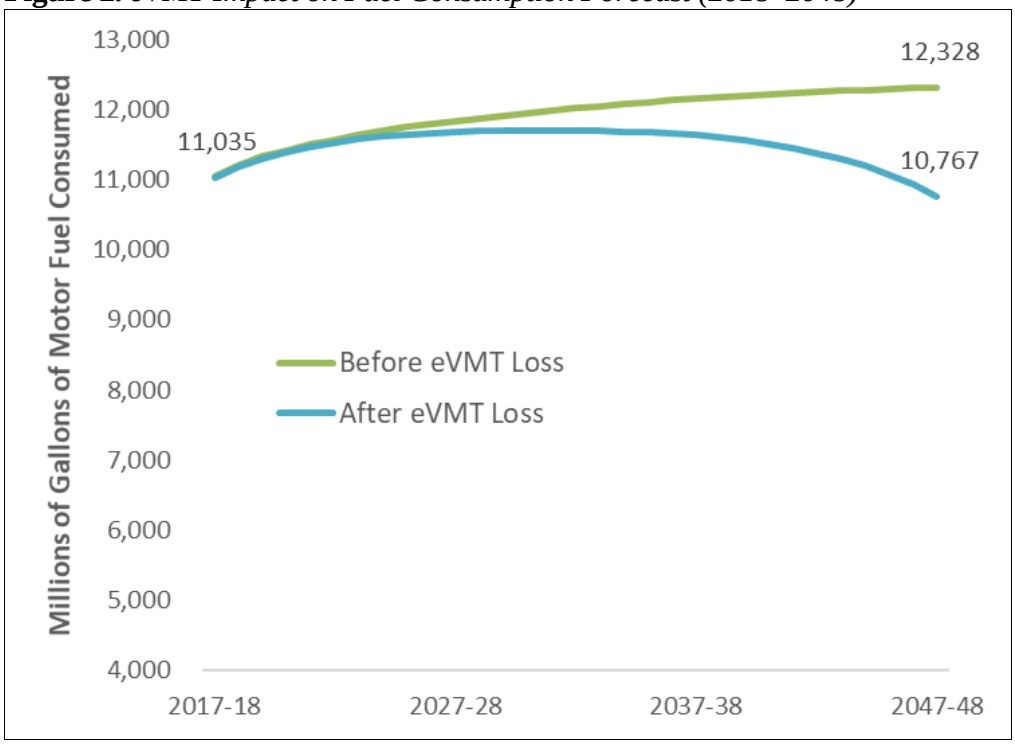

Average fuel economy of the fleet can be affected by multiple factors, including CAFE regulations, improvements in propulsion technology and vehicle materials, use of alternative fuels and other factors. Even with no EVs, Florida fleet fuel efficiency is projected to increase by almost 36.0% during 30-year forecast period, from 19.98 MPG in 2018 to 27.13 MPG in 2048. The use of EVs, that are projected to enter the fleet in large numbers after 2030, will accelerate average fleet fuel efficiency growth. Adoption of EVs is forecasted to add 1.01 MPG (an increase of 4.1% over base fuel efficiency) to the average fuel efficiency of the Florida fleet by 2037 and 3.93 MPG (an increase of 14.5% over base fuel efficiency) to the average fuel efficiency of the fleet by 2048.

Projected Revenue Loss Attributed to EV

In 2018, Florida's transportation tax revenue losses due to reduced motor fuel consumption from EV use were estimated at $17.5 million per year, including $6.4 million in Florida federal tax, $7.0 million in state transportation tax and $4.2 million in local use transportation tax collections. While tax revenue losses have been small to date, the loss rate from EV use is projected to increase over time, rising on a percentage loss basis from 0.2% of fuel tax revenues in FY 2019–2020 to 1.7% by the end of FY 2029–2030. Annual revenue losses are projected to increase from $9.5 million in FY 2019–2020 to $121 million by FY 2029–2030. Cumulative tax revenue losses in Florida through FY 2029–2030 are projected to total over $583 million, including $194 million federal taxes, $263 million state taxes and $127 million in local use taxes. The state share of total losses increases

from 41.4% in FY 2019–2020 to 46.6% in FY 2029–2030 as state fuel taxes are annually adjusted to CPI while federal and local taxes are not.

An approximate nine-fold increase in the percentage share of motor fuel tax revenue lost from plug-in vehicle use is projected to occur from 2028–2029 through 2047–2048. By 2048, the percentage share is estimated to increase to nearly 13% loss in revenues, totaling $1.2 billion annually, with $651 million per year, or 56%, of the total losses coming from Florida state fuel taxes. Figure 3 demonstrates projected fuel tax revenue loss for the state of Florida through 2048.

Figure 3. *Lost Fuel Tax Revenue from Plug-in Vehicle Use through 2048*

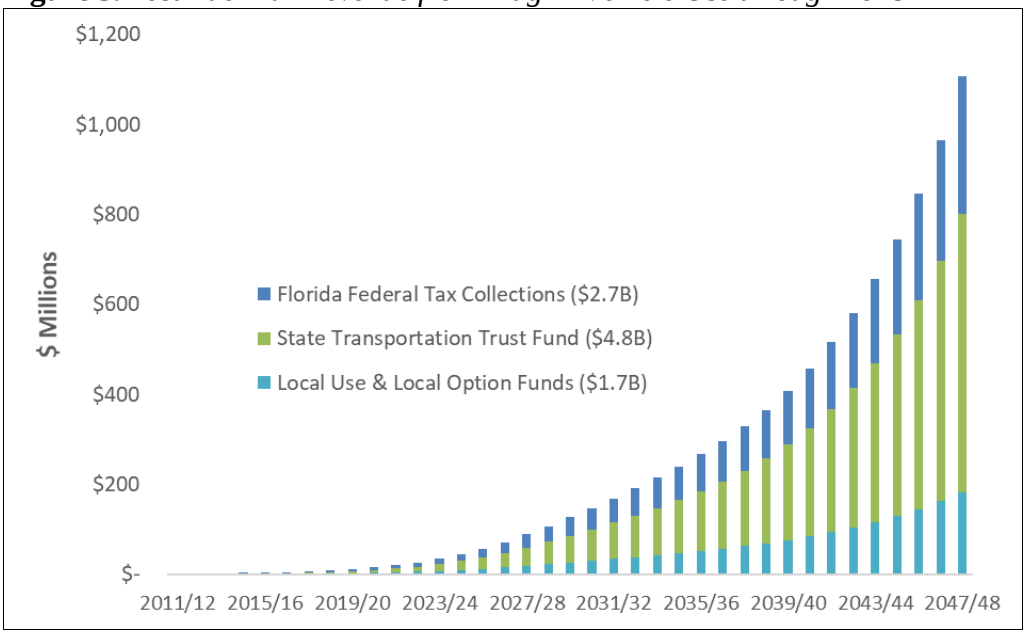

AV Impact on VMT

Vehicle automation is not expected to have a significant effect on VMT generation in Florida in the next decade. While many manufacturers are actively working on implementing AV technologies, significant technological and regulatory challenges remain.

The implementation of AV technologies will likely take evolutionary path. Initially, AV technologies will likely be available on high-end vehicles or as paid options. It is projected, that until 2050, less than 50% of vehicles on the road will have full automation capabilities.

Projected Revenue Losses Attributed to AV

Since AV technologies are not projected to constitute a relatively noticeable share of the state fleet at least until 2030–2035, revenue loss from AV VMT is expected to be insignificant during the first half of the 30-year forecast period. In FY 2029–2030, total annual funding shortfall from AV VMT is projected to be $3.8 million, including $1.4 million loss from federal fuel taxes, $1.7 million from

state fuel taxes and $0.6 million from local taxes. This annual shortfall is projected to grow to $119.5 million in FY 2034–2035, $453 million in 2039-2040 and $1.2 billion in 2047–2048. The cumulative impact of AV VMT on total Florida fuel tax collection shortfall is projected to reach $8.9 billion, in constant 2018 dollars, for the entire projection period of 2018–2048, including $2.5 billion loss from federal taxes, $4.8 billion loss from state taxes and $1.6 billion loss from local taxes.

Combined EV and AV Effect on Florida Transportation Revenue

While the impact of electric and autonomous vehicles on the overall fleet fuel efficiency are expected to be rather small during the first half of the 30-year forecast period, EVs and AVs are expected to result in a noticeable increase in the fuel efficiency of Florida fleet after 2035. By 2040, EVs are expected to add 1.39 MPG to the average fuel efficiency of the fleet while AVs are expected to add 1.83 MPG to the average fuel efficiency of Florida fleet. By 2048, EVs and AVs combined, are projected to add 8.42 MPG to the average fuel efficiency of Florida fleet (3.93 MPG from EV impact and 4.49 MPG from AV impact).

Over the period of 2018–2048, the combined cumulative impact of EV and AV market penetration on total Florida transportation revenue collection is projected to reach $18.3 billion, including $5.3 billion loss from federal transportation taxes, $9.7 billion loss from state taxes and $3.3 billion loss from local transportation taxes. Figure 4 demonstrates the combined projected effect of EV and AV technologies on Florida state transportation tax revenues.

Figure 4. *Combined Revenue Losses in State Fuel Taxes from EV and AV Market Penetration in Florida*

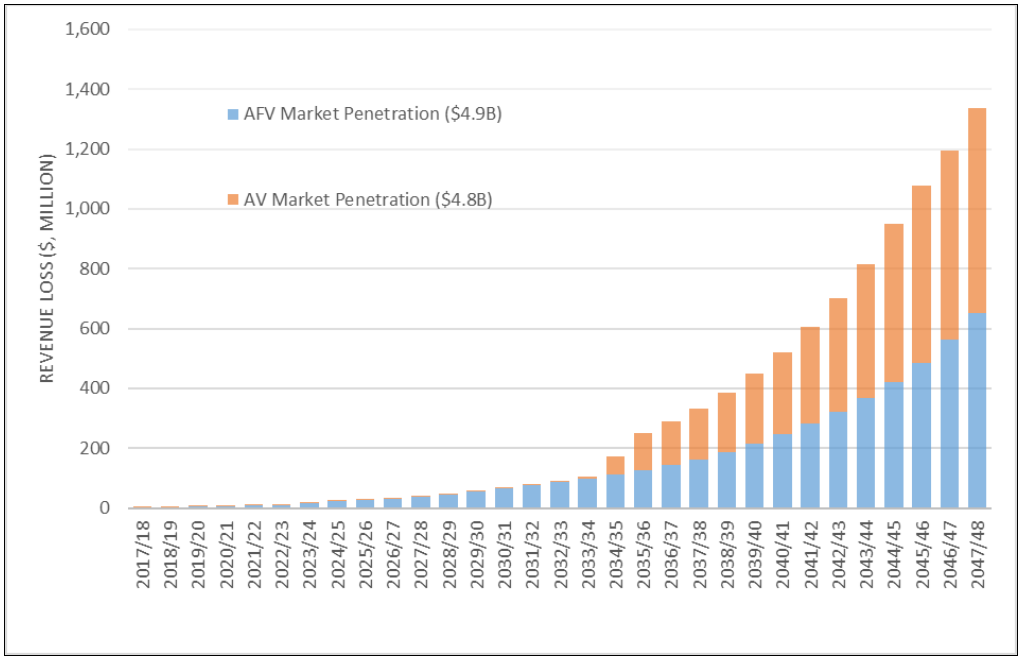

At the end of FY 2027–2028, lost revenues are projected to reach 1.3% of fuel-based state transportation tax collection. Rapid growth in EV and AV adoption is projected to increase state revenue losses to about 26% of the fuel-based transportation tax revenue in Florida by 2048.

These losses do not include potential reduction in capital and operating costs that AV might generate by roadway capacity improvements from cooperative driving. Recent simulation-based studies show potential capacity improvement ranging between 10% and 30% from high AV market penetration (60–100%) (Fagnant and Kockelman 2015).

Policy Considerations

Transportation infrastructure in the U.S. is funded by fuel taxes. Every gallon of diesel or gasoline sold is taxed and the proceeds from these taxes are used to build and maintain roads. Electric vehicles do not consume gasoline or diesel and, thus, do not contribute to gas taxes. Motor fuel-based taxes, which historically have served as an effective and administratively efficient surrogate for a user-fee based collection system, are becoming increasingly less effective in this role as vehicle fuel efficiencies continuously increase and as non-motor-fuel powered vehicles are adopted in greater numbers.

If the current trends in vehicle electrification and automation continue, government entities in Florida (as well as other states) will have to face increasing deficits in transportation revenues due to higher adoption of EV and AV technologies. Even if EV/AV adoption remains relatively low, the projected improvement in fuel efficiency of conventional vehicles alone will present significant challenges for traditional infrastructure funding model by continuing to erode gas tax revenues.

Some of the potential policy options that may help address tax revenue shortfalls, include: 1) adjusting gas taxes to address growing fuel efficiency of vehicles, 2) implementing EV fees and taxes, 3) implementing road use fees, or VMT fees, that are not based on fuel consumption, 4) employing public-private partnerships (PPP) to construct transportation infrastructure, and other approaches.

All of these approaches have their advantages and limitations that need to be evaluated carefully. Gas tax adjustment is relatively easy to implement, but such a measure is unlikely to provide a long-term solution (can only be effective in short-to-medium term). EV fees and taxes are very unpopular with EV owners and will face strong opposition from the growing number of EV customers. VMT fees, while providing equitable treatment of all road users, regardless of vehicle fuel efficiency, fuel or propulsion type, also have privacy implications that extend beyond the issue of revenue collection and allocative efficiency that will have to be addressed. PPP model for funding transportation infrastructure often faces negative public perception since it allows the private sector to profit from the public-sector investment. Finally, some of these options will involve uphill political battles, so their implementation and success will depend heavily on political will and the ability of decision-makers to demonstrate the urgency of proposed measures.

Conclusions

Although currently EVs have a relatively small impact on Florida state transportation revenue, fuel tax revenue losses from increased electric VMT are projected to increase from $9.5 million in FY 2019–2020 to $121 million by FY 2029–2030, totaling over $583 million for the ten-year period. The increased adoption of EVs, that will likely reach critical mass by 2030–2035, is projected to result in substantial tax revenue losses. By 2048, the total loss of tax revenue associated with the use of EVs is projected to reach $1.2 billion annually.

Tax revenue loss from AVs is projected to be insignificant during the first half of the 30-year forecast period but will accelerate in later years, reaching $969 million in 2044–2045. The period 2027–2028 through 2047–2048 will see increased AV adoption and market penetration, which will accelerate revenue losses. The cumulative impact of AV VMT on Florida transportation funding shortfall is projected to reach almost $9.0 billion, in constant 2018 dollars, for the period of 2018–2048.

The combined effect of increased EV and AV market penetration on total transportation revenue collection in Florida is projected to reach $18.3 billion for the entire period of 2018–2048, including $5.3 billion loss in federal transportation taxes, $9.7 billion loss in state transportation taxes and $3.3 billion loss in local use and local option taxes. At the end of FY 2027–2028, lost revenues due to the adoption of EV and AV technologies are not expected to exceed 1.3% of total fuel-based tax collections. By 2048, the projected rapid increase in EV and AV adoption in Florida will substantially increase revenue losses that are forecasted to reach 26% of the total fuel-based transportation revenues in Florida. Given the constantly growing transportation revenue shortfall, there will be continuous pressures on future legislative bodies to increase tax and fee rates or transfer funds away from other programs and into transportation, or to accept the consequences of degradation in transportation service levels.

In addition to gas tax revenue losses due to increased eVMT, wider adoption of EVs and AVs may require additional infrastructure investment to accommodate these technologies. For example, adequate public charging infrastructure will be required to support a large EV fleet. Additionally, upgrades to pavement markings and signage may be needed to enable vehicle automation technologies to recognize lane boundaries, pavement edge and road signs in all weather conditions.

It is expected that most of the benefits of AV adoption will be realized only after a large share of vehicles on the road are equipped with automation technologies. Similarly, the infrastructure investment requirements associated with AV technologies are expected to be rather minor in the short-to-medium term. The need for a relatively significant amount of infrastructure investment to address AV technologies will likely arise after 2040.

Future legislative bodies will encounter continuous pressure to increase tax and fee rates or transfer funds away from other programs and into transportation. While federal, state, and local legislative bodies in the U.S. have demonstrated a propensity in recent years to partially accommodate transportation funding shortfalls, continued ad hoc adjustments may become increasingly difficult to

achieve as vehicle fuel efficiency continues to improve and EVs and AVs gain market share.

References

AAM – Alliance of Automobile Manufacturers (2019) *Advanced technology vehicle sales dashboard*. Retrieved from: https://autoalliance.org/energy-environment/advanced-technology-vehicle-sales-dashboard/. (Accessed 15 March 2019.)

AFDC – Alternative Fuels Data Center (2019) *Alternative fueling station locator*. U.S. Department of Energy. Retrieved from: https://afdc.energy.gov/stations/#/find/nearest. (Accessed 21 April 2019.)

Bansal P, Kockelman KM (2017) Forecasting Americans' long-term adoption of connected and autonomous vehicle technologies. *Transportation Research Part A: Policy and Practice* 95: 49–63.

Bierstedt J, Gooze A, Gray C, Peterman J, Raykin L, Walters J (2014) *Effects of next-generation vehicles on travel demand and highway capacity*. Retrieved from: https://orfe.princeton.edu/~alaink/Papers/FP_NextGenVehicleWhitePaper012414.pdf(Accessed 22 January 2019.)

CARB – California Air Resources Board (2017) *Midterm review report: advanced clean cars*. Sacramento, CA: CARB.

EIA – U.S. Energy Information Administration (2018) *Annual energy outlook 2018 (AEO 2018)*. Washington, DC: Office of Integrated and International Energy Analysis.

EPA – Environmental Protection Agency (2016) *Light-duty automotive technology, carbon dioxide emissions and fuel economy trends: 1975 through 2016*. EPA.

Fagnant D, Kockelman K (2015) Preparing a nation for autonomous vehicles: opportunities, barriers and policy recommendations. *Transportation Research Part A: Policy and Practice* 77(Jul): 167–181.

FDOT – Florida Department of Transportation (2017) *Transportation funding sources*. Tallahassee: Office of the Comptroller.

Haboucha C, Ishaq R, Shiftan Y (2017) User preferences regarding autonomous vehicles. *Transportation Research Part C: Emerging Technologies* 78(May): 37–49.

Harper CD, Hendrickson CT, Mangones S, Samaras C (2016) Estimating potential increases in travel with autonomous vehicles for the non-driving, elderly and people with travel-restrictive medical conditions. *Transportation Research Part C: Emerging Technologies* 72(Nov): 1–9.

Howard D, Dai D (2014) Public perceptions of self-driving cars: the case of Berkeley, California. In *Transportation Research Board 93rd Annual Meeting*. Washington, DC.

Kyriakidis M, Happee R, de Winter J (2015) Public opinion on automated driving: results of an international questionnaire among 5000 respondents. *Transportation Research Part F: Traffic Psychology and Behaviour* 32(Jul): 127–140.

Loveday S (2019) Monthly plug - In EV sales scorecard - Archive. InsideEVs. Retrieved from: https://insideevs.com/news/344006/monthly-plug-in-report-card-archive. (Accessed 21 September2019.)

Lutsey N, Nicholas M (2019) *Update on electric vehicle costs in the United States through 2030*. Washington, DC: International Council on Clean Transportation.

Nielsen TAS, Haustein S (2018) On sceptics and enthusiasts: what are the expectations towards self-driving cars? *Transport Policy* 66(Aug): 49–55.

Nordhoff S, de Winter J, Kyriakidis M, van Arem B, Happee R (2018) Acceptance of driverless vehicles: results from a large cross-national questionnaire study. *Journal of Advanced Transportation* 2018: 5382192.

SAE – Society of Automotive Engineers (2018) *Taxonomy and definitions for terms related to driving automation systems for on-road motor vehicles*. SAE.

Schaller B (2018) *The new automobility: lyft, uber and the future of American cities*. Brooklyn, NY: Schaller Consulting.

Schoettle B, Sivak M (2014) A survey of public opinion about connected vehicles in the U.S., the U.K., and Australia. In *International Conference on Connected Vehicles and Expo, Vienna, Austria*.

Trommer S, Kröger L, Kuhnimhof T (2018) Potential fleet size of private autonomous vehicles in Germany and the US. In G Meyer, S Beiker (eds.), *Road Vehicle Automation 4*, 247–56. Cham: Springer International Publishing.

US Census – U.S. Census Bureau (2018). *Selected economic characteristics, 2012–2016 American community survey 5-year estimates*. Washington, DC: US Census.

Zmud J (2016) Self-driving vehicles: determinants of adoption and conditions of usage. *Transportation Research Record: Journal of the Transportation Research Board* 2565(1): 57–64.